The
Philosophical Magazine

FIRST PUBLISHED IN 1798

A Journal of Theoretical
Experimental and Applied Physics

Vol. 4 September 1959 **No. 45**
Eighth Series

UNIVERSITY OF HAWAII
LIBRARY
JAN 7 '60

£1 5s. 0d., plus postage
Annual Subscription £13 10s. 0d., payable in advance

ALERE FLAMMAM

Printed and Published by
TAYLOR & FRANCIS LTD
RED LION COURT, FLEET STREET, LONDON, E.C.4

THE PHILOSOPHICAL MAGAZINE

Editor
Professor N. F. Mott, M.A., D.Sc., F.R.S.

Editorial Board
Sir Lawrence Bragg, O.B.E., M.C., M.A., D.Sc., F.R.S.
Sir George Thomson, M.A., D.Sc., F.R.S.
Professor A. M. Tyndall, C.B.E., D.Sc., F.R.S.

Authors wishing to submit papers for publication in the Journal should send manuscripts directly to the Publishers.

Manuscripts should be typed in *double* spacing on one side of quarto (8 × 10 in.) paper, and authors are urged to aim at absolute clarity of meaning and an attractive presentation of their texts.

References should be listed at the end in alphabetical order of authors and should be cited in the text in terms of author's name and date. Diagrams should normally be in Indian ink on white card, with lettering in soft pencil, the captions being typed on a separate sheet.

A leaflet giving detailed instructions to authors on the preparation of papers is available on request from the Publishers.

Authors are entitled to receive 25 offprints of a paper in the Journal free of charge, and additional offprints can be obtained from the Publishers.

The *Philosophical Magazine* and its companion journal, *Advances in Physics*, will accept papers for publication in experimental and theoretical physics. The *Philosophical Magazine* publishes contributions describing new results, letters to the editor and book reviews. *Advances in Physics* publishes articles surveying the present state of knowledge in any branch of the science in which recent progress has been made. The editors welcome contributions from overseas as well as from the United Kingdom, and papers may be published in English, French and German.

UNIVERSITY OF HONG KONG

Applications are invited for the following newly-established posts in Mathematics :

1. Readership or Senior Lectureship in Applied Mathematics
2. Senior Lectureship or Lectureship in Pure Mathematics

Annual salary (superannuable) is :

Readership :	£2,500 (man) or £1,900 (woman)
Senior Lectureship :	£2,000 × £75–£2,300 (man) or £1,500 × £60–£1,740 (woman)
Lectureship:	£1,575 × £50–£2,175 (man) or £1,200 × £40–£1,680 (woman)

There is also an expatriation allowance of £300/£250/£225 a year if applicable. The equivalent of income tax in the Colony is comparatively low.

First class sea passages are provided for expatriate staff and their families on first appointment and leaves.

Applicants should have appropriate qualifications and teaching and research experience.

Further particulars and information as to the method of application may be obtained from the Secretary, Association of Universities of the British Commonwealth, 36 Gordon Square, London, W.C.1.

Applications close, in Hong Kong and London, on **31st December, 1959.**

UNIVERSITY OF SYDNEY

Senior Lectureship or Readership in Physics

Applications are invited from senior theoretical astrophysicists for the position of Senior Lecturer or Reader in Physics in the Theoretical Group of the School of Physics.

The salary for a Senior Lecturer is within the range £A2,200–80–£2,600 per annum plus cost of living adjustment. The salary for a Reader is £A2,850 per annum plus cost of living adjustment. Salaries are subject to deductions under the State Superannuation Act. The commencing salary will be fixed according to the qualifications and experience of the successful applicant.

Under the Staff Members' Housing Scheme in cases approved by the University and its Bankers, married men may be assisted by loans to purchase a house.

The Theoretical Group has a strong team at present in the fields of Field Theory, Low Temperature Theory, Nuclear Physics and Shower Theory. Silliac, the automatic digital computer, is housed in the School of Physics and first priority in its use is given to physicists in the School. The School also has a large experimental group active in the field of cosmic rays. Steps are now being taken in the School to establish a thermonuclear group as well as an astronomy group with its own telescope.

Further particulars and information as to the method of application may be obtained from the Secretary, Association of Universities of the British Commonwealth, 36 Gordon Square, London, W.C.1.

Applications close on **5th December, 1959.**

Announcing the new publication

CONTEMPORARY PHYSICS

A Journal of Interpretation and Review

Editor:
G. R. Noakes, M.A., F.Inst.P.

Editorial Board:
Consultant Editors: Sir Lawrence Bragg, O.B.E., M.C., M.A., D.Sc., F.R.S.
Sir George Thomson, M.A., D.Sc., F.R.S.

Advisory Editors: Professor L. F. Bates, Ph.D., D.Sc., F.R.S.
Dr. K. A. G. Mendelssohn, F.R.S.
Dr. F. A. Vick, O.B.E.

Contents of October, 1959

Molecular Beams. By O. R. Frisch, Cavendish Laboratory, Cambridge

The Structure of the Atomic Nucleus. By R. J. Blin-Stoyle, Fellow of Wadham College and Senior Research Officer in Theoretical Physics, University of Oxford

Alexander von Humboldt and the Organization of International Collaboration in Geophysical Research. By L. Kellner, Imperial College of Science and Technology, London

The Selection and Design of Experiments for Alternating Current Teaching. By H. V. Beck, Cavendish Laboratory, Cambridge

Skidding Friction. The Effect of Hysteresis Losses in Tyre Tread Rubber. By Barbara E. Sabey, Road Research Laboratory, Department of Scientific and Industrial Research

Light Sources using Radioisotopes. By E. J. Wilson and J. D. H. Hughes, Isotope Division, Harwell

Price per part 5s. 0d. (75 cents) plus postage

Subscription price per volume of 6 parts £1 7s. 0d. ($4.00), post free, payable in advance

Printed and Published by

TAYLOR & FRANCIS LTD

RED LION COURT, FLEET STREET, LONDON, E.C.4

Journal of Electronics and Control

A Philosophical Magazine Associated Journal

Editor:
J. Thomson, M.A., D.Sc., M.I.E.E., F.Inst.P.
Consultant Editor:
Professor N. F. Mott, F.R.S.
Editorial Board:
Professor P. Aigrain (France)
Professor H. B. G. Casimir (Holland)
J. F. Coales (U.K.)
Professor K. G. Emeleus (U.K.)
D. W. Fry (U.K.)
Dr. W. Klein (Germany)
Dr. R. Kompfner (U.S.A.)

Contents of June, 1959

Electronics Section

Some Experiments on Broad-band C.W. Power Klystrons at X-band. By M. O. Bryant and C. P. Lea-Wilson, Services Electronics Research Laboratory, Extension, Harlow, Essex

Necessary and Sufficient Trajectory Conditions for Dense Electron Beams. By W. M. Mueller, Research Laboratories, Hughes Aircraft Company, Los Angeles, California

Cavity Maser Experiments using Ruby at S Band. By W. S. C. Chang, J. Cromack and A. E. Siegman, Stanford University, Stanford, California

The Effect of Field Configuration on Gas Discharge Breakdown in Microwave Cavities at Low Pressure. By S. A. Self and H. A. H. Boot, Services Electronics Research Laboratory, Baldock, Herts

Asymptotic Contribution to Non-linear Theory of Plasma Oscillations. By Louis Gold, Edgerton, Germeshausen and Grier, Inc., 160 Brookline Avenue, Boston 13, Massachusetts

Control Section

The Application of a Pattern-recognition Technique to the Synthesis of Coding Circuits. By J. H. Calderwood, Royal Technical College, Salford and A. Porter, University of Saskatchewan, Canada

The Synthesis of a Parallel Adder Circuit using a Pattern-recognition Technique. By J. H. Calderwood, Royal Technical College, Salford and A. Porter, University of Saskatchewan, Canada

Price per part £1 5s. plus postage
Price per volume £7 post free, payable in advance
6 monthly issues per volume

Printed and Published by

TAYLOR & FRANCIS LTD
RED LION COURT, FLEET STREET, LONDON, E.C.4

Orders originating in U.S.A. and Canada should be sent to the Academic Press Inc., 111 Fifth Avenue, New York 3, N.Y., U.S.A.

INTERNATIONAL JOURNAL OF
RADIATION BIOLOGY
and related studies in Physics, Chemistry and Medicine

Editor
W. M. DALE, M.D., D.SC.
Dept. of Biochemistry, Christie Hospital & Holt Radium Institute, Withington, Manchester, 20
Assistant Editor
JOHN WAKEFIELD, B.A., F.Z.S.

Editorial Board
Charlotte Auerbach, *U.K.;* J. H. Baxendale, *U.K.;* D. W. van Bekkum, *Holland;* E. H. Betz, *Belgium;* H. A. S. van den Brenk, *Australia;* A. A. Buzzatti-Traverso, *Italy;* J. Coursaget, *France;* F. Devik, *Norway;* M. Haissinsky, *France;* A. Hollaender, *U.S.A.;* B. F. Kaufmann, *U.S.A.;* G. Klein, *Sweden;* H. Langendorff, *Germany;* M. Magat, *France;* M. Nakaidzumi, *Japan;* E. Paterson, *U.K.;* H. Ulrich, *Switzerland;* M. Westergaard, *Denmark.*

Contents of July, 1959

The Relative Biological Efficiency of Single Doses of Fast Neutrons and Gamma-rays on *Vicia faba* Roots and the Effect of Oxygen. Part I. Reduction of Root Growth. By G. J. Neary, S. M. Tonkinson and F. S. Williamson, Medical Research Council Radiobiological Research Unit, Harwell, Didcot, Berks

The Relative Biological Efficiency of Single Doses of Fast Neutrons and Gamma-rays on *Vicia faba* Roots and the Effect of Oxygen. Part II. Chromosome Damage: the Production of Micronuclei. By H. J. Evans, G. J. Neary and F. S. Williamson, Medical Research Council Radiobiological Research Unit, Harwell, Didcot, Berks

The Relative Biological Efficiency of Single Doses of Fast Neutrons and Gamma-rays on *Vicia faba* Roots and the Effect of Oxygen. Part III. Mitotic Delay. By G. J. Neary, H. J. Evans, S. M. Tonkinson and F. S. Williamson, Medical Research Council Radiobiological Research Unit, Harwell, Didcot, Berks

The Effects of X-radiation on the Processes Leading to DNA-synthesis in Regenerating Rat Liver. By J. J. Jaffe, L. G. Lajtha, June Lascelles, Margery G. Ord and L. A. Stocken, Department of Biochemistry and the Churchill Hospital, University of Oxford

Modification of Radiation-induced Intestinal Injury in Rats by Chilling after Irradiation. By W. D. Gude, A. C. Upton and T. T. Odell, Jr., Biology Division, Oak Ridge National Laboratory, Oak Ridge, Tennessee

The Modification of Acute Mortality in Mice by Variation of the Dose-rate and the Overall Time of Irradiation. By M. J. Corp and F. E. Neal, M.R.C. Radiobiological Research Unit, A.E.R.E., Harwell, Berks

Comparison of Protective Effects of Hind-leg Shielding and Isologous Bone-marrow Injection in X-irradiated Rats. By J. M. Loiselle, L. F. Lamerton and Kay Adams, Physics Department, Institute of Cancer Research, Royal Cancer Hospital, Fulham Road, London, S.W.3

Radiation-induced Tissue Breakdown. IV. The Source of Degraded Amino Acids in Irradiated Rats. By Georg Gerber, Gisela Gerber, K. I. Altman and L. H. Hempelmann, Division, of Experimental Radiology, School of Medicine and Dentistry, University of Rochester, Rochester, New York

The Effect of Triethylene-melamine on the Fertility of Female Mice. By B. M. Cattanach, Institute of Animal Genetics, University of Edinburgh

Modification of X-ray Damage to the Lens by Partial Shielding. By Antoinette Pirie and S. M. Drance, Nuffield Laboratory of Ophthalmology, University of Oxford

Enzymatic Activity Related to DNA-synthesis in Regenerating Liver of Irradiated Rats. By S. Okada and L. H. Hempelmann, From the Division of Experimental Radiology, University of Rochester School of Medicine and Dentistry, Rochester 20, N.Y.

Price per part £1 0s. 0d. plus postage
Subscription per volume (4 issues) £3 15s. 0d. post free, payable in advance

Printed and Published by
TAYLOR & FRANCIS LTD
RED LION COURT, FLEET STREET, LONDON, E.C.4
Orders originating in U.S.A. and Canada should be sent to the
Academic Press Inc., 111 Fifth Avenue, New York 3, N.Y., U.S.A.

A new International Journal

Molecular Physics

Editor: **H. C. LONGUET-HIGGINS, F.R.S.**
Associate Editor: **J. H. VAN DER WAALS**

Editorial Board:

J. Bjerrum, *Copenhagen*; G. Careri, *Padua*; C. A. Coulson, *Oxford*; F. H. C. Crick, *Cambridge*; P. J. W. Debye, *Cornell*; D. Hadži, *Ljubljana*; O. Hassel, *Oslo*; W. Heitler, *Zürich*; J. O Hirschfelder, *Wisconsin*; D. F. Hornig, *Princeton*; J. A. A. Ketelaar, *Amsterdam*; J. G. Kirkwood, *Yale*; R. Kronig, *Delft*; J.W. Linnett, *Oxford*; A. Liquori, *Rome*; Dame Kathleen Lonsdale, *London* ; P-O. Löwdin, *Uppsala* ; M. Magat, *Paris* ; R. S. Mulliken, *Chicago*; A. Münster, *Frankfurt*; L. J. Oosterhoff, *Leiden*; L. E. Orgel, *Cambridge*; J. A. Pople, *Teddington*; I. Prigogine, *Brussels*; R. E. Richards, *Oxford*; J. S. Rowlinson, *Manchester*; G. S. Rushbrooke, *Newcastle upon Tyne*; L. E. Sutton, *Oxford*; H. W. Thompson, *Oxford*; B. Vodar, *Bellevue, Paris.*

Contents of July, 1959

Long-range Interaction of Two 1s-hydrogen Atoms Expressed in Terms of Natural Spin-orbitals. By J. O. Hirschfelder, Theoretical Chemistry Laboratory, Chemistry Department, University of Wisconsin, Madison, Wisconsin and P. O. Löwdin, Quantum Chemistry Group, University of Uppsala, Uppsala, Sweden

Efficiencies of Third Bodies in the Reaction $H+O_2+M=HO_2+M$. By P. G. Dickens and J. W. Linnett, Inorganic Chemistry Laboratory, Oxford

Diffusion Coefficients of Gases from the Rate of Approach to the Steady State in Thermal Diffusion. By S. C. Saxena and E. A. Mason, Institute for Molecular Physics, University of Maryland, College Park

The Pairing of Electronic States in Alternant Hydrocarbons. By A. D. McLachlan, Department of Theoretical Chemistry, University Chemical Laboratory, Lensfield Road, Cambridge, England

The Electron Spin Resonance Spectrum of a γ-irradiated Single Crystal of Glycine. By D. K. Ghosh and D. H. Whiffen, Chemistry Department, University of Birmingham

Thallium Nuclear Resonance Spectra, Part II. By R. Freeman, R. P. H. Gasser and R. E. Richards, Physical Chemistry Laboratory, South Parks Road, Oxford

Electron Transfer Spectra of Hexahalide Complexes. By C. K. Jørgensen, Chemistry Department A, Technical University of Denmark, Copenhagen

Price per part £1 5s. 0d. plus postage
Subscription per volume (4 issues) £4 15s. 0d. post free, payable in advance

Printed and Published by
TAYLOR & FRANCIS LTD
RED LION COURT, FLEET STREET, LONDON, E.C.4

Orders originating in U.S.A. and Canada should be sent to the
Academic Press Inc., 111 Fifth Avenue, New York 3, N.Y., U.S.A.

A new International Journal

ERGONOMICS

HUMAN FACTORS IN WORK, MACHINE CONTROL AND EQUIPMENT DESIGN

General Editor
A. T. WELFORD
University of Cambridge, Psychological Laboratory, Downing Place, Cambridge

Associate Editor (Anatomy and Physiology)
W. F. FLOYD

Assistant Editor
Miss H. M. CLAY

Editorial Board

H. Bastenier, *Belgium*; R. B. Bromiley, *Canada* ; R. Bonnardel, Bernard Metz, *France*; E. A. Müller, *Germany*; M. G. Bennett, W. E. Hick, Sir Charles Lovatt Evans, L. G. Norman, *Great Britain*; F. H. Bonjer, *Netherlands*; S. P. M. Forssman, *Sweden*; E. Grandjean, *Switzerland*; H. S. Belding, P. M. Fitts, *U.S.A.*

Contents of May, 1959

Some Problems of Scientific Thinking. By Sir Frederic Bartlett, St. John's College, Cambridge

Accident-proneness in Motor-vehicle Drivers. By D. Russell Davis and Patricia A. Coiley, Medical Psychology Laboratory, University of Cambridge

A Note on Panel Layout for Numbers of Identical Items. By B. Shackel, Psychological Research Laboratory, E.M.I. Electronics Ltd., Hayes, Middlesex, England

The Effects of Aptitude, Fitness, Physical Working Capacity, Skill and Motivation on the Amount and Quality of Work. By F. H. Bonjer, Department of Occupational Health, Netherlands Institute for Preventive Medicine, Leiden, Holland

Circulatory Responses to Change from Recumbent to Erect Posture as an Index of Heat Stress. By J. R. Brown, G. P. Crowden and P. F. Taylor, Department of Applied Physiology, London School of Hygiene and Tropical Medicine

The Estimation of the Transfer Function of a Human Operator by a Correlation Method of Analysis. By J. G. Henderson, Electrical Engineering Department, University of Birmingham

The Judgment of Velocity and Prediction of Motion. By D. J. Gerhard, Department of Scientific and Industrial Research, London

E.P.A. Project No. 335. " Fitting the Job to the Worker "

Price £1 5s. 0d. per part plus postage
Subscription price per volume £4 15s. 0d. post free, payable in advance

Printed and Published by
TAYLOR & FRANCIS LTD
RED LION COURT, FLEET STREET, LONDON, E.C.4

Orders originating in U.S.A. and Canada should be sent to the
Academic Press Inc., 111 Fifth Avenue, New York 3, N.Y., U.S.A.

INTERNATIONAL JOURNAL

OPTICA ACTA

European Journal of Optics
Journal Européen d'Optique
Europäische Zeitschrift für Optik

English Editor: C. G. Wynne, 13 Elwill Way, Beckenham, Kent, U.K.

Rédacteur Français: A. Maréchal, 3 Boulevard Pasteur, Paris, France

Deutscher Herausgeber: G. Franke, Laufdorfer Weg 2, Wetzlar, Germany

Editorial Board

J. M. Otero y Navascues, *Madrid;* R. W. Ditchburn, *Reading;* A. Arnulf, *Paris;* A. Biot, *Gand;* J. Cabannes, *Paris;* P. Fleury, *Paris;* F. Gabler, *Vienna;* G. Hansen, *Oberkochen;* E. Ingelstam, *Stockholm;* H. Korte, *Braunschweig;* W. S. Stiles, *London;* G. Toraldo di Francia, *Florence;* A. C. S. van Heel, *Delft.*

Contents of April, 1959

Correction Approchée de l'Effet de Lobe en Radioastronomie. Par J. Arsac. Observatoire de Meudon

Colour Perception with the Peripheral Retina. By J. D. Moreland and A. Cruz, Technical Optics Section, Imperial College, London

A Fourier Analyser for Optical Frequency Response Determinations. By J. M. Naish, Royal Aircraft Establishment, Hampshire England

Photo-sensitive Reactions in Foveae of Normal and Cone-monochromatic Observers. By R. A. Weale, Visual Research Division, Ophthalmological Research Unit, (Medical Research Council), Institute of Ophthalmology, Judd Street, London, W.C.1

Contrast Transfer in the Grating Spectrograph. By A. Lohmann, Institute of Optical Research, Stockholm 70, Sweden

Doppelbrechungs-interferenzfarben sehr dünner Plättchen. Von S. Rösch, Wetzlar

Price per part £1 (1375 fr.), (DM 11.75), ($2.80), plus postage

Subscription price per volume (4 parts) £3 15s. (5155 fr.), (DM 44), ($10.50), post free, payable in advance

Printed and Published by

TAYLOR & FRANCIS LTD

RED LION COURT, FLEET STREET, LONDON, E.C.4

Physics in Medicine and Biology

A Taylor & Francis Journal published in association with The Hospital Physicists' Association

Editor: J. E. Roberts, D.Sc.
Consultant Editor: Professor N. F. Mott, F.R.S.

Editorial Board

N. W. Bellwood, *London*; R. Bonet-Maury, *Paris*; J. Dainty, *Edinburgh*; H. E. Johns, *Toronto*; W. A. Langmead, *Dumfriesshire*; D. A. McDonald, *London*; J. S. Mitchell, *Cambridge*; G. J. Neary, *Harwell*; B. Rajewsky, *Frankfurt*; J. Rotblat, *London*; S. Rowlands, *London*; H. P. Schwan, *Philadelphia*; R. Sievert, *Stockholm*; F. W. Spiers, *Leeds*; J. F. Tait, *Massachusetts*; A. J. H. Vendrik, *Nijmegen*.

Contents of July, 1959

The Basic Design Data of a Guarded-field Thimble Ionization Chamber: A Theoretical Investigation. By Barry Barber, M.A., A.Inst.P., Physics Department, London Hospital Research Laboratories, Ashfield Street, London, E.1

A Theoretical Approach to the Radiation Dose-rate Distribution from Combined X- or γ-ray Beams with special reference to Wedge-filtered Beams. By R. Sear, B.Sc., A.Inst.P., Physics Department, The London Hospital Research Laboratories, London, E.1

Miniature Ionization Chambers for Measurements in Body Cavities. By S. Benner, Ph.D., M.D., I. Ragnhult, M.Sc., and G. Gebert, Radiophysics Institute, University of Gothenburg, Sahlgrenska Sjukhuset, Gothenburg C, Sweden

A Simple Circuit for Simultaneous Dose-rate and Dose Measurements. By Sven Benner, Ph.D., M.D., Radiophysics Institute, University of Gothenburg, Sahlgrenska Sjukhuset, Gothenburg C, Sweden

A Note on the Calibration of X-ray Dosemeters. By John Tooze and Boyce Worthley, Anti-Cancer Committee, University of Adelaide, South Australia

The Stopping-power Correction for Graphite Cavity-chambers used with 2 mV X-rays. By G. P. Barnard, D.Sc., Ph.D., M.I.E.E., F.Inst.P. and A. R. S. Marsh, The National Physical Laboratory, Teddington, Middlesex

An Experimental Evaluation of Microspectrophotometry. By K. W. Keohane, B.Sc., Ph.D., and W. K. Metcalf, M.D., B.S., Department of Anatomy, The University, Bristol, 8

An Experimental Determination of the Propagation of Fluid Oscillations in a Tube with a Visco-elastic Wall; together with an Analysis of the Characteristics Required in an Electrical Analogue. By M. G. Taylor, M.D., Ph.D., Physiology Department, Medical College of St. Bartholomew's Hospital, London

Subscription price per volume £3 10s. post free, payable in advance
4 parts per volume—£1 per part plus postage

Printed and Published by

TAYLOR & FRANCIS, LTD

RED LION COURT, FLEET STREET, LONDON, E.C.4

Orders originating in U.S.A. and Canada should be sent to the
Academic Press Inc., 111 Fifth Avenue, New York 3, N.Y., U.S.A.

The Analysis of 4·5 BeV Negative Pion Interactions in Nuclear Emulsion†

By H. H. ALY, J. G. M. DUTHIE and C. M. FISHER
H. H. Wills Physical Laboratory, University of Bristol

[Received April 7, 1959]

ABSTRACT

Two hundred nuclear interactions produced in Ilford G5 nuclear emulsion by 4·5 BeV π^- mesons have been analysed. The transverse momentum of those secondary shower particles identified as pions has an average value over all angles of 290 ± 50 MeV/c. The mean multiplicity of shower particles from the interactions is $2{\cdot}0 \pm 0{\cdot}1$ and is independent of the number of heavily ionizing prongs N_h. About 90 % of the shower particles were estimated to be pions. The angular distribution in the C-system is anisotropic with a mean value for $|\cos\theta^*|$ of $0{\cdot}58 \pm 0{\cdot}03$.

Assuming that secondary pions are emitted symmetrically backwards and forwards from a single collision system, the observed angular distribution of shower particles has been used to determine the effective mass of the collision partner. It is found to be $1{\cdot}40^{+0{\cdot}47}_{-0{\cdot}27}$ proton mass units. If the total distribution is divided into groups with respect to N_h it is found that events having $N_h \leqslant 7$ yield a value of $0{\cdot}77^{+0{\cdot}36}_{-0{\cdot}19}$ proton mass units whilst those having $N_h > 7$ yield $2{\cdot}3^{+0{\cdot}9}_{-0{\cdot}4}$ proton mass units.

§ 1. INTRODUCTION

IN recent years there have been several investigations into the nature of interactions initiated by high energy pions (Eizberg *et al.* 1955, Johnson 1955, Maenchen *et al.* 1955, 1957, Sternheimer and Lindenbaum 1958, Walker 1957). In the diffusion chamber investigations, the Lorentz factor γ, of the centre of momentum system (hereafter referred to as the C-system) is easily calculated if the gas employed is hydrogen. This is not true of experiments carried out using nuclear emulsions. In the analysis of cosmic ray jets it has usually been assumed that the collision partner has nucleonic mass where the term 'collision partner' is used in this discussion to describe the particle which, with the primary particle, forms the C-system of the interaction. Our analysis assumes, as in the analysis of jets, that in these interactions there are on average, equal numbers of shower particles produced in the backward and forward directions of the C-system. From this assumption of backward-forward symmetry, and observations of the angular distribution of shower particles in jets, estimates have been made of the energy of the primary particle. In this paper we have examined events with known primary energy and by investigating the angular distribution of the shower particles we have estimated the mean rest mass of the collision partner.

---

† Communicated by the Authors.

Fermi (1950), Landau (1953), Kraushaar and Marks (1954) and others have predicted the angular distribution of the mesons produced in high energy nucleon–nucleon collisions. The energy here is somewhat below that discussed in these models, but it is of interest to compare the observed distribution of shower particles produced in pion-nucleus collisions with the extrapolated theoretical predictions for nucleon–nucleon collisions. A composite distribution has been obtained of all shower particles from the 200 stars and is discussed in § 10.

The mean transverse momentum of the shower particles has been determined by several authors (Daniel *et al.* 1952, Edwards *et al.* 1958 and Fenyves *et al.* 1958) over a wide range of primary energies (300 BEV–25 000 BEV). Results indicate that this parameter is remarkably independent of energy. In this experiment the mean value of the transverse momentum $\bar{p}_T$ of the secondary mesons has been determined and the dependence of p_T on the angle of emission to the primary direction investigated.

§ 2. EXPERIMENTAL PROCEDURE

The observations were made in a stack of stripped Ilford G5 emulsions exposed to a beam of 4·5 BEV negative pions from the Berkeley Bevatron. The stack consisted of 80 emulsion sheets each 30 cm × 20 cm × 600 μ with the pion beam traversing the longer axis. This stack had previously been examined by Brisbout *et al.* (1956) and has been shown to be relatively free from spurious scattering.

Tracks of the primary pions were followed independently in the direction of the beam until an interaction, recognized by the production of heavily ionizing tracks or at least two shower tracks, was found. Interactions observed on neighbouring beam tracks were neglected to ensure that an unbiased sample was obtained. Two hundred interactions were found in this way.

On finding an interaction the following quantities were determined:

(1) The number of heavily ionizing tracks emerging (N_h) having normalized blob density $b^* > 1{\cdot}4$, where b^* is defined as the ratio of the blob density of the track under consideration to that of a 4·5 BEV pion track in the same vicinity.

(2) The number of shower tracks (n_s) having $b^* \leqslant 1{\cdot}4$.

(3) The space angles of the shower tracks with respect to the primary direction.

(4) For those shower particles travelling at least 5 mm in the emulsion in which they originated, the scattering parameter $\bar{\alpha}$.

(5) The normalized blob density b^* of the shower particles on which scattering measurements were made.

The interactions were classified in groups defined by their values of N_h and n_s. The nomenclature $N_h + n_s$ is used to define a particular group of interactions. There was uncertainty in the interpretation of $0 + 1$ and

$0+0$ events which may have been due to elastic scattering and charge exchange scattering respectively. These events have therefore been omitted.

The primary beam was fairly intense and the scattering criterion was chosen to avoid following shower particles out of the emulsion in which they were created. The scattering criterion introduces a bias against scattering tracks at large angles to the primary direction but this can be corrected by the application of a readily calculated geometric factor.

The normalized blob density b^* was measured on those tracks for which the value of $p\beta$ was determined. The identity of these shower particles was then investigated using the method described by Daniel *et al.* (1952), depending on the variation of the ionization with velocity in nuclear emulsion. On each track 4000 blobs were counted and a further 4000 on a nearby 4·5 BeV π^- track. The latter value was taken as the plateau ionization in the vicinity and used to normalize the former. A considerable variation was found in the blob density of the beam tracks with depth in the emulsion. Thus it was necessary to obtain a series of values of the normalizing density corresponding to different depths of the secondary track. The results of these measurements are discussed in § 3.

§ 3. IDENTIFICATION OF SHOWER PARTICLES

Out of the 39 tracks measured using the method described in the previous section, 29 were found to be pions. Of the remaining tracks, 5 could be ascribed to protons and 5 could not be identified. When the selection bias is taken into account the proportion of shower particles which were not pions becomes about 10%.

Table 1

θ N_h group	0–10°		10–30°		> 30°	
	π	p	π	p	π	p
$N_h \leqslant 7$	6	3	6	0	2	0
$N_h > 7$	4	1	4	1	7	0
All N_h	10	4	10	1	9	0

This method of identification of high energy singly charged particles has been investigated in some detail by Alexander and Johnston (1957) and by Shapiro and Stiller (1952). The exact shape of the curves below $b^* = 1$ are not well established for emulsions; however, for our purpose it is sufficient to know the general shape in this region and the exact position of the curves above the plateau, which is defined by several tracks having $b^* \sim 1{\cdot}4$.

Of the five particles which were probably protons four were emitted at angles of less than 10° to the primary direction and all lay inside the median angle of the distribution. An analysis of the C-system dynamics shows that no protons can be emitted from the primary interaction at an angle greater than 52° to the primary direction in the laboratory system such that the normalized blob density of their tracks is less than 1·4.

The characteristics of the identified shower particles when divided into groups with different laboratory angles of emission are shown in table 1.

§ 4. THE N_h AND n_s DISTRIBUTIONS

The distribution of the number of heavily ionizing prongs, having normalized blob density greater than 1·4, associated with the 200 stars is shown in fig. 1, together with the distributions obtained in the work on jets at very high energies. The increase in N_h as the primary energy decreases is clearly seen; however, it should be remembered that these jets were found in stacks flown at very high altitudes where the primaries are probably nucleons. The median value of N_h for the distribution

Fig. 1

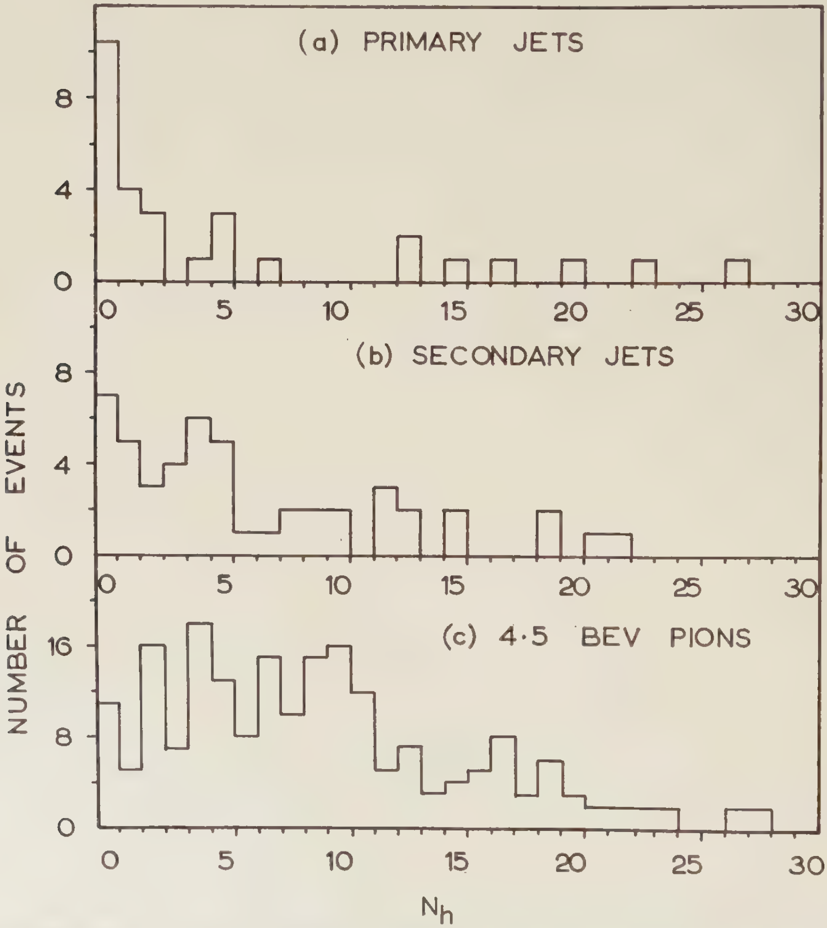

The distribution in the number of heavily ionizing prongs N_h. (*a*) Primary jets $\bar{E}\sim5000$ BEV. (*b*) Secondary jets $\bar{E}\sim300$ BEV. (Edwards *et al.* 1958.)

obtained in this experiment, corrected for 0+0 and 0+1 events, is 7 whilst the mean N_h per star is 9. Camerini *et al.* (1951), examining cosmic ray interactions, obtained a value of 10 for the mean N_h of stars having $\bar{n}_s = 2$ and $N_h \geqslant 3$. If stars having $N_h \leqslant 3$ are omitted this experiment yields a similar result.

The distribution in the number of shower particles n_s is shown in table 2. Since there was no observed dependence of n_s on N_h, the calculation of the mean multiplicity has been effected assuming that the number of true non-elastic collisions of the form 0+1 and 0+0 was equal to the mean number of events of the form N_h+0 and N_h+1 for all $N_h \leqslant 7$. Adding a correction of four events missed in this way it is found that the mean multiplicity is $2{\cdot}0 \pm 0{\cdot}1$.

Table 2

Multiplicity	0	1	2	3	4	5	6	7
No. of events	17	52	66	41	19	1	3	1

Within the error quoted, the same value of the mean multiplicity was obtained for events having $N_h > 7$ as for those having $N_h \leqslant 7$.

If the production process is assumed to be charge independent and all shower particles are taken as pions, then the mean number of created pions is 3·0. From considerations discussed in § 3 the number of protons included in the above data is small (< 10%).

However, pions emitted backwards in the C-system with velocities comparable to that of the C-system in the laboratory, will appear as grey tracks. From considerations discussed in § 7 the number of slow pions missed in this way represents about 5% of the total. Thus the two effects partly compensate each other; a corrected value for the mean number of secondary pions would be $\bar{n}_\pi \sim 2{\cdot}8$.

§ 5. TRANSVERSE MOMENTUM OF SECONDARY PIONS

A total of 39 particles satisfied the scattering criterion described in § 2. Of these, 29 were probably pions, 5 were probably protons and 5 could not be identified. The weighted mean value of the transverse momentum for those shower particles identified as pions was

$$\bar{p}_T = 290 \pm 50 \text{ MeV}/c.$$

The arithmetic mean without weighting factors was 202 ± 30 MeV/c.

In fig. 2 the transverse momenta are plotted as a function of the C-system angles of emission. Curve I represents an upper limit imposed by the condition that the pions cannot have momentum greater than 1·3 BeV/c in the C-system of a 4·5 BeV pion–nucleon collision. Curve II represents the cut-off imposed by the condition that the tracks should have $b^+ \leqslant 1{\cdot}4$. Bearing in mind these limitations we are unable to conclude that there is any variation in the transverse momentum with the angle of emission. A similar distribution has been obtained by one of us (Aly, to be published) working with 6 BeV proton interactions in emulsion.

Fig. 2

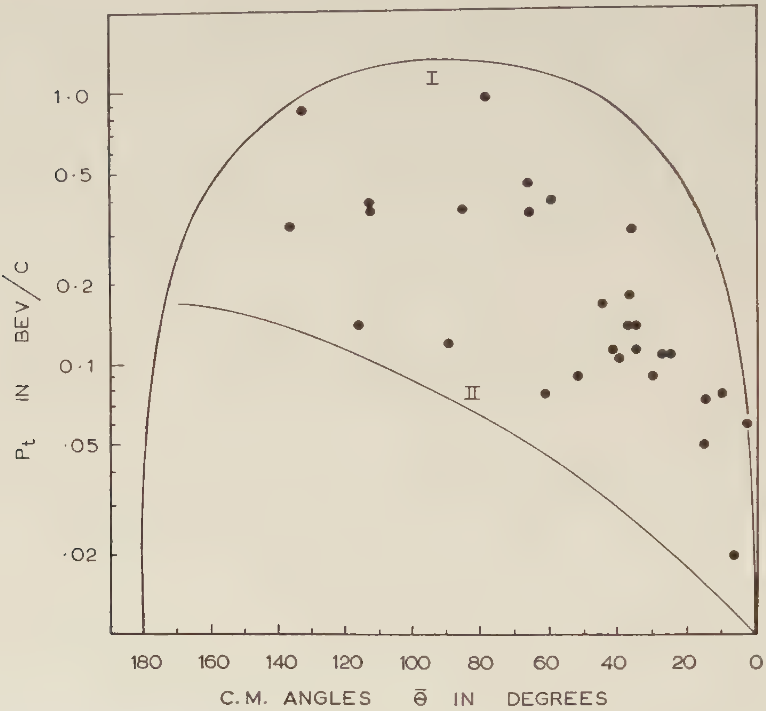

Transverse momentum as function of C-system angle of emission θ^*.

Table 3 shows the mean value of the transverse momentum of secondary particles produced in interactions at a variety of primary energies. The relative constancy of the transverse momentum is apparent. The values for very high primary energies are taken from the results of Edwards *et al.* (1958).

Table 3

$\bar{E}$ BeV	$\bar{p}_T$ BeV/c
4·5	0·29 ± 0·05
~ 300	0·34 ± 0·07
~ 2500	0·77 ± 0·14
~ 23,000	0·91 ± 0·20

In the present experiment the total kinetic energy before collision in the C-system, assuming a collision partner of nucleonic mass is 2·0 BeV. Since the mean number of created pions is three, then if energy is to be conserved, the upper limit of $\bar{p}_T$ is ~700 MeV/c, and occurs when all pions are emitted at 90° to the primary direction in the C-system. However, in order to conserve angular momentum the distribution must be peaked in the forward and backward directions as predicted by Fermi (1951) and confirmed experimentally (see § 10). From these considerations the mean value of p_T is expected to be somewhat smaller in this experiment than in interactions produced with much greater primary energies.

The distribution in the values of p_T obtained in this experiment is shown in fig. 3.

Fig. 3

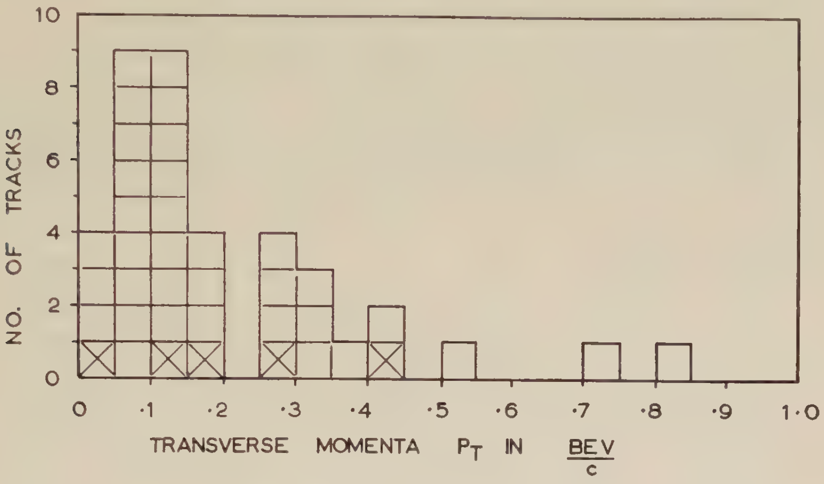

Transverse momentum histogram.

§ 6. The Energy Balance

In an interaction between a pion and a nucleon, the kinetic energy in the laboratory system, neglecting the Fermi energy of the nucleon, before the collision is 4·5 BeV. After the collision this energy must appear in the form of secondary particles or as excitation energy of the nucleus associated with the target nucleon.

The mean energy of the shower particles identified as pions has been calculated and is found to be 1·1 ± 0·2 BeV. Thus 3·3 ± 0·4 BeV of the available energy can be accounted for in terms of secondary π-mesons. The remaining 1·2 ± 0·4 BeV must be accounted for in terms of fast nucleons projected from the target nucleus and the excitation energy of the nucleus.

Camerini *et al.* (1951) have suggested the following relation between the number of heavily ionizing prongs associated with an interaction and the excitation energy communicated to the nucleus

$$E_{N_h} = 124N_h + 30\ \text{MeV}.$$

In this experiment the mean value of N_h is 9 so that using this relation E_{N_h} is 1·15 BeV. Therefore the energy carried away by fast nucleons in each interaction is small and confirms the small number of shower protons observed by direct measurement.

§ 7. THE LABORATORY ANGULAR DISTRIBUTION OF SHOWER PARTICLES

The laboratory angular distribution of shower particles has been divided into two groups for interactions of different N_h and is shown in fig. 4. The median angles of the distributions, with the proton component removed and a correction applied for those particles emitted backwards in the C-system but appearing as grey tracks in the laboratory, are given below.

Median angle for all events $= 35{\cdot}4 \pm 2{\cdot}4°$

Median angle for events having $N_h > 7 = 43{\cdot}2 \pm 4{\cdot}2°$

Median angle for events having $N_h \leqslant 7 = 27{\cdot}0 \pm 2{\cdot}7°$

Fig. 4

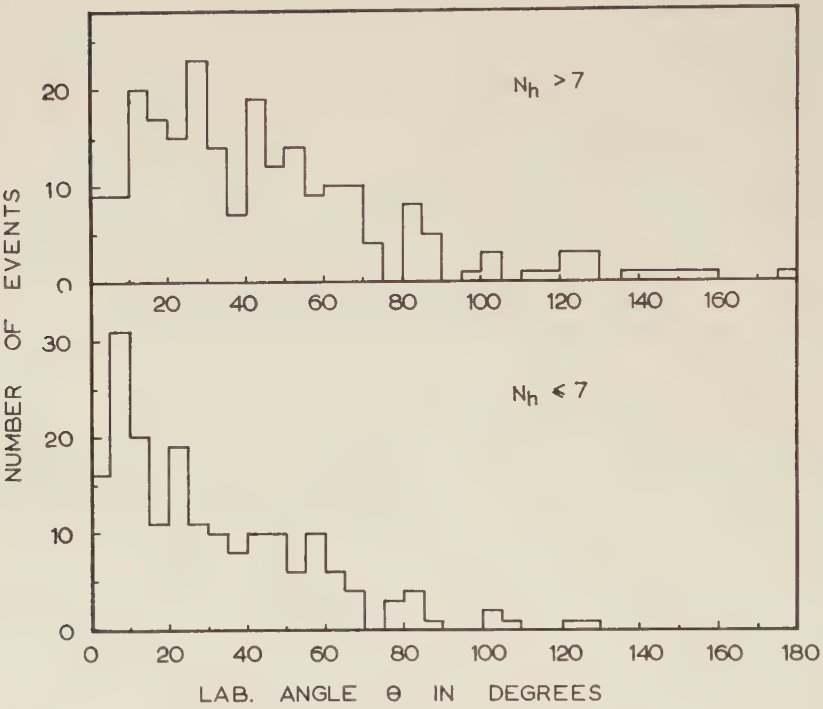

Laboratory angular distribution of shower particles for stars of $N_h > 7$ and $N_h \leqslant 7$.

The correction for slow pions was estimated using the results of Kamal (1957). He examined grey and black prongs from 2500 stars found by area scanning in this stack and has shown that approximately 5% of the grey prongs having $1{\cdot}4 \leqslant b^* \leqslant 3$ are in fact slow pions.

Qualitatively it is reasonable to expect a higher value of the median angle with higher N_h. If, in events of high N_h, the secondary particles traverse a large amount of nuclear matter, a resulting spread of the distribution due to secondary scattering interactions within the nucleus and a consequent increase in median angle is easily understood. However, since there was no observed increase in multiplicity with N_h, the number of potentially minimum ionizing particles absorbed in secondary interactions must have been equal to the number created.

The angular distribution was also investigated as a function of n_s; however, no significant difference between the median angles of the distributions for $n_s=2$ and $n_s\geqslant 3$ was found.

§ 8. REDUCTION OF EXPERIMENTAL RESULTS

The analysis of the results has been carried out assuming that the production of secondary particles occurs in a single collision such that the particle forming the centre of momentum system with the primary pion has a mean rest mass of M proton mass units.

The following notation is employed:

m_π is the pion rest mass.
E_0 is the total energy of the incident pion in the laboratory system.
p_0 is the momentum of the incident pion in the laboratory system.
$E_0{}^*$ and $p_0{}^*$ are the corresponding quantities in the C-system.
$E_M{}^*$ is the total energy of the collision partner in the C-system.
$p_M{}^*$ is the momentum of the collision partner in the C-system.
$\beta_c c$ is the velocity of the C-system in the laboratory frame.
γ_c is the Lorentz factor of the C-system; $\gamma_c=1/\{1-\beta_c{}^2\}^{1/2}$.

We then have

$$M=\frac{E_0}{c^2}\left\{\frac{1}{\beta_c}-1\right\}, \quad \text{if } E_0 \gg m_\pi c^2. \quad . \quad . \quad . \quad . \quad (1)$$

Thus, knowing E_0 and β_c we can determine M.

Now

$$\gamma_c \tan\theta=\frac{\sin\theta^*}{\beta_c/\beta_s{}^*+\cos\theta^*} \quad . \quad . \quad . \quad . \quad . \quad . \quad . \quad (2)$$

where θ^* is the C-system angle corresponding to the laboratory angle of emission θ of a shower particle having velocity $\beta_s{}^*c$ in the C-system.

If $\theta^*=\pi/2$ let $\theta=\eta$; then

$$\gamma_c \tan\eta=\beta_s{}^*/\beta_c,$$

yielding

$$\beta_c{}^2=\frac{1}{1+(\tan\eta/\beta_s{}^*)^2}. \quad . \quad . \quad . \quad . \quad . \quad . \quad . \quad (3)$$

Hence the problem is reduced to determining η and $\beta_s{}^*$. If we assume that in the C-system the shower particles are emitted equally in the backward and forward directions then η is the laboratory angle which divides the shower particle distribution into two equal groups. Thus η is the corrected median angle of the laboratory distribution.

Now $\gamma_s{}^*$, the Lorentz factor of the shower particles in the C-system, may be determined using the relation

$$(1-\beta_c\beta_x)\gamma_\mathrm{L}\gamma_c=\gamma_s{}^* \quad . \quad . \quad . \quad . \quad . \quad . \quad . \quad . \quad . \quad (4)$$

where $\beta_x c$ is the component of the velocity of the shower particles in the laboratory system in the direction of the primary, and γ_L is the Lorentz factor of the shower particles in the laboratory system.

$$\gamma_\mathrm{L}=\frac{1}{\{1-\beta_\mathrm{L}{}^2\}^{1/2}} \quad \beta_\mathrm{L}\cos\theta=\beta_x \quad \gamma_s{}^*=\frac{1}{\{1-\beta_s{}^{*2}\}^{1/2}}.$$

The scattering measurements yield values of γ_L and β_L.

Thus to determine $\beta_s{}^*$ requires that we assume values of γ_c and β_c to substitute in (4). We therefore proceed by a method of successive approximation. We start by assuming a collision partner of one proton mass. This yields by (1) $\gamma_c=1{\cdot}76$ and $\beta_c=0{\cdot}823$. Using these values we calculate from (4) a set of values of $\beta_s{}^*$. The values obtained showed no dependence on θ or θ^*. The mean value of $\beta_s{}^*$ is then substituted in (3) and using the measured value of the median angle a new value of β_c is found. This process is repeated until values of β_c and γ_c are obtained which are consistent with the experimental value of $\tan\eta$ and the $p\beta$ values obtained from the scattering measurements. Relation (1) then yields the mean mass of the collision partner.

Table 4

N_h group	$N_h \leqslant 7$	$N_h > 7$	All N_h
Median angle	27·0° ± 2·7°	43·2° ± 4·2°	35·4° ± 2·4°
M	$0{\cdot}77^{+0{\cdot}36}_{-0{\cdot}19}$	$2{\cdot}38^{+0{\cdot}9}_{-0{\cdot}4}$	$1{\cdot}40^{+0{\cdot}47}_{-0{\cdot}27}$

§ 9. THE MEAN MASS OF THE COLLISION PARTNER

The laboratory angular distribution of the shower particles has been described in § 7. The values of $\beta_s{}^*$, to be substituted in relation (3), were calculated using only those particles identified as pions, and yielded the result $\bar{\beta}_s{}^*=0{\cdot}865\pm0{\cdot}024$, which corresponds to a value of 0·775 for β_c and a value of M of $1{\cdot}40^{+0{\cdot}47}_{-0{\cdot}27}$ proton mass units for the total angular distribution. Table 4 shows the values of M calculated from the median angles corresponding to the groups of different N_h. In all cases the median angles used in the calculation are those of the distributions taking into account slow pions and omitting protons as described in § 3.

These results indicate that, at least for low values of N_h the assumptions of (*a*) equal numbers of particles emitted backwards and forwards in the C-system, and (*b*) that the interaction occurs with a single nucleon, lead to a substantially correct value of the primary energy and further, that for high N_h events, the result may be incorrect by only a factor of about 2. It is therefore not unreasonable to extend this type of analysis to high energies as a method of determining the primary energy.

§ 10. THE ANGULAR DISTRIBUTION OF SHOWER PARTICLES IN THE C-SYSTEM

The angles of emission of shower particles in the C-system can be obtained using the relation (2) of § 8, with the appropriate values of γ_c, β_c and $\bar{\beta}_s{}^*$. The transformation has been effected using the value of $\bar{\beta}_s{}^*$ found for secondary pions. All particles having laboratory angles of emission less than the median angle, are plotted in the forward direction in the C-system. All five particles identified as protons lie in this region. The C-system distribution is shown in fig. 5 as a function of the cosine of the C-system angle θ^*. The mean value of $|\cos\theta^*|$ for this distribution is found to be $0{\cdot}58 \pm 0{\cdot}03$.

Fig. 5

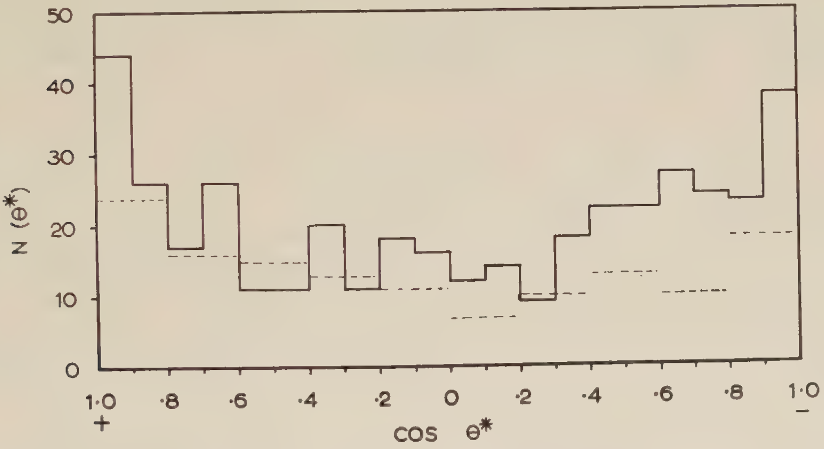

C-system angular distribution. The mean value of $|\cos\theta^*|$ for the distribution is $0{\cdot}58 \pm 0{\cdot}03$.

The transformation of the proton angles to the C-system cannot be achieved using the transformation curve applied to pions because the values of $\beta_s{}^*$ in expression (2) are not the same.

If all the particles are treated as pions the C-system distribution is symmetrical, however if the results of § 3 and § 7 are used to subtract out the proton component and to include slow pions, the resulting pion distribution is slightly peaked in the backward direction. The distribution obtained by the Berkeley group working with a hydrogen filled diffusion chamber (Maenchen *et al.* (1957)) for π^--mesons produced in 4 and 6-prong interactions is shown in fig. 5 as a dotted histogram. This is based on a total of 137 identified pions.

§ 10. SUMMARY OF RESULTS

The results of this analysis may be summarized as follows.

(*a*) About 90% of the shower particles are π-mesons. The remaining 10% are probably knock-on protons.

(*b*) The assumptions of (1) collision with a single nucleon, and (2) equal numbers of particles produced forwards and backwards in the C-system, are consistent with the known primary energy for low N_h ($\leqslant 7$) interactions.

(*c*) For interactions having $N_h > 7$ the primary energy may be determined if one assumes a collision partner of about two proton mass units.

(*d*) The mean multiplicity of the interactions is given by

$$\bar{n}_s = 2{\cdot}0 \pm 0{\cdot}1.$$

(*e*) The mean transverse momentum for all shower pions is 290 ± 50 Mev/c.

(*f*) The C-system angular distribution of shower particles is anisotropic. The mean value of $|\cos\theta^*|$ is 0·58 ± 0·03.

ACKNOWLEDGMENTS

We wish to express our indebtedness to Professor C. F. Powell for extending to us the hospitality of his laboratory.

This experiment would not have been possible without the co-operation of Professor W. H. Barkas and others of the staff of the Radiation Laboratory, Berkeley who exposed the π-meson stack.

We are particularly thankful to Dr. D. H. Perkins of this laboratory who suggested this experiment and to both Dr. D. H. Perkins and Dr. P. H. Fowler for many helpful discussions.

One of us (H.H.A.) would like to thank the government of Iraq, whilst (C.M.F.) and (J.G.D.) wish to thank the Department of Scientific and Industrial Research, for maintenance grants.

REFERENCES

ALEXANDER, G., and JOHNSTON, R. H. W., 1957, *Nuovo Cim.*, **5**, 363.

CAMERINI, V., DAVIES, J. H., FOWLER, P. H., FRANZINETTI, C., MUIRHEAD, H., LOCK, W. O., PERKINS, D. H., and YEKUTIELLI, G., 1951, *Phil. Mag.*, **42**, 1241.

BRISBOUT, F. A., DAHANAYAKE, C., ENGLER, A., FOWLER, P. H., and JONES, P. B., 1956, *Nuovo Cim.*, **3**, 1400.

DANIEL, R. R., DAVIES, J. H., MULVEY, J. H., and PERKINS, D. H., 1952, *Phil. Mag.*, **43**, 753.

Edwards, B., Losty, J., Perkins, D. H., Pinkau. K., and Reynolds, J., 1958, *Phil. Mag.*, **3,** 237.

Eizberg, L. M., Fowler, W. B., Lea, R. M., Shephard, W. D., Shutt, R. P., Thorndike, A. M., and Whittemore, W. L., 1955, *Phys. Rev.*, **97,** 797.

Fermi, E., 1950, *Prog. theor. Phys.*, **5,** 570; 1951, *Phys. Rev.*, **81,** 683.

Fenyves, E., Gombosi, E., and Suranyi, P., 1958, Report of Annual International Conference of High Energy Physics at CERN.

Johnson, W. R., 1955, *Phys. Rev.*, **99,** 1049.

Kamal, A., 1957, Thesis, University of Bristol.

King, D. T., 1958, *Phys. Rev.*, **109,** 1344.

Kraushaar, W. L., and Marks, L. J., 1954, *Phys. Rev.*, **93,** 326.

Landau, L. D., 1953, *Dokl. Akad. Nauk. S.S.S.R.* **12,** 51.

Lewis, H. H., Oppenheimer, J. R., and Wouthuysen S. A., 1948, *Phys. Rev.*, **73,** 127.

Maenchen, G., Powell, W. M. Saphir, G., and Wright, R. W., 1955, *Phys. Rev.*, **99,** 1619.

Maenchen, G., Fowler, W. B., Powell, W. M., and Wright, R. W., 1957, *Phys. Rev.*, **108,** 850.

Shapiro, M., and Stiller, B., 1952, *Phys. Rev.*, **87,** 682.

Sternheimer, R. M., and Lindenbaum, S. J., 1958, *Phys. Rev.*, **109,** 1723.

Walker, W. D., 1957, *Phys. Rev.*, **108,** 872.

Magnetic Moments and Electron Transfer in Nickel-rich Binary Alloys†

By J. Crangle and M. J. C. Martin‡
Physics Department, The University, Sheffield 10

[Received May 8, 1959]

Abstract

New measurements of the ferromagnetic saturation magnetization of nickel-rich binary alloys containing dissolved Al, Si, Sb or Ge are reported, and previous work on NiZn and NiSn alloys is re-assessed. It is shown that electrons are transferred from the solute atoms to the 3d band of nickel at rates lower than the maximum available valencies in every case.

§ 1. Introduction

Several elements in the central groups of the periodic table form substitutional alloys with the transition elements, and it is generally supposed that they can often act as donors of electrons to the structure, becoming ionized themselves.

In the case of alloys with nickel, the variation of the magnetic moment of the alloy with composition indicates directly the extent of the electron transfer to the vacant electron states responsible for the ferromagnetism. Previously, Sadron (1932) and Marian (1937) measured the magnetic moments of binary nickel alloys containing *inter alia* Al, Si, Zn, Sn and Sb. The basis of a collective electron model on which the observations could be explained was given by Stoner (1933) and Mott (1935). Approximate agreement was found in many cases between the number of loosely bound electrons ('valence' electrons) outside the inner closed shells in the atoms of the solute element, and the initial rate of decrease of magnetic moment with composition. It was implied that the 'valence' electrons were being transferred completely to the electron levels associated with the nickel atoms.

The present work was undertaken with a view to providing a check on the reliability of the previous measurements, and to extending or improving on the work where necessary; and thus providing more accurate estimates of the amount of the electron transfer.

All the solute elements chosen dissolve in nickel to an appreciable degree, with no changes in the face-centred cubic structure within the ferromagnetic range. Their solubility limits, according to Hansen (1958), are at 10 at% Si, 10% Al, 12% Ge and 8·4% Sb respectively.

---

† Communicated by the Authors.

‡ Now at Mullard Research Laboratories.

§ 2. PREPARATION OF THE ALLOYS

All the alloys except the nickel–aluminium series were prepared by melting the pure constituents in an argon arc furnace. The negative electrode of a direct current arc was a water-cooled tungsten rod, and the positive electrode consisted of the specimen to be melted, which rested on a water-cooled copper base. Experience has shown that significant contamination of alloys by either tungsten or copper when they are made in this way is rare. In every case alloys were inverted and remelted five or six times to ensure complete mixing. Each melt weighed about 15 g.

The nickel–aluminium alloys were made by melting the pure nickel and aluminium together in a high-frequency induction furnace. Recrystallized alumina crucibles of high purity were used, and the melts were allowed to solidify in the crucibles.

Table 1

	At % solute	θ °K	σ_{00}	p (Bohr magnetons/atom)
NiAl	2·66	568	52·0	0·538
	6·40	471	42·8	0·422
	10·57	334	31·2	0·309
	12·01	293	27·5	0·265
NiSi	2·50†	521	46·5	0·482
	6·68	385	34·9	0·354
	10·07	224	22·5	0·224
NiGe	2·36	568	49·1	0·518
	4·93	465	39·6	0·421
	7·40	372	31·3	0·335
NiSb	0·96	609	53·4	0·567
	1·86	559	46·8	0·502
	2·72	519	42·8	0·462

† 2·5 at % NiSi alloy contaminated with about 0·3 at % of tungsten.

All the alloys were heated *in vacuo* at about 1100°C for rather longer than three days, in order to ensure homogeneity.

All alloys were analysed for their solute content, and for the presence of significant impurities. Their compositions are included in table 1. Only one alloy contained more than a spectroscopic trace of any impurity. This was that with 2·50% of silicon, which contained about 0·3 at % of tungsten. The contamination probably arose during arc melting. Points measured for this alloy were neglected in constructing the appropriate graphs.

§ 3. MAGNETIC TECHNIQUES

All the magnetization measurements were made using a Sucksmith ring balance (Sucksmith 1939). They were made relative to measurements at room temperature on pure Johnson-Matthey nickel, for which the absolute data of Weiss and Forrer (1926) were assumed to apply. Magnetic isothermals were obtained for a range of ten applied fields between 4·3 and 16·4 kilo-oersteds, at temperatures between 23°K and 650°K. For obtaining temperatures above room temperature a small electric furnace was attached to the ring balance. Below room temperature another attachment (Crangle and Martin 1959) was used in conjunction with cooling baths of liquid hydrogen or liquid nitrogen to obtain the steady temperatures necessary to measure the isothermals.

Fig. 1

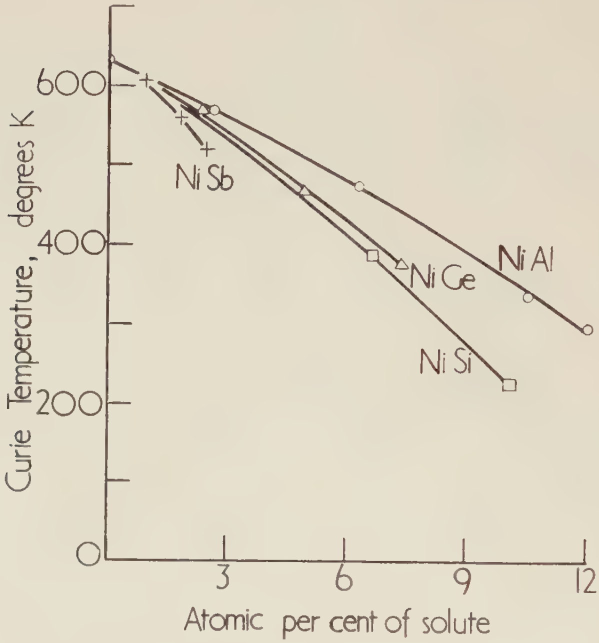

Measured Curie temperatures plotted as a function of alloy composition.

A 'Pallador' thermocouple (PdAu against PtIr) placed in good thermal contact with the specimen was used to measure temperature, giving an adequate sensitivity over the whole range.

To estimate the spontaneous (or domain) magnetization σ_{0T} at each temperature, the established extrapolation techniques were employed (for details see, for example, Crangle, 1955). These were:

(*a*) at the lower temperatures, by extrapolation of the linear parts of the isothermals to zero field, and (*b*) by the construction of sets of curves of constant magnetization and extrapolating these to zero field, at temperatures near the respective Curie points where the isothermals are curved.

Values of the spontaneous magnetization σ_{00} at zero temperature were obtained by extrapolation of the straight parts of graphs of σ_{0T} against T^2. Curie points θ were found by plotting $\sigma_{0T}{}^2$ against T and extrapolating the part with steepest slope to the temperature axis. Bohr magneton numbers were obtained from the values of σ_{00}, taking the magnetic moment of one Bohr magneton to be 5586 c.g.s. units per gram molecule.

The respective Curie points are plotted against alloy composition in fig. 1. That all the alloys examined were within their ranges of solid solution is confirmed by the graphs showing no discontinuities which would characterize a phase boundary or the existence of a superlattice. It is tentatively suggested on this evidence that the solubility of aluminium in nickel is somewhat greater than the value of 10% indicated by Hansen (1958), and tends to agree rather with Marian (1937). In each case the lines in fig. 1 extrapolate towards 0°K at percentages approximately equal to those at which the appropriate magnetic moments given in fig. 2 become zero.

§ 4. RESULTS AND DISCUSSION

Bohr magneton numbers p are plotted against composition for the various systems in fig. 2. Where appropriate, the old measurements of Marian and Sadron are also shown. The reduced scatter of the present experimental points does substantially reduce the uncertainty in the estimation of the initial slopes of the lines. The previous measurements on NiSn and NiZn alloys, where there is little scatter, are included as well. Values of the initial slopes dp/dc are given in table 2.

The measurements provide evidence on the transfer of electrons from the atoms of the various solute elements to the electron levels in nickel which are responsible for the ferromagnetic moment.

We assume that in pure nickel the number of unoccupied 3d states per atom is n_0, all being of the same spin. In an alloy containing a fractional amount c of a solute element, each solute atom is supposed to provide q electrons for transfer to the empty 3d states in nickel. The number of unoccupied states in the alloy is then

$$n_c = n_0(1-c) - c\,.\,q.$$

Now the experimentally observed magneton number p is related to n by

$$p = \tfrac{1}{2}gn,$$

where g is the spectroscopic splitting factor.

Resonance measurements by Standley and Reich (1955) have shown that in the nickel–aluminium and nickel–antimony systems, and also in the related nickel–copper system, g is effectively independent of composition, at least over the range of c considered here. In the absence of any information on the other systems, it is assumed that they behave likewise.

Thus $$p=\tfrac{1}{2}g[n_0(1-c)-c\,.\,q],$$

or $$dp/dc=-\tfrac{1}{2}g(n_0+q).$$

That is $$-q=2/g\,dp/dc+n_0.$$

Fig. 2

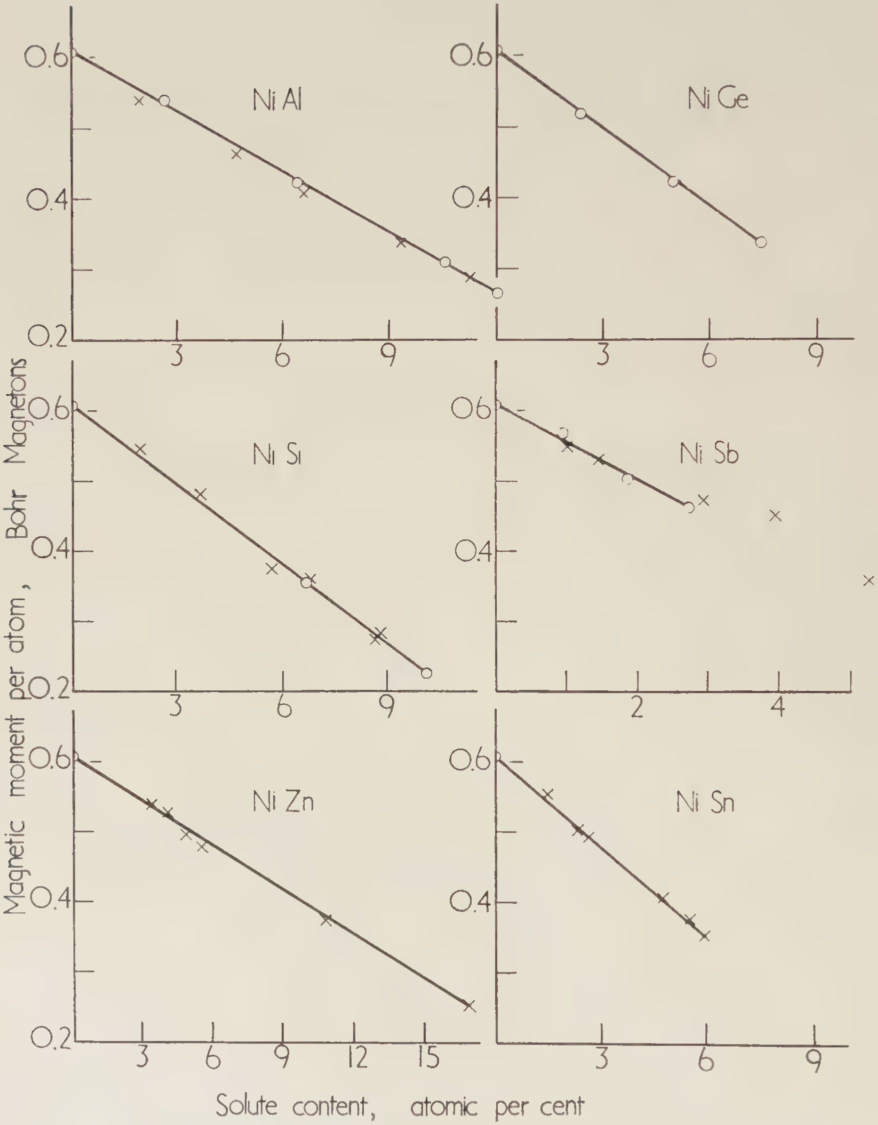

Magnetic moments plotted against alloy composition. The circles indicate present measurements and the crosses the previous work by Marian and Sadron.

There seems to be good evidence that the value of the number of unoccupied 3d states in pure nickel (n_0) is rather less than the value of 0·61. The value of g for nickel has been measured independently by Meyer (1952), by Standley and Reich (1955) and by Bagguley (1955). All the measurements are within the range $g = 2{\cdot}20 \pm 0{\cdot}03$. If we accept the value of $p = 0{\cdot}606$ for nickel (Stoner 1934), n_0 becomes 0·55.

Table 2

Solute element	Valency	dp/dc	q	δ
Cu	1	1·14	0·48 ± 0·02	0·5
Zn	2	2·11	1·37 ± 0·05	0·6
Al	3	2·80	1·99 ± 0·04	1·0
Si	4	3·77	2·87 ± 0·05	1·1
Ge	4	3·70	2·81 ± 0·05	1·2
Sn	4	4·22	3·29 ± 0·06	0·7
Sb	5	5·31	4·27 ± 0·12	0·7

Values of q for the various systems, estimated on the basis of $n_0 = 0{\cdot}55$ and $g = 2{\cdot}20$, are given in table 2. In addition the earlier measurements on nickel–zinc and nickel–tin alloys have been treated similarly, and are included as well as the data for nickel–copper alloys given by Ahern *et al.* (1958). The probable errors quoted are estimated on the basis of the observed scatter in fig. 2, and an error of ± 0·03 in the value taken for g.

It is clear that in none of these cases does the solute element give up all its outer electrons to the unoccupied states in the magnetic electron levels in the nickel.

Subtraction of the respective q values for the available number of electrons outside inner closed shells for the various elements gives the differences δ given in the last column of table 2. These are the number of 'valence' electrons in the solute for which no magnetic effect is observed. They are presumably either transferred to non-magnetic conduction levels in the alloy, or remain bound to the solute atoms. The present work gives no evidence on what happens to these electrons. However, it would be very surprising if the added elements were each only ionized to the extent of the number q of electrons transferred to the nickel 3d band.

In the cases of Cu, Sb, Zn and Sn, δ is quite close to the number of 4s electrons per atom in pure nickel. It thus seems likely that in these elements their remaining valence electrons are being transferred to the 4s level, which thus maintains a constant population. But for Al, Si and Ge, δ seems significantly greater than the 4s electron density. In the absence of any obvious reason for an increase in conduction electron population when these particular elements are alloyed with nickel, it is tentatively suggested that Al, Si and Ge are retaining an average of about 0·5 electrons per atom in bound states.

Acknowledgment

The authors are grateful to Professor W. Sucksmith for his interest and advice during the course of this work.

References

Ahern, S. A., Martin, M. J. C., and Sucksmith, W., 1958, *Proc. roy. Soc.* A, **248,** 145.
Bagguley, C. F., 1955, *Proc. roy. Soc.* A, **221,** 549.
Crangle, J., 1955, *Phil. Mag.*, **46,** 499.
Crangle, J., and Martin, M. J. C., 1959, *J. sci. Instrum.*, **36,** 100.
Hansen, M., 1958, *Constitution of Binary Alloys* (New York: McGraw-Hill).
Marian, V., 1937, *Ann. Phys. Paris*, **7,** 459.
Meyer, A. J. P., 1952, *C. R. Acad. Sci., Paris*, **235,** 1382.
Mott, N. F., 1935, *Proc. phys. Soc.*, **47,** 571.
Sadron, C., 1932, *Ann. Phys., Paris*, **17,** 371.
Standley, K. J., and Reich, K. H., 1955, *Proc. phys. Soc. Lond.*, **68,** 713.
Stoner, E. C., 1933, *Phil. Mag.*, **15,** 1018; 1934, *Magnetism and Matter* (London: Methuen).
Sucksmith, W., 1939, *Proc. roy. Soc.* A, **170,** 551.
Weiss, P., and Forrer, R., 1926, *Ann. Phys., Paris*, **5,** 153.

The Multiple Scattering of Particles of Opposite Charge†

By I. S. Hughes and D. Sinclair‡
Department of Natural Philosophy, University of Glasgow

[Received May 20, 1959]

Abstract

Earlier investigations by a number of workers have revealed an apparent difference in the multiple scattering of positively and negatively charged particles which is much greater than that predicted by theory. Experiments have been carried out in which the existence of such a difference was investigated for the multiple scattering of positive and negative μ mesons, π mesons and electrons in nuclear emulsions. No significant difference was found.

§ 1. Introduction

Several experiments in which measurements have been made of the multiple scattering of electrons and positrons of the same momentum have shown a difference in the magnitude of the scattering of particles of opposite charge which is much greater than that predicted by theory (Corson 1951, Groetzinger *et al.* 1952, Bosley and Hughes 1955, Heymann and Williams 1956). In all of these experiments the scattering of the positrons has been reported to be less than that of the electrons. Cusack and Stott (1955), on the other hand, find no difference in the scattering of 0·4 Mev electrons and positrons in nitrogen although their measurements are not sufficiently accurate to exclude a difference compatible with that observed by the other workers, Henderson and Scott (1957), also using electrons and positrons of 0·4 Mev, find only differences in agreement with the calculated values of Mohr (1954).

In an attempt to resolve this problem a series of experiments was undertaken in this laboratory to investigate the multiple scattering of positively and negatively charged particles in nuclear emulsions. These experiments were specifically designed to detect *differences* in the scattering, and particular precautions were taken to avoid all possible spurious differences, whereas in certain of the earlier experiments the examination of such differences was a secondary objective of the work.

§ 2. Exposures and Measurements

2.1. π^+ and π^- Mesons

π^+ and π^- mesons were produced by placing a target in the γ-ray beam of the Glasgow 300 Mev electron synchrotron and were allowed to pass into G5 nuclear emulsions. The mesons which stopped in the emulsion were identified by their endings. Those tracks having endings such that the charge of the meson could be unambiguously established were selected for measurement provided that they had a track length greater than 1300 μ in the emulsion. Measurements of the multiple scattering of the selected tracks were made by the method of Fowler (1950). The measurements were on a 1000 μ section of each track starting 300 μ from the ending. The average value of $p\beta$ thus selected was 10·5 MeV/c.

---

† Communicated by the Authors.
‡ Now at Department of Physics, University of Michigan, U.S.A.

2.2. μ^+ *and* μ^- *Mesons*

Magnetically separated beams of μ^+ and μ^- mesons from the Liverpool cyclotron were stopped in G5 nuclear emulsions. To avoid the inclusion of a contamination of π mesons in the sample only those primaries which decayed to minimum ionizing secondaries were accepted for measurements. Measurements of the multiple scattering of the selected tracks were made in the same way as for the π mesons. The average value of $p\beta$ thus selected was 9·5 MeV/c.

2.3. *Positrons and Electrons*

The collimated γ-ray beam from the Glasgow 300 MeV synchrotron was allowed to strike a target at the centre of a cylindrical vacuum chamber. The target consisted of a rod of graphite 0·05 in. in diameter. The vacuum chamber was placed in a uniform magnetic field of 4·46 kG and positive and negative electrons from pair production in the target were deflected through semicircles of radius 3 in. to enter nuclear emulsions placed symmetrically on a diameter of the vacuum chamber perpendicular to the γ-ray beam. The desired particles entered the nuclear emulsions at angles near grazing incidence with a momentum of 10·2 MeV/c. In order to cancel any possible asymmetries in the arrangement, halfway through the exposure the field was reversed and at the same time the positions of the two emulsions were interchanged. Multiple scattering measurements were made on tracks entering the emulsion surface within a small area near the centre of the plates and satisfying the selection criteria in angle, dip and length. The method of measurement was the same as that used for π and μ mesons. As previously, the measurements for all particles of both signs were made by a single observer using the same microscope. When allowance was made for energy loss in the emulsion the mean momentum for the electrons and positrons was 9·66 MeV/c.

§ 3. RESULTS

Values of the scattering constant K for the emulsion were calculated from the relation

$$K = \langle\phi\rangle_{\text{chord}} \frac{p\beta c}{Z}\left(\frac{100}{t}\right)^{1/2}$$

where, in the usual notation, $\langle\phi\rangle_{\text{chord}}$ is the mean angle of scattering measured by the coordinate method, p and βc are the momentum and velocity of the scattered particle, Z is the ratio of its charge to that of the electron, and t is the cell size in microns. Small corrections to the values of K thus obtained were made to eliminate the effects of reading and microscope 'noise', ($\sim$1·5%), and inclination of the tracks to the coordinate axes, ($\sim$3%). These corrections were identical for particles of both signs.

The values of K for particles of positive and negative charge and for three cell sizes are shown in the table. 'Cut' values K_c, of the scattering constant are also given, these values having been obtained by omitting angles greater than four times the median value.

Cell size	K					
	π		μ		Electrons	
	+	−	+	−	+	−
50 μ	25·1 ± 0·6	25·5 ± 0·6	25·8 ± 0·6	26·1 ± 0·6	27·9 ± 0·4	28·4 ± 0·4
100	24·8 ± 0·9	25·6 ± 0·9	25·8 ± 0·9	26·4 ± 0·9	26·9 ± 0·6	27·6 ± 0·6
200	25·1 ± 1·4	27·2 ± 1·6	24·5 ± 1·4	25·4 ± 1·4	27·2 ± 0·8	26·6 ± 0·8
	K_c					
50 μ	23·5 ± 0·6	23·8 ± 0·6	24·5 ± 0·6	24·4 ± 0·6	26·1 ± 0·4	26·0 ± 0·4
100	23·6 ± 0·9	24·2 ± 0·9	24·4 ± 0·9	24·4 ± 0·9	25·3 ± 0·6	25·8 ± 0·6
200	24·2 ± 1·4	25·6 ± 1·5	23·5 ± 1·4	24·4 ± 1·4	25·2 ± 0·8	25·9 ± 0·8

The errors shown are all standard deviations.

It is clear from the table that no significant difference has been found between the scattering of particles of opposite charge, in agreement with the theoretical predictions of Mohr (loc. cit.), of a difference of less than 1%, for the circumstances of the present experiment, and in contradiction with the results of the earlier experiments. Differences in the relative values of the scattering constants for π mesons, μ mesons and electrons are not significant. Although particles of the same mass are known to have the same value of $p\beta$ to high accuracy the relative values of $p\beta$ for π mesons, μ mesons and electrons are less precise.

ACKNOWLEDGMENTS

The authors wish to express their gratitude to Dr. H. Muirhead for helpful discussions during the course of this work. We are also grateful to Professor H. W. B. Skinner for providing the facilities of the Liverpool cyclotron, to Mr. B. Halliday and the crew of that accelerator, and to Dr. W. McFarlane and the crew of the Glasgow synchrotron.

We are indebted to the Department of Scientific and Industrial Research for the receipt of a fellowship (I.S.H.) and a studentship (D.S.), during the course of this work.

References

Bosley, W., and Hughes, I. S., 1955, *Phil. Mag.*, **46,** 1281.
Corson, D. R., 1951, *Phys. Rev.*, **84,** 605.
Cusack, N., and Stott, P., 1955, *Phil. Mag.*, **46,** 632.
Fowler, P. H., 1950, *Phil. Mag.*, **41,** 169.
Groetzinger, G., Humphrey, W., and Ribe, F. L., 1952, *Phys. Rev.*, **85,** 78.
Heymann, F. F., and Williams, W. F., 1956, *Phil. Mag.*, **1,** 212.
Henderson, C., and Scott, A., 1957, *Proc. phys. Soc. Lond.*, A, **70,** 188.
Mohr, C. B. O., 1954, *Proc. phys. Soc. Lond.*, A, **67,** 730.

A Study of Growth Defects in Face-centred Cubic Metal Foils Prepared by Evaporation†

By J. W. MATTHEWS
University of the Witwatersrand, Johannesburg

[Received August 31, 1959]

ABSTRACT

Single crystal foils of copper, silver and gold were prepared by evaporation of the metal onto the cleavage face of a hot rock salt crystal. Examination of the foils in a transmission electron microscope showed the presence of dislocations and stacking faults. Many of the stacking faults had part of their area on one {111} plane and the remainder on another. A number of defects which involved three faulted planes were also observed. In addition, the foils contained dislocation loops and tetrahedral stacking faults similar to those discovered recently in quenched metals.

The formation of defects during film growth has been considered. Stacking faults result from the coalescence of 'out of phase' metal nuclei. Experimental evidence for this is presented.

§ 1. INTRODUCTION

WHELAN *et al.* (1957) have demonstrated that direct observation of total dislocations, partial dislocations, and stacking faults can be made with the transmission electron microscope. Their specimens were stainless steel foils prepared by electropolishing sheets of the metal until small holes appeared. The foil near the holes was of thickness suitable for electron microscopy. The advantage of this preparation technique over most others is that the specimen is a sample of the bulk material.

The image contrast arising from stacking faults in the specimen has been discussed by Whelan and Hirsch (1957 a, b) and Hirsch *et al.* (1956) have given a qualitative discussion of electron scattering by the strained crystal around a dislocation line. Whelan (1959) has emphasized that not all dislocations may be visible. The three factors on which he considers their visibility to depend are (*a*) the Burgers vector, (*b*) the degree of dissociation into partial dislocations and (*c*) the orientation of the specimen with respect to the incident electron beam.

The work reported here is an application of the techniques of Whelan *et al.* to the study of growth defects in evaporated films of gold, silver and copper which are all face-centred cubic metals of low stacking fault energy. This is closely related to an investigation carried out recently by Pashley (1959), but our results do not overlap greatly. Section 3 is a description of the defects found, and a discussion of their mode of formation is given in § 4.

---

† Communicated by Professor F. R. N. Nabarro.

§ 2. Experimental Details

Foils were prepared by evaporation of the metal off a tungsten filament onto the cube face of a hot, freshly cleaved, rock salt crystal. The gas pressure in the evaporation chamber was less than 0·1 microns of mercury. The substrate temperatures used for gold, silver and copper foils were 450, 300 and 450°c respectively. The foils were removed from the salt crystal by lowering it, coated surface upward, into water. The metal floated off on the water surface and was caught on copper specimen grids.

Single crystal foils with the (001) plane parallel to the surface were obtained if the rate of metal deposition was greater than 100 Å per second. Slow evaporation gave polycrystalline foils with a preferred (001) orientation. The thickness of most foils was between 400 and 1000 Å, but a few gold foils with an average thickness of less than 100 Å have also been prepared. These were backed with carbon to prevent them from collapsing when placed on the specimen carriers and were used to study the formation of the growth faults.

Specimens were examined in a Siemens and Halske (Elmiskop I) electron microscope at magnifications of from 20 000 to 80 000 times. Electron accelerating voltages of 80 and 100 kv were used and the aperture, α, of the objective lens was 10^{-2} radians. Foils were mounted in the stereo-holder, as a small tilt of the specimen often produced an improvement in the appearance and contrast of dislocations and stacking faults.

§ 3. Description of Defects Observed in the Foils

Figures 1 to 11† are electron micrographs of the foils ; figs. 1 to 7 are of silver foil ; fig. 8 is of copper, and the remainder are of gold. Most of the examples of the defects described are in figs. 1 to 7. This is because almost all the experimental work has been carried out on silver. The majority of the defects are common to the three metals.

Complete dislocations are visible at A and A′ in figs. 1 and 2. It is interesting that some of the dislocation lines, particularly those at A′, do not take the shortest route from the top of the foil to the bottom but lie approximately along $\langle 110\rangle$ directions. Pure screw dislocations would have their lines parallel to these directions and one is tempted to say that the A′ dislocations are of screw type and that their energy would increase if they decreased their length and became partly of edge type in the process. It appears, however, that dislocations will often be formed in evaporated foils with their lines along a $\langle 110\rangle$ direction which need not be parallel to their Burgers vector. They would probably remain in this orientation after growth is complete as dislocations in evaporated foils are rather immobile. Pashley (1957) has shown that it is possible to strain evaporated gold foils elastically by 0·7%. This elastic strain is far greater than that observed in bulk specimens.

---

† Figures 1 to 11 are plates.

The density of dislocations varied from one silver foil to the other but was usually between 1×10^{10} and 3×10^{10} per cm². The density in copper and gold was approximately the same as that in silver.

The sets of parallel interference fringes in the micrographs result from stacking faults in the foil. The faults extend from one surface of the foil to the other and lie on any of the four $\{111\}$ planes. These planes all make an angle of 54° 44′ with the foil surface. The plane of the foil has been labelled (001), so that the (111) and $(\bar{1}11)$ planes intersect the surface along [110] while the $(1\bar{1}1)$ and $(\bar{1}11)$ planes intersect it along [110]. We have not been able to determine which of the fault boundaries is in the upper surface of the foil, so that the stacking fault at B in fig. 2, for example, is either on the $(1\bar{1}\bar{1})$ or on the $(\bar{1}1\bar{1})$ plane.

Many stacking faults in the foils had part of their area on one plane and the remainder on another non-parallel plane. Bent stacking faults of this type have been discussed by a number of authors (Cottrell 1952, Thompson 1953, Frank and Nicholas 1953, Friedel 1955, Whelan 1959), and Whelan (1959) has recently observed them in stainless steel using the electron microscope. The bend itself contains an imperfect dislocation which Thompson, following a suggestion by Nabarro, has called the ‘ stair rod ’. The Burgers vector of the stable stair-rod dislocations have been listed by Frank and Nicholas (1953).

Two types of bent stacking fault are distinguishable in the micrographs ; examples of them are shown in figs. 3 and 4. In fig. 3 the angle between the faulted planes is acute (70° 32′) and in fig. 4 it is obtuse (180°–70° 32′). Line drawings of the two types have been made (figs. 12 and 13). The convention used is as follows. The intersections of the stacking fault with the upper and lower surfaces of the foil are indicated by thick full and thick dotted lines respectively. Fine full lines represent the electron interference fringes caused by the fault and the fine dotted lines are imperfect dislocations.

Bent stacking faults in which the stair-rod dislocations are parallel to one of the two $\langle 110 \rangle$ directions in the plane of the foil have been observed. They are often difficult to identify with certainty. Possible examples are present at positions C and C′ in figs. 1 and 2. Stair rods parallel to the foil surface occurred with about one-hundredth the frequency of those inclined at 45° to the surface. The total stair-rod dislocation density in silver foils was about 3×10^{8} per cm² ; the density in copper and gold was somewhat lower. Bent stacking faults with an obtuse angle between the faulted planes outnumbered the acute angled variety by about 20% in all the foils examined.

More than half the stair rods were found in stacking faults that contained two or more bends. Line drawings of six of these faults with

Fig. 12

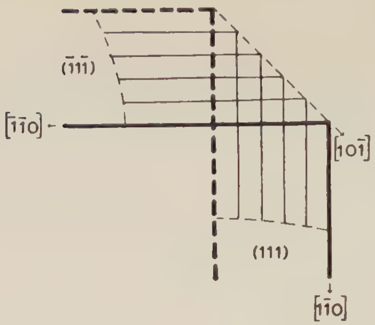

Fig. 13

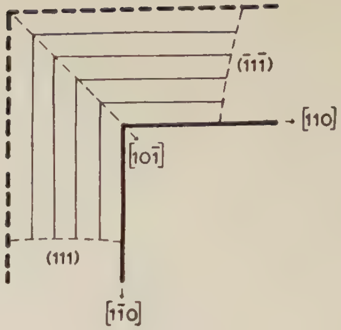

Fig. 14

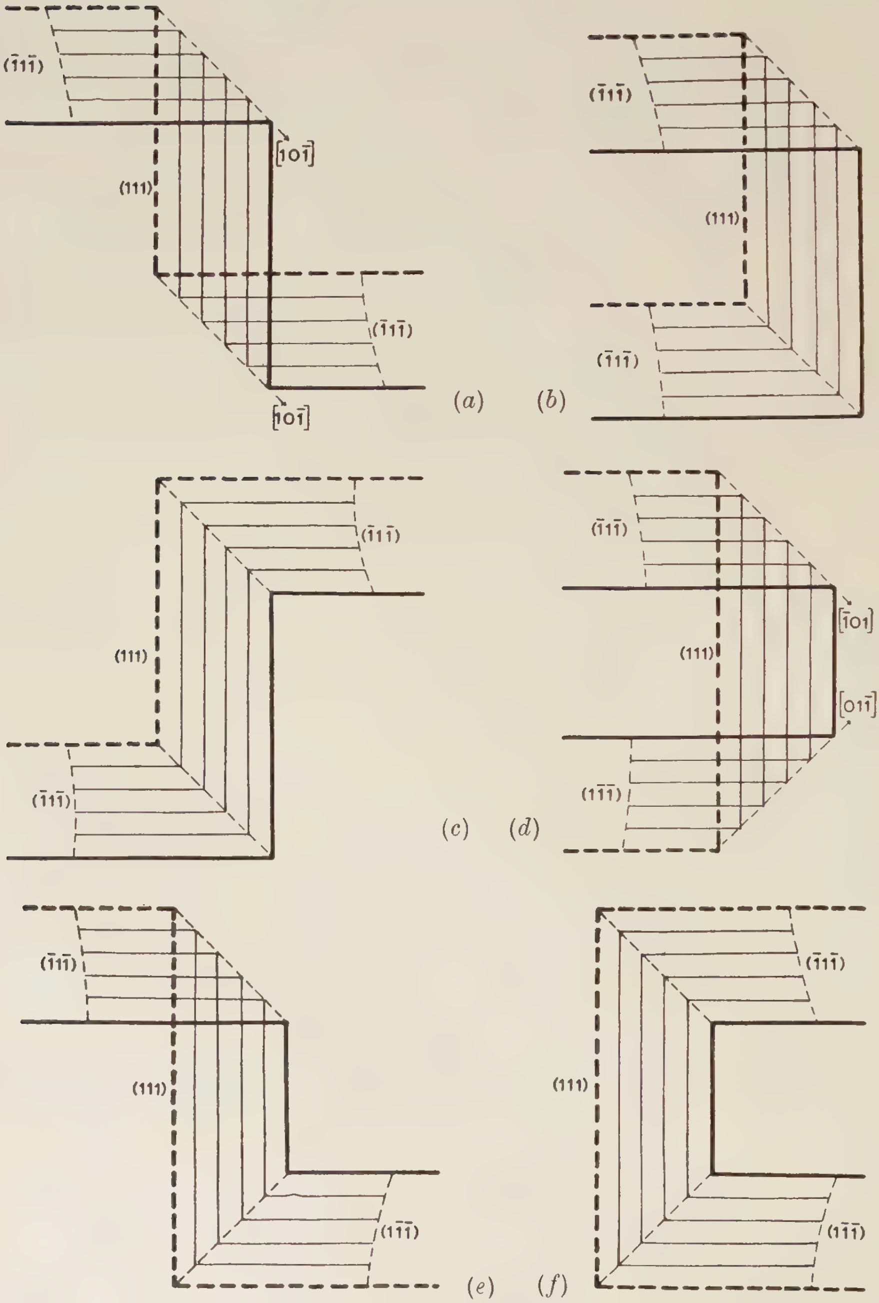

(*a*) (*b*)

(*c*) (*d*)

(*e*) (*f*)

two bends have been made (fig. 14) and examples of each of them have been found in the foils. Their positions in the micrographs are indicated in table 1.

Table 1

Defect	Position of defect in the micrographs
14 (*a*)	Fig. 1D
(*b*)	Fig. 1E, fig. 2E
(*c*)	Fig. 2F
(*d*)	Fig. 1G, fig. 2G
(*e*)	Fig. 1N, fig. 5
(*f*)	Fig. 2H, fig. 9

The first three defects (14 (*a*), (*b*) and (*c*)) have two parallel stair rods and involve two sets of non-parallel planes. Each of the three defects can occur in 16 ways, of which eight are distinguishable in the micrographs. (The cases in which the stair rods are parallel to the foil surface have been ignored.) The stair rods in 14 (*d*), (*e*) and (*f*) are inclined at 60° to one another so that the three faulted planes are non-parallel. Each of these defects can occur in eight ways, of which four are distinguishable in the micrographs. (Again, defects which have a stair rod parallel to the foil have not been considered.)

Fig. 15

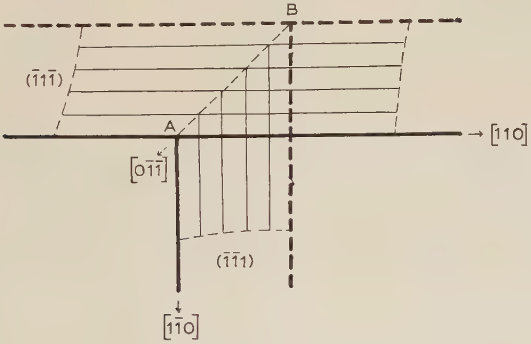

A few two-bend stacking faults in which the stair rods were inclined at 120° to one another were found. If there is a stair rod at C′ in fig. 2 then those at C″ are inclined at 120° to it.

Figure 15 shows a defect which was frequently observed in the foils. Examples of it are seen at positions labelled J in figs. 1 and 2. It is possible for the line of intersection of the three stacking faults to be parallel to the plane of the foil. Identification of the defect in this orientation would however be difficult, and no convincing example of this case has been found. The stable Burgers vectors of the dislocation along the line AB in fig. 15 have been listed by Frank and Nicholas (1953).

Another common growth defect is shown in fig. 16. Examples of it are present at K in figs. 1 and 2. A special case of it in which AB and CD are in the same straight line may easily be confused with the imperfection in fig. 17. The defect at L in fig. 1, for example, may be interpreted in two ways. A dislocation node with geometry similar to that of the defect in fig. 17 has been discussed by Thompson (1953).

Fig. 16

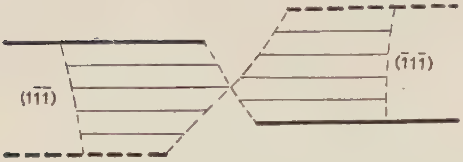

Fig. 17

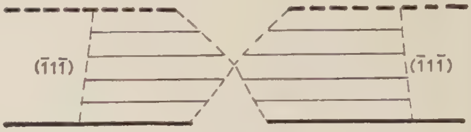

Fig. 18

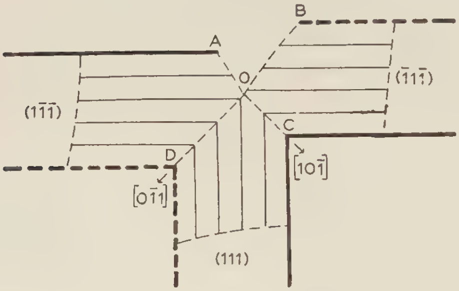

Fig. 19

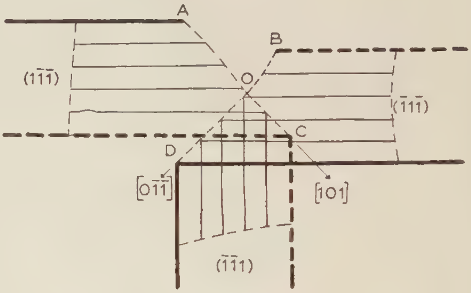

An interesting growth defect is present in fig. 6 and at P in fig. 2. It should probably be interpreted as in fig. 18. At the point O is a four-fold imperfect dislocation node which consists of two stair-rod dislocations (OC and OD), and two partial dislocations (OA and OB) which are either sessile or glissile (Frank and Nicholas 1953). The angles between the faulted planes joined along OC and OD are obtuse. The defect in which these angles are acute is drawn in fig. 19, but no examples of this case were seen in the foils. Its rarity is, however, expected from the growth mechanism given in § 4. Defects similar to those in figs. 18 and 19 have been discussed by Thompson (1953).

Another four-fold imperfect dislocation node which is expected to be fairly common in the foils is shown in fig. 20. It is made up of two stair rods (OA and OC), a dislocation similar to that along AB in fig. 15 (OD), and one partial dislocation (OB). The angle between the faulted planes that meet along the stair rods is obtuse.

A search for this defect in the foils has given disappointing results. The best example that has been found is seen in fig. 7. The node is either in the foil surface or very near to it. The defect in which the faulted planes joined along AC are separated by an acute angle (fig. 21) has not been found in the foils but its rarity is not unexpected.

The evaporated foils contained tetrahedral stacking faults and dislocation loops similar to those discovered recently (Hirsch *et al.* 1958; Hirsch and Silcox 1958) in quenched metals. Tetrahedral stacking faults appear as small squares with sides parallel to the (100) and (010) directions when observed along the normal to the foil plane. Examples of them in silver foil are seen at M in fig. 1. These are approximately the same size as those found by Hirsch and Silcox in quenched gold. Their average size and number per unit volume in the silver foils was, however, difficult to determine. This was due to numerous small spots of ill-defined shape which were present in the micrographs and which may or may not have been tetrahedra of stacking fault. No dislocation loops were observed in the silver foils but some defects whose interpretation is in doubt have been found (see A in fig. 6).

Fig. 20

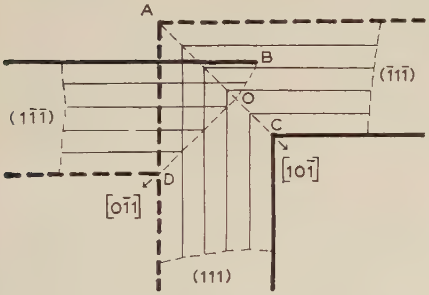

Fig. 21

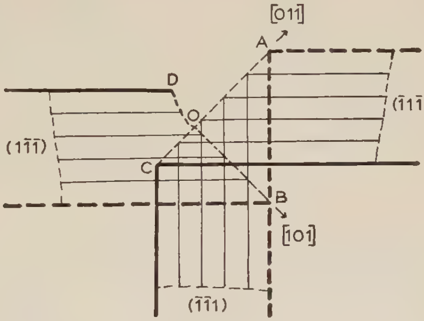

Small spots were present in the micrographs of gold foil but so far no defect whose appearance corresponds closely with that of a tetrahedral stacking fault or a dislocation loop has been found. Dislocation loops in evaporated gold foils have, however, been observed by Pashley (1959). The surfaces of the foils in which loops were found were parallel to the (111) plane.

Dislocation loops similar to those observed by Hirsch and Silcox (1958) in quenched copper were present in the evaporated copper foils. An example is seen at A in fig. 8. No tetrahedral stacking faults were found in the copper foils.

§ 4. Formation of Growth Defects

Many metal nuclei are formed on the salt in the early stages of film growth. The majority of these nuclei are epitaxially aligned on the substrate. Figure 10 is a micrograph of a thin deposit of gold which confirms these statements. One cannot, however, regard a deposit of metal, composed of separate nuclei, as a single crystal which is perfect if its vacant lattice sites are neglected. This is because the lattice of one nucleus may be displaced from that of another by a non-integral number of lattice spacings. This results from the misfit between the lattices of the metal and of the substrate and means that when two nuclei meet they will not always do so in perfect register.

The nuclei would be expected to grow with facets that coincide with low index crystal planes. An examination of thin (± 70 Å) deposits of gold in the electron microscope has shown that this is in fact so. The facets are parallel to the {111}, {110} and {001} planes. It is possible to deduce this from a single observation of nuclei containing stacking faults. This is illustrated in fig. 22.

Fig. 22

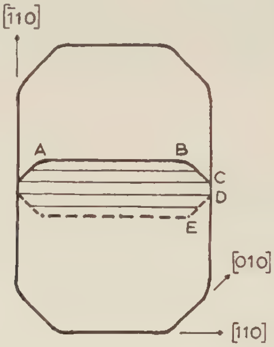

If there is a straight upper boundary, AB, to the stacking fault, then the (001) plane is a growth face. Also, if the stacking fault has boundaries like BC and DE which are at right angles to one another and at 45° to AB then the nucleus has (111) and $(\bar{1}11)$ facets. The presence of a boundary CD indicates that the nucleus has a (110) face as well. A nucleus which has an (001) facet and {111} facets is seen in fig. 11.

When two nuclei grow together the joint plane will probably be a {111}, a {110} or a {100} plane. If they meet on a {110} or a {100} plane then no stacking fault can form between them although the nuclei may have to strain slightly to get into perfect register. It is, however, possible for a stacking fault to form between nuclei that join on a {111} plane.

It is important to notice that nuclei can only meet on {111} planes when they are of different height. This is illustrated in fig. 23. If a stacking fault is formed between nuclei A and B in fig. 23 it will be on the {111} plane. If B were larger than A the faulted plane would be $\{\bar{1}\bar{1}1\}$.

Both intrinsic and extrinsic stacking faults can result from the coalescence of two nuclei. Consider a pair of growing nuclei which are separated from one another by a single {111} plane of vacancies. Three possible configurations are shown in fig. 24. Full lines are {111} planes seen from the side and the dotted line is the plane of vacancies.

Adjacent planes cannot have the same letter, so the bracketed letters give the only ways in which the vacant plane can be filled. The sequences of planes when growth is complete are as follows :

(i)	(ii)	(iii)
a b c b a b c Δ Δ ∇ ∇ Δ Δ	b c a b a b c Δ Δ Δ ∇ Δ Δ b c a c a b c Δ Δ ∇ Δ Δ Δ	c a b c a b c Δ Δ Δ Δ Δ Δ

The Δ and ∇ convention is due to Frank (1951). The successions a to b, b to c and c to a are indicated by Δ and b to a, c to b and a to c by ∇. There is an extrinsic stacking fault in sequence (i) ; both sequences in (ii) contain an intrinsic stacking fault ; (iii) is an unfaulted sequence.

Fig. 23

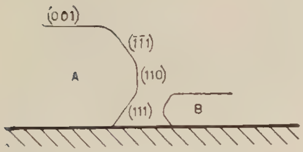

Fig. 24

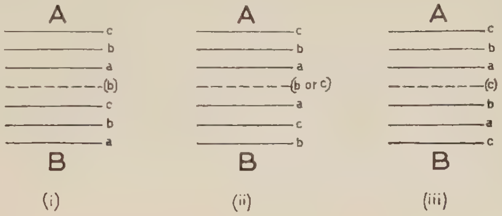

(i) (ii) (iii)

Figure 24 is a little misleading because (i), (ii) and (iii) are special cases. Before nuclei join they can be ‘ out of phase ’ by a quite arbitrary amount. The sequence of planes on either side of the gap between the nuclei may, for example, be somewhere between sequences (ii) and (iii). It is, however, unlikely to be midway between these sequences and there will be a tendency for the planes to go into the sequence to which they approximate most closely. There is also a tendency for them to take up the unfaulted sequence and as a result of this a perfect joint will sometimes be formed when the sequence before coalescence is nearer to (ii) than to (iii). In other words, a perfect joint will be formed more often than one which contains an intrinsic stacking fault. Similarly, if the surface energy of an extrinsic stacking fault is greater than that of the intrinsic variety it will be formed less frequently in the foils.

It is perhaps possible, when two nuclei are in the situation considered above, for the stacking sequence over a portion of the joint plane to differ from that over the remainder. The probability of this is greatly increased if the nuclei concerned are not in exactly parallel orientation. The misalignment necessary is roughly 0·1° and it is probable that nuclei misoriented by this amount do exist. Evidence for the presence of nuclei misaligned by a much greater amount has been obtained. An example is seen at A in fig. 10.

Nuclei may also grow together so that the stacking fault in the joint plane contains a ‘ jog ’. Suppose two nuclei are separated by two empty {111} planes (fig. 25).

Fig. 25

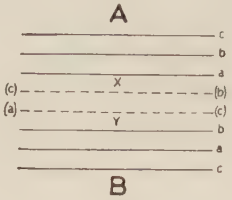

The planes can be filled in the two ways indicated by the letters in brackets. Both the sequences contain extrinsic stacking faults. If the upper nucleus (A) grows downwards towards the lower one (B) then the upper dotted plane will be ‘ c ’ and the lower one ‘ a ’. On the other hand, if the lower plane is the first to be filled it will be ‘ c ’ and the upper one ‘ b ’. If a growth step one atomic layer in thickness advances from the left of A towards XY and a similar step advances from the right of B towards XY then an extrinsic stacking fault jogged at XY will be formed. To the left of XY the sequence will be c a b a c a b c and to the right of XY it will be c a b c b a b c.

Fig. 26

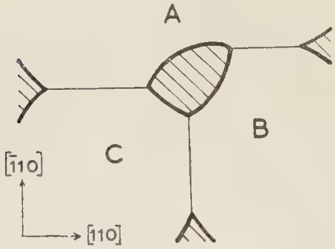

Fig. 27

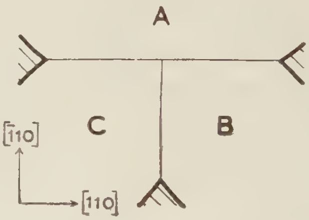

Many of the intersecting stacking faults described in § 3 can result from the coalescence of three nuclei. There are two essentially different ways in which three nuclei may join so that any one nucleus is in contact with the other two (figs. 26 and 27).

In the following discussion AB, BC, and CA represent the joint planes between nuclei A and B, B and C, and C and A. The conditions that need be satisfied for the defect in fig. 18 to result from the joining up of the three nuclei in fig. 26 are (i) AB, BC and CA must all contain stacking faults ; (ii) the height of C along the [001] direction must be greater than that of A and the height of A must be greater than that of B; (iii) each joint plane must intersect with the other two inside the completed foil. Other defects which can result from nuclei joined as in fig. 26 are listed in table 2.

Table 2

Joint planes that contain stacking faults	Relative heights of nuclei	Other conditions which are necessary	Figure in which the defect is illustrated
AB, BC, CA	$C > A > B$	Each joint plane must intersect the other two inside the foil	Fig. 20
AB, CA	$C > A > B$	AB and CA must intersect in the foil	Fig. 16
AB, BC	C and $A > B$	—	Fig. 13
BC, CA	$A > C > B$	—	Fig. 12

It is obvious from table 2 that the conditions required for the formation of a bent stacking fault with an acute angle between the faulted planes are more exacting than those needed for an obtuse angled bent fault. A bent stacking fault of the obtuse type may in fact be formed when only two nuclei join together (see fig. 11). The growth mechanism thus provides an explanation for the higher density of obtuse angled bends.

It is interesting to consider what happens in fig. 26 if none of the joint planes contains stacking faults. A large perfect nucleus may be formed but it is also possible for the hole in the middle to contain one or more complete dislocations. The orientation of the dislocation line (or lines) depends on the relative heights of A, B and C. The line will, for example, be approximately parallel to the [011] direction if $A > B > C$. The Burgers vector of the dislocation need not be parallel to its line. (See the discussion in § 3 of the dislocations at A′ in figs. 1 and 2.)

Bent stacking faults may result from nuclei joining as in fig. 27. However, the interesting defect that may be produced is that in fig. 15. Examples of three nuclei meeting as in fig. 27 to give the defect in fig. 15 are seen at B in fig. 10.

The imperfections drawn in figs. 19 and 21 have not been observed. This is not surprising since rather special conditions are needed for their formation. Firstly, four nuclei meeting as in fig. 28 are required. Secondly, BC, CD and DA must contain stacking faults and each faulted plane must intersect the other two. Thirdly, the height of B must be greater than that of C, the height of C must be greater than that of D, and the height of D must be greater than that of A.

Any of the two-bend stacking faults in fig. 14 may be formed when four nuclei meet in the manner illustrated in fig. 29. If every joint plane in fig. 29 contains a stacking fault an imperfection like the one near O in fig. 1 is obtained.

Fig. 28

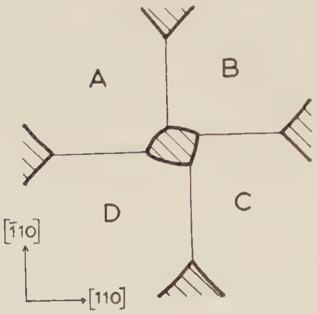

Fig. 29

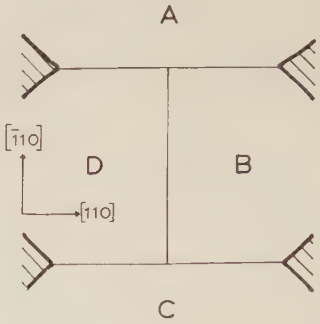

The density of stair-rod dislocations was higher in silver than it was in either copper or gold. This is likely to be due to the substrate temperatures used and not to differences in the physical properties of the metals themselves. Raising the substrate temperature has two effects. The average distance a metal atom diffuses on the salt surface is increased. This leads to an increase in the average size of nuclei and to a decrease in the number per unit area. The number of joint planes is therefore reduced, and this results in a lowering of the stair rod density. The second effect of a higher substrate temperature is that more annealing of the foil takes place after it has formed.

Acknowledgments

The author would like to thank Professor F. C. Frank for suggesting to him that the stacking faults in the foils might result from the joining together of nuclei with {111} facets. The author is also deeply indebted to Professor F. R. N. Nabarro and Dr. D. B. Holt for many helpful discussions and to Mr. J. Siebert who prepared a number of the foils. In addition, the author wishes to thank the University Council Research Committee for financial support.

References

Cottrell, A. H., 1952, *Phil. Mag.*, **43**, 645.
Frank, F. C., 1951, *Phil. Mag.*, **42**, 1014.
Frank, F. C., and Nicholas, J. F., 1953, *Phil. Mag.*, **44**, 1213.
Friedel, J., 1955, *Phil Mag.*, **46**, 1169.
Hirsch, P. B., Horne, R. W., and Whelan, M. J., 1956, *Phil. Mag.*, **1**, 677.
Hirsch, P. B., Silcox, J., Smallman, R. E., and Westmacott, K. H., 1958, *Phil. Mag.*, **3**, 897.

HIRSCH, P. B., and SILCOX, J., 1958, *Proceedings of International Conference on Crystal Growth held at Cooperstown, New York* (New York : John Wiley and Sons).

PASHLEY, D. W., 1957, *Proceedings of the Conference on Electron Microscopy held at Bangor, Wales.* (Summarized by Emerson, H. W., 1958, *Brit. J. appl. Phys.*, **9**, 306) ; 1959, *Phil. Mag.*, **4**, 324.

THOMPSON, N., 1953, *Proc. phys. Soc. Lond.*, B, **66**, 481.

WHELAN, M. J., 1959, *Proc. roy. Soc.* A, **249**, 114.

WHELAN, M. J., and HIRSCH, P. B., 1957 a, *Phil. Mag.*, **2**, 1121 ; 1957 b, *Ibid.*, **2**, 1303.

WHELAN, M. J., HIRSCH, P. B., HORNE, R. W., and BOLLMANN, W., 1957, *Proc. roy. Soc.* A, **240**, 524.

Observation of the Suppression Effect on Bremsstrahlung†

By P. H. Fowler, D. H. Perkins and K. Pinkau
H. H. Wills Physics Laboratory, University of Bristol

[Received May 22, 1959]

Abstract

The distance y between the primary pair of a photon-initiated cascade and its first daughter pair has been measured on 58 electromagnetic showers of energy below 1000 Bev, and on 47 above 1000 Bev. An average value of y of 10 mm was found for the low energy group, in agreement with the predictions of the Bethe–Heitler and Migdal theories. For the high energy cascades the average value for y was 13·5 mm, in agreement with the one predicted by Migdal's calculations, and in disagreement with the value predicted by the Bethe–Heitler theory.

§ 1. Introduction

Landau and Pomerančuk (1953) predicted that the probability of emission of low energy photons by high energy electrons would be reduced by multiple scattering. This effect is expected to be important in dense media, like nuclear emulsion. Later, Migdal (1956, 1957) derived detailed formulae for the cross sections for pair production and radiation as a function of photon and electron energies.

Up to the present date, several attempts have been made to observe such effects in high-energy electromagnetic cascades recorded in nuclear emulsions (Debenedetti *et al.* 1955, 1956. Miesowicz *et al.* 1957. Benisz *et al.* 1958, Varofolmeev *et al.* 1958). In these experiments the aim was to determine the energy spectrum of individual electrons in electromagnetic cascades close to their origins. The authors claim. in accordance with the predictions of Migdal, to have observed a deficiency of low energy electrons. In comparing experimental results of the number and energy of electrons with theory, some authors have carried out Monte Carlo calculations, taking into account the Migdal effect (Varofolmeev *et al.* 1958), while others tried to distinguish between electron pairs of the first and later generations (Benisz *et al.* 1958).

The most thorough investigation carried out so far seems to be that of Varofolmeev *et al.* (1958) who made measurements upon three cascades of 1000 Bev primary energy. These authors made no attempt to distinguish between pairs of different generations, but compared the experimental energy spectrum of electrons with the theoretical one obtained from Monte Carlo calculations. They found that their results lay closer to the curve predicted according to the Migdal theory, than to that of Bethe and Heitler. A number of objections can be raised to their experiment. They are: (*a*) that the accuracy of the energy determination must be high for each event to allow comparison with the theory; (*b*) their conclusions rest largely on a deficiency of about five pairs per cascade over the whole energy range out of a total of about 12. Some of these could easily have been missed in scanning for cascade electrons at a distance of 1·5 radiation lengths; and finally, (*c*) the difference in number of electrons according to the two theories is only comparable with the large inherent fluctuations in the number of electrons at a given small distance from the origin of the cascade.

---

† Communicated by the Authors. A preliminary report on this experiment was given at the Physical Society Conference on Cosmic Rays. Durham. 1958.

§ 2. EXPERIMENTAL TECHNIQUE

In the present experiment, only electromagnetic cascades initiated by single photons were analysed. The showers resulted either from the entry of isolated photons into the emulsion stacks from outside, or from high energy nuclear interactions in the stacks. The stacks employed were sufficiently large so that any fluctuations in the initial stages of the cascade development would have a negligible effect on the probability of detection of the cascade. Following the primary electron-pair from the point of its creation, the distance y between the primary pair and the first daughter pair was measured in each event. In a few cases, only a lower limit to y could be given, owing to confusion with neighbouring tracks or appreciable multiple scattering of one of the electrons.

A rough energy estimate was made of the energy of the primary pair, i.e. that of the initiating photon, E_γ. No great accuracy was necessary since it served only to divide the events into two groups, according to whether their energy was above or below 1000 BEV.

The results of the measurements are shown in fig. 1.

§ 3. COMPARISON WITH THEORY

Let k be the number of photons with $E > 2\,mc^2$ radiated per unit path length by the two electrons of the primary pair, and λ be the conversion length ($= 3{\cdot}75$ cm in emulsion). Over the distances y investigated (~ 1 cm), the electrons lose on average only a small amount of energy, and k, which is approximately proportional to $\ln E$, will remain essentially constant. The probability that no second pair appears within the distance y from the origin of the primary pair is then

$$P(>y) = \exp\left\{-k\lambda\left[\frac{y}{\lambda} - 1 + \exp\left(-\frac{y}{\lambda}\right)\right]\right\}. \quad . \quad . \quad . \quad (1)$$

The conversion length for photons depends on photon energy at low energies decreasing to an asymptotic value of 9/7 radiation lengths above 1 BEV. Combining the Bethe–Heitler energy spectrum of bremsstrahlung photons with the known variation of the conversion cross-section below 1 BEV,

Fig. 1

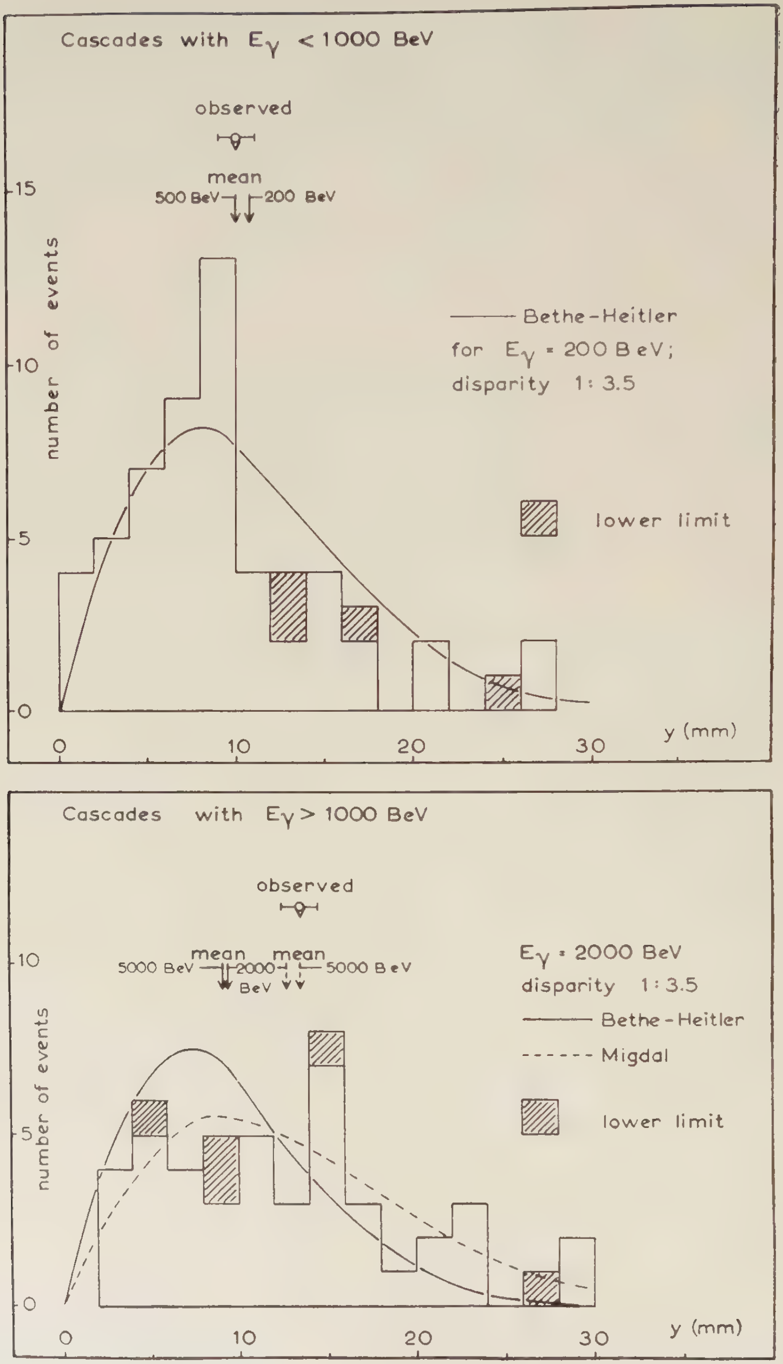

Distribution of y for (a) 58 events with an energy $E_\gamma < 1000$ BeV, and (b) 47 events with $E_\gamma > 1000$ BeV.

The error of one standard deviation is drawn to the observed mean value of y, and theoretical mean values are indicated for a few different primary energies.

it can be shown that the number of pairs converting will be the same as that obtained assuming a constant conversion length, with a sharp cut-off in the photon energy spectrum at 25 Mev. We therefore find that, according to the Bethe–Heitler theory, the effective number of photons k' radiated per radiation length by electrons of energy above 1 Bev is given by

$$k' = \ln\left(\frac{E}{25\ \text{Mev}}\right). \qquad \tag{2}$$

The value of k' according to Migdal's theory is obtained by dividing k' of eqn. (2) by the appropriate value of R taken from fig. 2.

For the application of formulae to this experiment, an average would have to be taken of eqn. (1) over all possible disparities. However, to within an accuracy of a few per cent, it is sufficient to assume a value of k' for the pair of electrons corresponding to the median value of the disparity, viz. 3·5 : 1.

Fig. 2

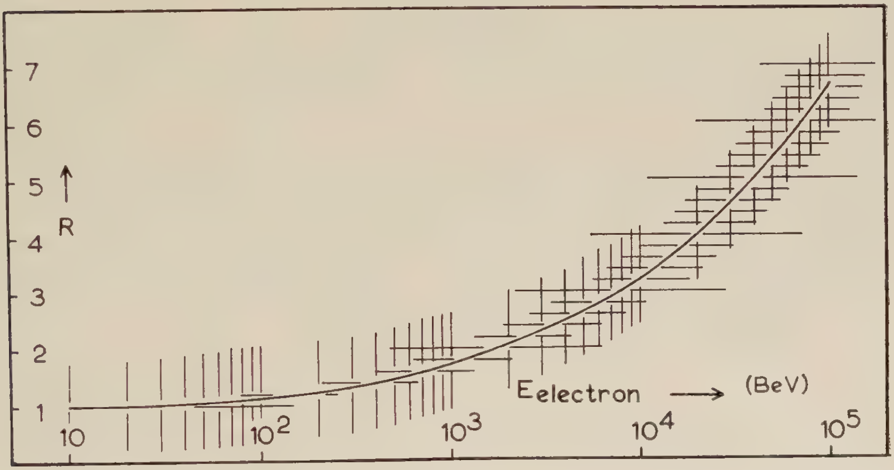

The variation of the quantity R with electron energy; R is the ratio of the number of photons radiated according to the Bethe–Heitler theory, to that calculated according to Migdal.

Comparing the two graphs in fig. 1, one can see that with increasing energy the observed distribution shifts towards larger values a y, rather than shifting in towards the origin, as would be expected from the logarithmic increase in k according to the Bethe–Heitler theory. The observations thus clearly support the theory of Landau, Pomerančuk and Migdal. For a more detailed comparison, the average values of y according to these theories are indicated in fig. 1, together with the observed values. We find good agreement between the observations and theory for cascades with energies below 1000 Bev where there is no great difference between Bethe–Heitler's and Migdal's predictions. For the higher energy cascades, the observed mean is more than three standard deviations away from the mean given by the Bethe–Heitler theory, while agreeing well with that predicted from Migdal.

The detection of the suppression effect does not as such invalidate other calculations in quantum electrodynamics, because it stems from an addition effect which was not considered by Bethe and Heitler. Bell (1958), on the basis of classical arguments, concludes, contrary to the Migdal theory, that the suppression in the number of photons at the low energy end of the spectrum should be compensated by an enhancement at the high energy end, which should lead to the same total energy loss per unit length. If in fact it should be found that the radiation loss of electrons decreases at very high energies, this would have to be ascribed to an essentially quantum mechanical effect. It should be noted that, in the present experiment, we have not shown that electrons become more penetrating particles as their energy increases. What has been demonstrated clearly is that there is a suppression in the total number of photons radiated.

REFERENCES

BELL, J. S., 1958, *Nuclear Phys.*, **8,** 613.
BENISZ, J., CHYLINSKY, S., and WOLTER, W., 1958, Polish Acad. Sci., Rep. No. 39/VI.
DEBENEDETTI, A., GARELLI, C. M., TALLONE, L., VIGONE, M., and WATAGHIN, G., 1955, *Nuovo Cim.*, **2,** 220; 1956, *Ibid.*, **3,** 226.
LANDAU, L., POMERANČUK, I., 1953, *Dokl. Akad. Nauk. S.S.S.R.*, **92,** 535, 735
MIESOWICZ, M., STANISZ, O., and WOLTER, W., 1957, *Nuovo Cim.*, **5,** 513.
MIGDAL, A. B., 1956, *Phys. Rev.*, **103,** 1811; 1957, *JETP*, **32,** 633.
VARFOLMEEV, A. A., GERATSIMOVA, R. I., GUREVICH, I. I., MAKARINA, L. A., ROMANTSEVA, A. S., SVETLOBOV, I. A., and CHUEVA, S. A., 1958, Annual Conference on High Energy Physics, Geneva.

Threshold Effects in High Energy Reactions†

By A. I. BAZ
Atomic Energy Institute, Moscow, USSR

[Received September 14, 1959]

ABSTRACT

The resonances which occur in high energy phenomena are interpreted in terms of threshold states. Tentative conclusions are drawn regarding the parities of some of the elementary particles.

---

§ 1. INTRODUCTION

MANY resonances are known to-day in elementary particle physics. Apart from the famous $(\frac{3}{2}, \frac{3}{2})$ resonance in $\pi + \mathrm{p}$ scattering, there are definite indications of

(*a*) a resonance at $\sim 0{\cdot}9$ BeV in $\pi^- + \mathrm{p}$ scattering;

(*b*) a resonance at very low energies in $\mathrm{K}^- + \mathrm{p}$ scattering;

(*c*) a resonance at $\sim 0{\cdot}95$ BeV in the reaction $\gamma + \mathrm{p} \rightarrow \Lambda + \mathrm{K}^+$.

A common feature of all these resonances is that their positions are very close to some thresholds. Thus, the $\pi^- + \mathrm{p}$ resonance (*a*) is very close to the $\mathrm{K} + \Sigma$ production threshold, the $\mathrm{K}^- + \mathrm{p}$ resonance at around 20 MeV is very close to the $\mathrm{K}^- + \mathrm{p}$ threshold itself, and the $\gamma + \mathrm{p}$ resonance coincides with the threshold for $\Lambda + \mathrm{K}^+$ production.

These surprising coincidences give rise to a conjecture that the resonances are connected in some way with the corresponding thresholds: it seems extremely unlikely that the resonances should occur so close to thresholds unless there were a special reason for it. The conjecture is especially plausible because there exists in general a simple reason for expecting resonances close to two-body thresholds owing to the presence of a final-state interaction. Let us assume that the interaction between a pair of particles $b + Y$ may be represented by an attractive potential $U(r)$ for distances $r \geqslant R_0$ (the form of the interaction for $r < R_0$ is unimportant for the present argument). It has been shown by the present author (Baz 1959; we refer to this paper as I) that the cross section for a reaction

$$a + X \rightarrow b + Y,$$

as well as the cross sections for all other reactions

$$a + X \rightarrow c + Z,$$

---

† Communicated by B. H. Flowers. Work performed during the author's leave of absence at the Universities of Oxford and Manchester.

are expected to show a resonance-like structure in the neighbourhood of the $b+Y$ threshold provided only that the potential $U(r)$ is not too weak. If the potential begins at $r=R_0=\hbar/m_\pi c$, and has the form

$$U(r)=-\tfrac{1}{4}m_\pi c^2\exp(-r/R_0), \qquad (r\geqslant R_0),$$

for example, full-scale resonance phenomena are to be expected in the $\pi^-+\mathrm{p}$ system near to the $\mathrm{K}+\Sigma$ threshold between which latter particles we have supposed $U(r)$ to act. Paper I dealt exclusively with threshold effects in low energy nuclear physics, but the essential results remain valid for the collisions of any particles.

If we therefore assume that the $\mathrm{K}+\Sigma$, $\mathrm{K}+\mathrm{N}$ and $\Lambda+\mathrm{K}^-$ interactions include attractive potential tails of the rough order of magnitude suggested above, the appearance of resonances close to thresholds involving these pairs of particles receives a natural explanation. This explanation, if correct, enables us to draw from the experimental cross sections close to threshold some interesting conclusions regarding the relative parities of the K, Σ and Λ particles. First of all, however, we briefly recapitulate some results of paper I.

To see how threshold resonances arise we consider the simple case of a two-channel s-wave system where below the threshold energy $E=E_{\mathrm{th}}$ only elastic scattering $X(a,a)X$ is possible, while if $E>E_{\mathrm{th}}$ the reaction channel $X(a,b)Y$ is also open. Here E is the centre-of-mass kinetic energy of particles $a+\mathrm{X}$. Elements of the scattering matrix for elastic scattering, U_{aa}, and for the reaction, U_{ab}, may be written in the usual way in terms of boundary conditions at the surface $r=R_0$ (see, for example, Lane and Thomas 1958):

$$\left.\begin{aligned} U_{aa}&=\exp(2i\phi)\left[\frac{1-\tau/\Delta^*}{1-\tau/\Delta}\right]_{R_0}, \\ U_{ab}&=\frac{k^{1/2}}{\psi^{(+)}(R_0)}\left[\frac{c}{\Delta-\tau}\right]_{R_0}. \end{aligned}\right\} \quad . \quad . \quad . \quad . \quad . \quad (1)$$

Here k is the wave number of $b+Y$ at infinite separation, $\psi^{(+)}(r)$ is the wave function of $b+Y$ in the outer region $(r\geqslant R_0)$ which behaves asymptotically as $\exp(ikr)$, and τ is the logarithmic derivative of $\psi^{(+)}$. The quantities ϕ, Δ and c, where $|c|^2=-\tfrac{1}{4}\,\mathrm{Im}\,\Delta$, can be regarded as constants near to threshold; whereas k, $\psi^{(+)}$ and τ depend upon $E-E_{\mathrm{th}}$ rather than upon E, the former quantities depend upon E itself.

Now it is usually supposed that the strong interaction inside the sphere $r<R_0$ vanishes abruptly at $r=R_0$ so that $\psi^{(+)}$ and τ are equal to their free-particle values which, in the case of s-waves, are

$$\psi_{\mathrm{free}}^{(+)}(R_0)=\exp(ikR_0), \qquad \tau_{\mathrm{free}}(R_0)=ik. \quad . \quad . \quad . \quad (2)$$

However, if the interaction does not vanish abruptly, but assumes the form of an attractive potential tail for $r>R_0$, then $\psi^{(+)}(R_0)$ and τ differ from the values (2) considerably. In I it is argued that the following formulae should be quite general near to the threshold provided the attractive potential is not too weak:

$$\left.\begin{aligned}\psi^{(+)}(R_0)&=\exp(ikr_0)\Lambda(\delta-i\epsilon^{1/2}),\\ \tau(R_0)&=\frac{1}{R}\frac{1}{\delta-i\epsilon^{1/2}},\end{aligned}\right\} \quad . \quad . \quad . \quad . \quad (3)$$

where r_0, Λ, δ and R are constants, and $\epsilon=E/U_0$, where U_0 is the depth of the potential at $r=R_0$. The constant R is a measure of the range of the potential; $\Lambda\simeq 1$, and $|\delta|\ll 1$. For definitions of these various quantities, reference should be made to 1. These formulae are valid for $|\epsilon|\ll 1$ whenever the potential

$$\begin{aligned}V(r)&=U(r) \quad \text{for} \quad r\geqslant R_0\\ &=+\infty \quad \text{for} \quad r<R_0\end{aligned}$$

has a bound or virtual state at an energy which is small compared to U_0. For potentials $U(r)$ which are weaker than we have been considering the expressions for $\psi^{(+)}$ and τ are more complicated, taking values intermediate between (2) and (3).

On inserting (3) into (1) we obtain immediately formulae looking very similar to the Breit–Wigner resonance formulae. The reaction cross section, for example, is

$$\sigma_{ab}=\frac{4\pi}{k_a{}^2}\frac{\Gamma_a\Gamma_b}{E_0{}^2+(\Gamma_a+\Gamma_b)^2} \quad . \quad . \quad . \quad . \quad (4)$$

where k_a is the wave number of the colliding particles $a+X$, Γ_a and E_0 are constants derived from δ, R, Λ and Δ, and the inelastic width Γ_b is extremely large:

$$\Gamma_b=(k_bR_0)\gamma_b{}^2\approx(k_bR_0)\frac{\hbar^2}{\mu R_0{}^2}. \quad . \quad . \quad . \quad . \quad (5)$$

The elastic scattering cross section also has a resonance form. Note that the 'resonance denominator' contains the *constant* energy E_0, rather than the usual factor.

It is easy to see, by considering the wave function of the system at $r>R_0$, that the 'resonance' is due to a peculiar quasi-stationary state a little below, or just at, the threshold, composed of particles $b+Y$ moving at a large distance from each other: the state resembles the normal deuteron state in that the two particles are nearly always outside their interaction radius. The state can exist only below the threshold (for s-waves) because at positive energies the particles $b+Y$ immediately disperse.

If we remove the purely kinematic factors from (4) the reduced cross section

$$\frac{\sigma_{ab}}{4\pi\lambda_a{}^2k_b}\sim\frac{1}{E_0{}^2+(\Gamma_a+\Gamma_b)^2} \quad . \quad . \quad . \quad . \quad . \quad (6)$$

is a monotonically decreasing function of energy (fig. 1 *a*).

Everywhere above we have considered only s-waves. We can in the same way consider cases where $l > 0$. The result is again that a resonance is very likely to occur near to the threshold, except in this case, owing to the presence of the repulsive potential barrier, the resonances can occur above threshold as well as below. The reaction cross section has the form

$$\sigma_{ab} = \frac{4\pi}{k_a^2}(2l+1)\frac{\Gamma_a\Gamma_b}{(E-E_r)^2+(\Gamma_a+\Gamma_b)^2} \quad . \; . \; . \; . \quad (7)$$

Fig. 1

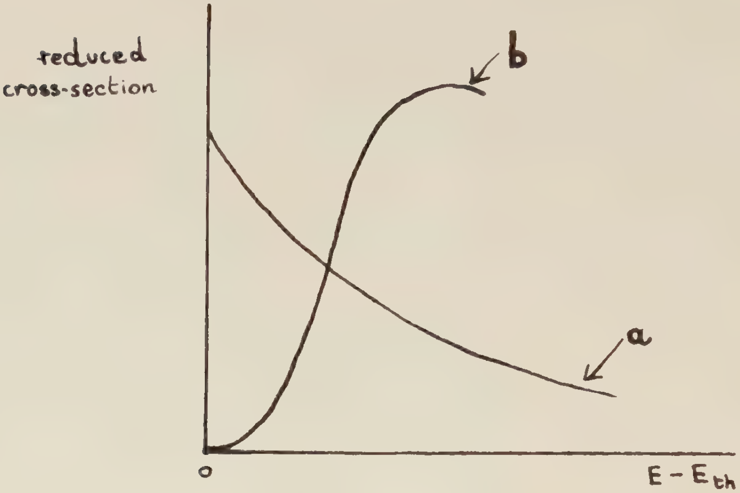

with $\Gamma_b = (k_b R_0)^{2l+1}\gamma_b^2$. Again, we find that γ_b^2 is close to the Wigner limit $\hbar^2/\mu R_0^2$. It was shown in I that the most probable position of the resonance E_r is, in this case, just above threshold in the interval

$$0 < (E_r - E_{\text{th}}) < U_1,$$

where U_1 is the height of the centrifugal barrier at the outer edge of the attractive potential $U(r)$.

The reduced cross section

$$\frac{\sigma_{ab}}{4\pi\lambda_a^2 k_b} \sim \frac{(k_b R_0)^{2l}}{(E-E_r)^2+(\Gamma_a+\Gamma_b)^2} \quad . \; . \; . \; . \quad (8)$$

correspondingly has the form shown in fig. 1 *b*.

The above formulae are not exact, especially when more than two channels are open. However, if experimental data suggest that threshold phenomena are of importance, then (6) and (8) give the type of energy dependence to be expected. Henceforth we shall take the point of view that the resonances (*a*), (*b*) and (*c*) have a threshold origin.

§ 2. The $\pi+p$ Resonance at 0·9 BeV

Data† on $\pi^- + p$ cross sections are shown in fig. 2, the total cross section being that of Burrowes *et al.* There is a marked disagreement between the Columbia and the Brookhaven values at 1·09 Bev/c (654 Mev in the centre of mass) and for the moment we disregard the Brookhaven data completely (the reasons being given below). The experimental errors are very large, even larger than are shown in fig. 2 where uncertainties in the pion energy are not taken into account, but we shall optimistically suppose that the solid lines of fig. 2 do describe the general trends of the cross sections correctly.

Fig. 2

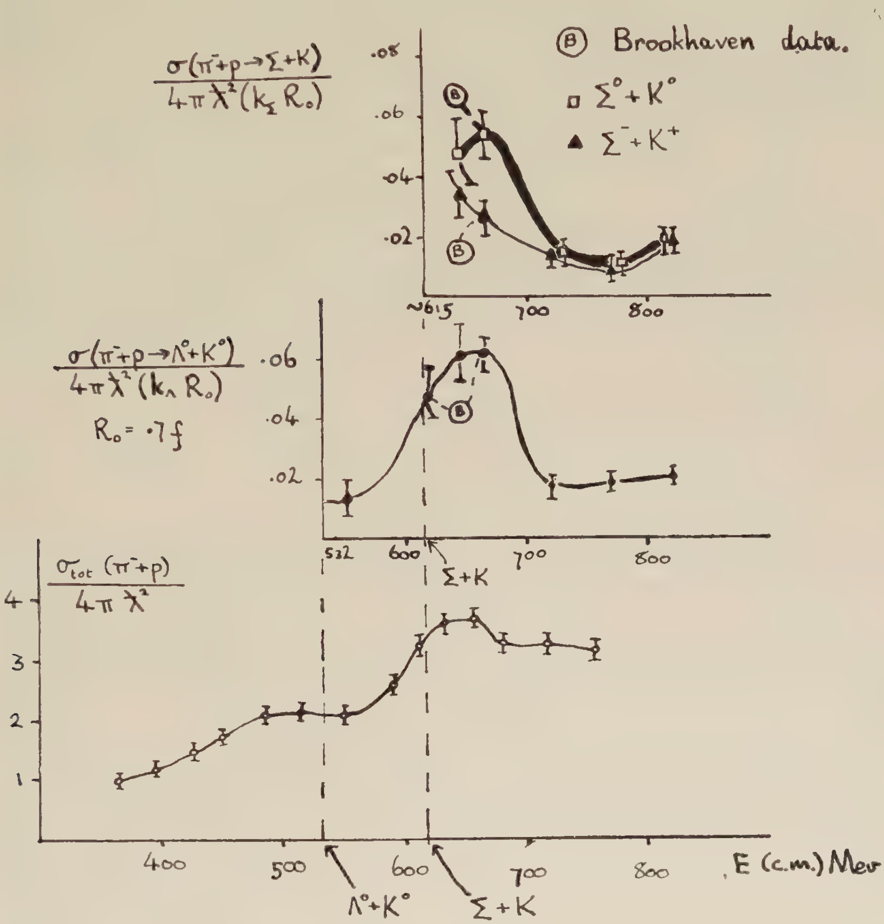

---

† All the experimental data used below, unless otherwise stated, are taken from the ‘ Report on Geneva Conference 1958 ’.

It is also known that near the $K+\Sigma$ threshold the $\Lambda+K^0$ and Σ^0+K^0 production cross sections are strongly anisotropic, while the Σ^-+K^+ cross section is consistent with isotropy.

If we accept the hypothesis of the threshold origin of the resonance, then all the data lead to the conclusions

(i) that Λ and Σ^0 have the same parity,

(ii) that $(K^0+\Sigma^0)$ and $(K^+ +\Sigma^-)$ have opposite relative parities and so cannot belong to the same isotopic spin multiplet.

The argument runs as follows. The resonance is due either to the $K^0+\Sigma^0$ or to the $K^++\Sigma^-$ interaction. It can be seen, however, that only an attractive interaction between K^0 and Σ^0 in a p-state can link together consistently the following facts:

1. The resonance occurs about 30 MEV *above* threshold, thus excluding $l=0$.
2. The energy dependence of the $K^0+\Sigma^0$ and $K^++\Sigma^-$ production cross sections suggests that $K^++\Sigma^-$ are produced in an s-state (compare fig. 1*a*) while $K^0+\Sigma^0$ are produced in a state with $l>0$ (fig. 1*b*). For $l>1$, the cross section would be extremely small near threshold.
3. The angular distributions of $K^++\Sigma^-$ and $K^0+\Sigma^0$ are also consistent with s-wave and p-wave production respectively.
4. The maxima of the total cross sections, the $K^0+\Lambda$, and the $K^0+\Sigma^0$ cross sections, all coincide.
5. The large value of the $K^0+\Sigma^0$ cross section near threshold compared with that for $K^++\Sigma^-$ production is consistent with p-wave production of $K^0+\Sigma^0$ only if there is a resonance in the p-state.

No one of these facts is conclusive by itself. Taken together, however, they are most suggestive and argue strongly for the conclusions (i) and (ii) above.

Let us now consider $\Lambda+K^0$ production in some detail. We have treated the resonance as if it were solely due to the $K^0+\Sigma^0$ interaction. It is likely, however, that the bump in the cross section is due to the superposition of two resonances, one due to the $K^0+\Sigma^0$ interaction in a p-state, the other to the $K^++\Sigma^-$ interaction in an s-state. The latter is fairly strong, as can be seen from the production cross section. According to the discussion in § 1 an s-state resonance must be situated just at or a little below the $K^++\Sigma^-$ threshold (i.e. about 30 MEV below the $K^0+\Sigma^0$ resonance) and it follows from the energy dependence of the $K^++\Sigma^-$ production cross section that its width is about 100 MEV.

If the resonances have different parities we would expect the angular distribution of $K^0+\Lambda$ production to change drastically with energy. Experiment shows, however, that the angular distribution in the interval 610–720 MEV (centre of mass) changes quite steadily and could be accounted for in terms of a monotonically increasing s-wave background together with a wide p-wave resonance (or rather two p-wave resonances). This indicates that both $K^0+\Sigma^0$ and $K^++\Sigma^-$ resonances contribute to the p-wave production of $K^0+\Lambda$. Consequently $K^0+\Sigma^0$ and $K^++\Sigma^-$ have opposite intrinsic parities.

To confirm this conclusion, better data on the energy dependence, and especially on the angular distribution, of the $K^0+\Lambda$ production cross section are badly needed.

From the data which exist at present it seems possible to fix an absolute parity for $K^0+\Lambda$. The angular distribution of scattering seems to suggest that the 0·9 BeV resonance occurs in a p-state of π^-+p. From the point of view of the total cross section this is quite possible because the change in $\sigma_{\text{tot}}\ 4\pi\lambda^2$ over the region of the resonance is not large. From our picture of a threshold state it then follows that the intrinsic parities of π^-+p and $K^0+\Lambda$ (or $K^0+\Sigma^0$) are the same.

Before concluding this section we must remember that we have rejected the Brookhaven data on the total cross section at 645 MeV (centre of mass). If these data prove to be correct, and the Columbia data wrong, we immediately run into difficulties. The energy dependence of $K^0+\Sigma^0$ production would then indicate that these particles are produced in an s-state and $K^++\Sigma^-$ in a p-state. This would conflict directly with the observed angular distributions.

§ 3. THE $\gamma+p$ RESONANCE

Experimental data on the cross section for the reaction $\gamma+p\to K^++\Lambda$ are shown in fig. 3. The cross section displays an energy dependence typical of an attractive s-wave final state interaction, and the assumption of an attractive potential tail between K^+ and Λ explains the existing data to any desired degree of accuracy.

There are some immediate consequences. The first is that $K^++\Lambda$ production occurs mainly in an s-state near threshold, and this supports Moravcsik's (1959) conclusion regarding the pseudoscalar character of the K^+ particles. His conclusion is based on dispersion relations, and is valid only if s-wave production is predominant.

The second consequence concerns the relation between K^0 and K^+ particles. The shape of the $\pi^-+p\to K^0+\Lambda^0$ cross section (fig. 2) suggests that the s-wave part of the cross section has the conventional energy dependence

$$\sigma_{l=0}\sim 4\pi\lambda^2(k_\Lambda R_0)\times 0{\cdot}15$$

where the numerical constant is based on the assumption that $R_0=0{\cdot}7\times 10^{-13}$ cm. This suggests that there is no attractive potential tail between K^0 and Λ in an s-state, while the $K^++\Lambda$ interaction has one. In agreement with our previous results we conclude that K^+ and K^0 are different particles. This conclusion is indirectly supported by the behaviour of the total π^-+p cross section near to the $K^0+\Lambda$ threshold which also suggests the absence of an attractive tail in the $K^0 + \Lambda$ interaction. The small-scale variation which is observed to occur can be accounted for in terms of the usual cusp theory.

Fig. 3

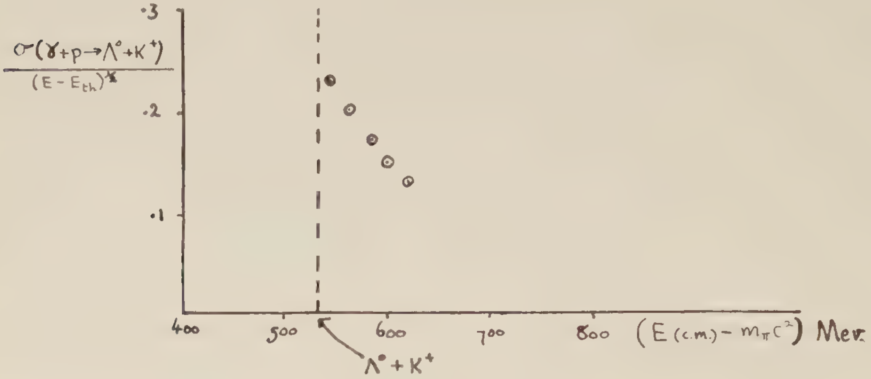

§ 4. THE $K^- + p$ RESONANCE

Data on the total elastic scattering of $K^- + p$, on the charge exchange reaction $K^- + p \rightarrow \overline{K^0} + n$, and on $\pi + \Sigma$ production are shown in fig. 4. They seem to suggest a resonance at about 15 MeV (centre of mass) above the $\overline{K^0} + n$ threshold. The position, the large width of the $\overline{K^0} + n$ channel, and the trend of the charge exchange cross section with energy, suggest that the resonance is of the threshold type and is due to $\overline{K^0} + n$ interaction in a p-state. From the established isotropy of the low energy $K^- + p$ scattering it then follows that K^- and $\overline{K^0}$ have opposite parities.

Data on $\pi + \Sigma$ production are very poor and controversial. However, if we accept the Berkeley results on the total cross section and on Σ^- and Σ^+ production rates (fig. 5), we have two points to make. Firstly, the $\pi + \Sigma$ cross section participates in the resonance. Secondly, the Σ^-/Σ^+ ratio changes rapidly in the vicinity of the threshold.

The first point is a weak one because the $\pi + \Sigma$ threshold is about 100 MeV below the $K + N$ threshold. Consequently $\pi + \Sigma$ production can occur through both s- and p-waves. Neither parity, nor spin, selection rules can be expected.

The second point is more interesting. It may always be interference between different states that causes the Σ^-/Σ^+ ratio to change so rapidly. A more straightforward explanation is possible, however, if we assume that $\pi^- + \Sigma^+$ production goes predominantly through the $\overline{K^0} + n$ resonance while the $\pi^+ + \Sigma^-$ production does not. It would be sheer speculation beyond even the scope of this paper to decide at present which possibility is the more plausible.

§ 5. CONCLUDING REMARKS

To understand the degree of certainty of the above results we repeat here very briefly the main points. The basic assumption about the 'threshold origin' of the observed resonances looks very attractive because it explains in a natural way why all the resonances are so close to threshold and pin-points a reason why they should exist at all. The potential required to produce such resonances is in itself such a reasonable one that it would be difficult to find objections to its existence. It cannot be overlooked, however, that there may be some other, presumably more complicated, explanation of the striking threshold–resonance correlation.

Fig. 4

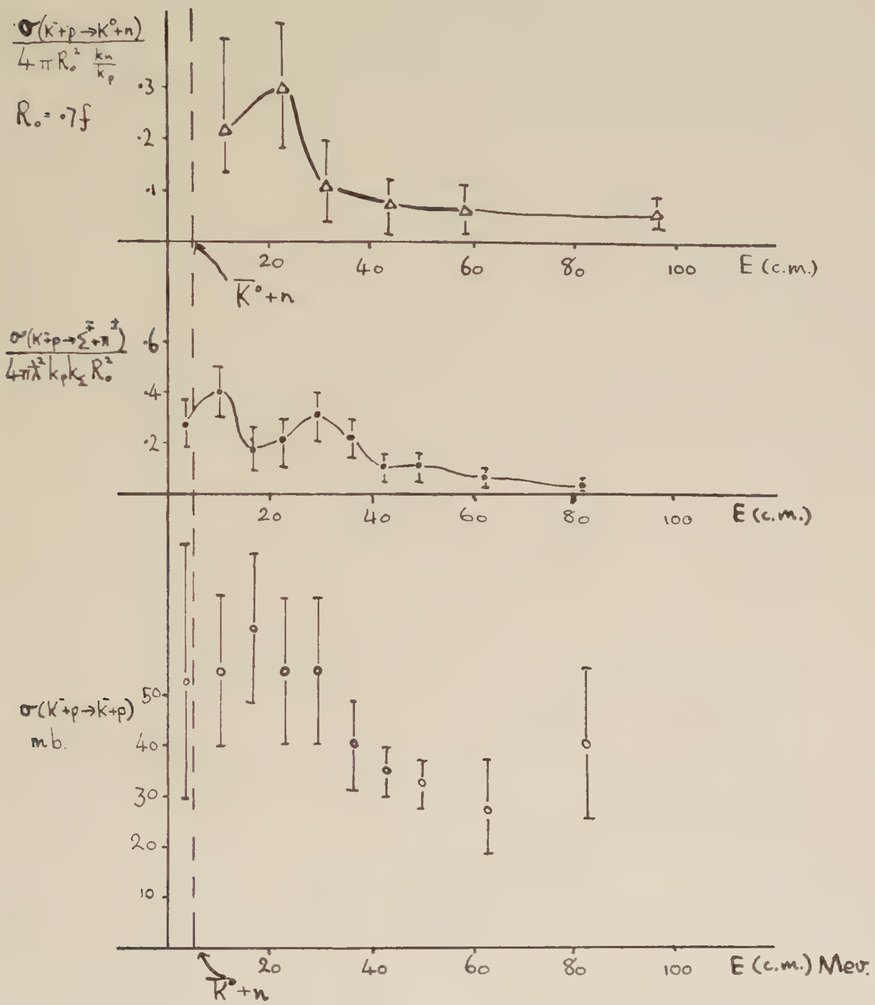

After this assumption is made the arguments become very straightforward and the validity of the results depends only on the quantity and quality of the experimental data used. Unfortunately, the experimental errors are so large as to make meaningless any attempt to achieve numerical agreement of theory with experiment. All except the most respectable of theories have a few adjustable parameters which can be chosen to fit the data within experimental error. With all this in mind we have simply been trying to find the simplest assumptions about the various particles and their interactions which would enable overall agreement with the existing data, such as it is, to be obtained without recourse to such unsatisfactory devices as the chance cancellation of matrix elements. We have seen, however, that in order to obtain a logically consistent picture we had to anticipate some trends in the cross sections which cannot as yet be regarded as proven. Although unsatisfactory, this procedure at least has the advantage of providing a ready means of checking experimentally the internal consistency of the picture.

Fig. 5

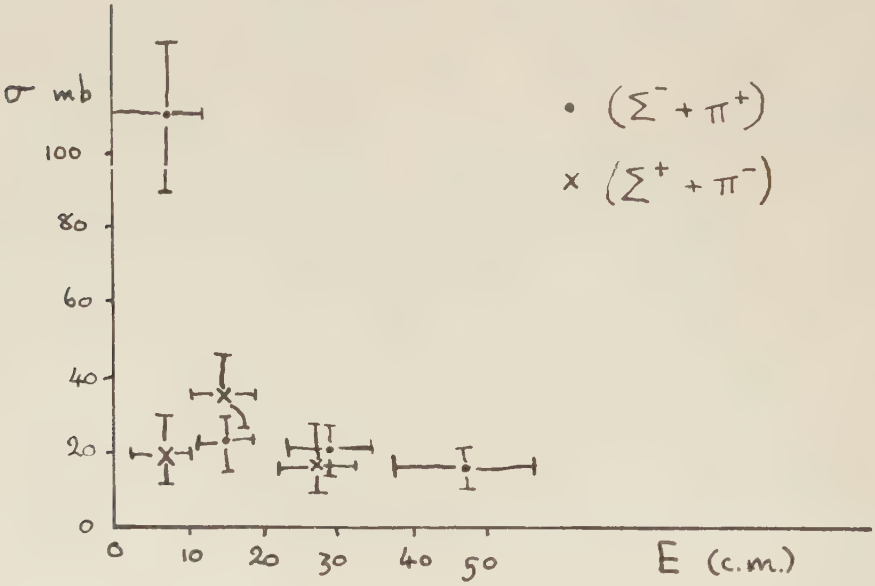

After these preliminaries we dare to summarize our results as follows. The simplest way to understand the observed resonances in high energy phenomena is to postulate an attractive potential tail between some of the particles and effective near to their thresholds. Having made this assumption the most natural links between the different data are provided by the hypotheses that

(i) Σ^0 and Λ^0 have the same parity,
(ii) K^- and $\overline{K^0}$ have opposite parity,
(iii) $K^0+\Sigma^0$ and $K^++\Sigma^-$ have opposite parity,
(iv) π^-+p and $K^0+\Lambda^0$ have the same intrinsic parity.

References

Baz, A. I., 1959, *Advanc. Phys.* (in the press).

Burrowes, H. C., Caldwell, D. O., Frisch, D. H., Hill, D. A., Ritson, D. M., Schluter, R. A., and Wahlig, M. A., 1959, *Phys. Rev.*, **2**, 119.

Lane, A. M., and Thomas, R. G., 1958, *Rev. mod. Phys.*, **30**, 257.

Mathews, P. T., and Salam, A., 1959, *Phys. Rev.*, **2**, 226.

Moravcsik, M. J., 1959, *Phys. Rev.*, **2**, 352.

On a New Mode of Deformation in Indium Antimonide†

By J. W. Allen
Services Electronics Research Laboratory, Baldock, Herts

[Received May 11, 1959]

Abstract

Dislocations can be introduced into indium antimonide by local impact. The particular configuration of dislocations produced has been called a 'dislocation-crack', because of its close resemblance in macroscopic features to an ordinary crack. The stress required to produce a dislocation-crack is shown to be of the same order as the fracture stress. A mechanism which explains the observations is proposed. Dislocation-cracks also occur in InAs, GaAs, GaP and Ge.

§ 1. Introduction

The deformation properties of single crystals of indium antimonide have been described in previous papers (Allen 1957, 1958; these will be called papers I and II in this work). Briefly, the material is brittle at room temperature and shows elastic behaviour up to its fracture point, whereas at higher temperatures it becomes ductile and considerable dislocation multiplication occurs. This latter process is characterized by a time delay in the plastic strain after a stress is applied. It was mentioned in paper I that dislocations could also be introduced into indium antimonide by the application of a sudden localized impact, although the mechanism of their production was not understood. In this paper we describe the phenomenon in more detail and suggest a possible explanation of it.

In this work we have chosen the etch-pit technique to reveal the positions of the dislocations. Details of the method are contained in paper I.

§ 2. Qualitative Observations

If a crystal of InSb is subjected to a local impact and then etched it frequently happens that markings are seen which resemble cracks passing through part of the crystal. An example is shown in fig. 1 (Pl. 124). Such features are few in number and it frequently happens that only one is produced by a single impact. They may be several millimetres in linear dimensions or they may be as small as a few microns. In all cases that we have observed they extend to the crystal surface, but they do not extend right across the crystal in such a way as to divide it into two parts. There is a marked preference for them to lie in (110) planes although they can show considerable curvature. At higher magnification it is seen that the apparent crack in fact consists of a wall of dislocations (fig. 2, Pl. 124) and for this reason we call the features 'dislocation-cracks'. The dislocations show wide variations in linear density along the length of the dislocation-crack, although they may be uniformly spaced along short sections. Along some sections some tens of microns long there may be no dislocations at all, as in parts of fig. 2, while elsewhere the dislocations may be so closely spaced as to be unresolved by the techniques used here. Very high densities occur more often the more nearly the plane of the dislocation-crack approaches (110). High densities also frequently occur at changes of direction of a dislocation-crack, as may be seen in fig. 3 (Pl. 125).

---

† Communicated by the Author.

§ 3. QUANTITATIVE OBSERVATIONS

A very simple method of applying a high local stress to the surface of a crystal for a short time under controlled conditions is to drop a small steel sphere onto it. The height of drop and the mass of the sphere are experimentally variable parameters which control the stress, duration and radius of contact. The relations between these quantities are well known (see, for example, Timoshenko 1934) and are as follows:

The maximum radius of contact, a:

$$a=[\{\tfrac{5}{4}\pi^2\rho(\kappa_1+\kappa_2)\}^{1/5}]v^{2/5}R. \qquad \ldots \ldots \quad (1)$$

The duration of contact, t:

$$t=[2{\cdot}94\{\tfrac{5}{4}\pi^2\rho(\kappa_1+\kappa_2)^{2/5}]v^{-1/5}R. \qquad \ldots \ldots \quad (2)$$

The maximum pressure, q_m:

$$q_m=\left[\frac{2}{\pi^2}\{\tfrac{5}{4}\pi^2\rho(\kappa_1+\kappa_2)^{-4}\}^{1/5}\right]v^{2/5}. \qquad \ldots \ldots \quad (3)$$

In these expressions the quantities within the square brackets are determined by the mechanical properties of the sphere and crystal and are constants of the experiment, while the velocity of approach at impact, v, and the sphere radius, R, are the variables. The quantities κ_1 and κ_2 refer to the sphere and the crystal respectively and are defined by

$$\kappa_i\equiv\frac{1-\nu_i^2}{\pi E_i} \qquad \ldots \ldots \quad (4)$$

where ν is Poisson's ratio and E is Young's modulus. The other quantity ρ is the density of the sphere.

The maximum pressure q_m occurs at the centre of the area of contact while the maximum shear stress is of the order of $\frac{1}{3}q_m$ and is at a point about $\frac{1}{2}a$ below the centre of the contact area. The maximum tensile stress is along the perimeter of the contact area and has the value

$$\sigma_m=\frac{(1-2\nu_2)}{3}q_m. \qquad \ldots \ldots \quad (5)$$

There is a shear stress along the perimeter with the same magnitude as σ_m.

In an experiment the crystal surface, which was approximately a $(\bar{1}\bar{1}\bar{1})$ plane, was ground flat, polished chemically with CP4A diluted with nitric acid, and etched with 111 solution (detailed procedures and the composition of the etches are given in paper I). The surface was then examined under the microscope to ensure that there was no surface damage. A steel sphere, in actual fact a ball-bearing, was next dropped from a pre-determined height onto the surface, care being taken that the ball should strike the surface only once. For heights of drop h from 2 cm to 10 cm the ball was held vertically above the crystal by an electromagnet and fell freely when the electromagnet current was broken. Draught shields were found to be essential if the smaller spheres were to fall vertically. For heights of drop of 2 cm and below the ball was affixed to a length of cotton and was used as a pendulum bob, h being calculated from the horizontal displacement x. After the ball had struck the surface the crystal was etched for about 15 sec in 111 etch. The surface was then examined microscopically and measurements were made of the damage done. Before each drop the surface was re-polished until an undamaged surface was obtained.

Three quite distinct types of damage were revealed by the etch. Firstly, there was general pitting over a roughly circular area corresponding to the area of contact. This damage was quite superficial and disappeared after a few microns had been removed from the surface. Secondly, arcs of 'ring-cracks' appeared near the perimeter of the contact area, showing some tendency to lie in (110) planes. Occasionally concentric arcs occurred. By etching away the crystal surface it was shown that the ring-cracks penetrated the crystal for several tens of microns, and that they were actually dislocation-cracks. A typical contact area showing these two types of damage is shown in fig. 4 (Pl. 125). Thirdly, radial cracks were sometimes seen, but these were associated with slight irregularities of the surface contour and did not occur if sufficient care was taken in the initial surface preparation.

The superficial damage occurred with all sphere sizes and heights of drop used in these experiments, while for a given size of sphere there seemed to be a minimum height of drop below which a ring-crack was not produced. In fig. 5 the occurrence or non-occurrence of a ring-crack is plotted as a function of the mass of the balls and the height from which they were dropped. Most of the points on this graph are the result of more than one experiment. It can be seen that there are two regions with a rather well-defined boundary separating them. In fact the sharpness of the boundary is quite surprising when it is remembered that the stresses involved vary only as $h^{1/5}$ and that in most systems the statistical spread of fracture or deformation stresses is fairly wide. This suggests that the criterion for the occurrence of a ring-crack represented by the boundary is either an intrinsic property of the crystal or is the statistical sum of a very large number of processes. We shall return to this point in the discussion below.

Fig. 5

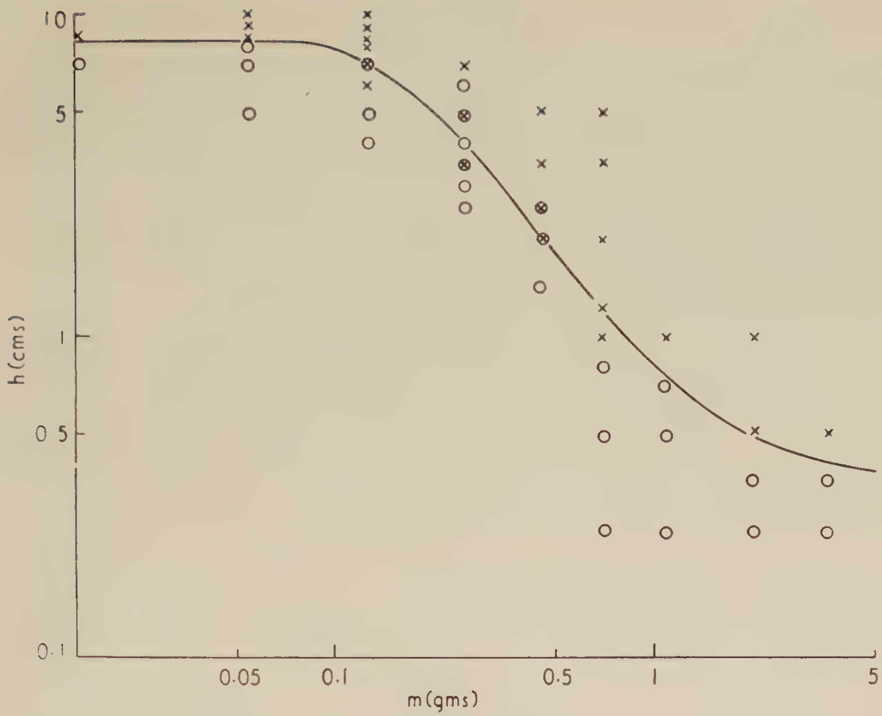

Damage produced by the impact of a steel sphere as a function of the height of drop h and the sphere mass m.

○, superficial damage only; ×, superficial damage and ring-cracks; ⊗, ring-cracks produced in some cases but not in all.

Fig. 6

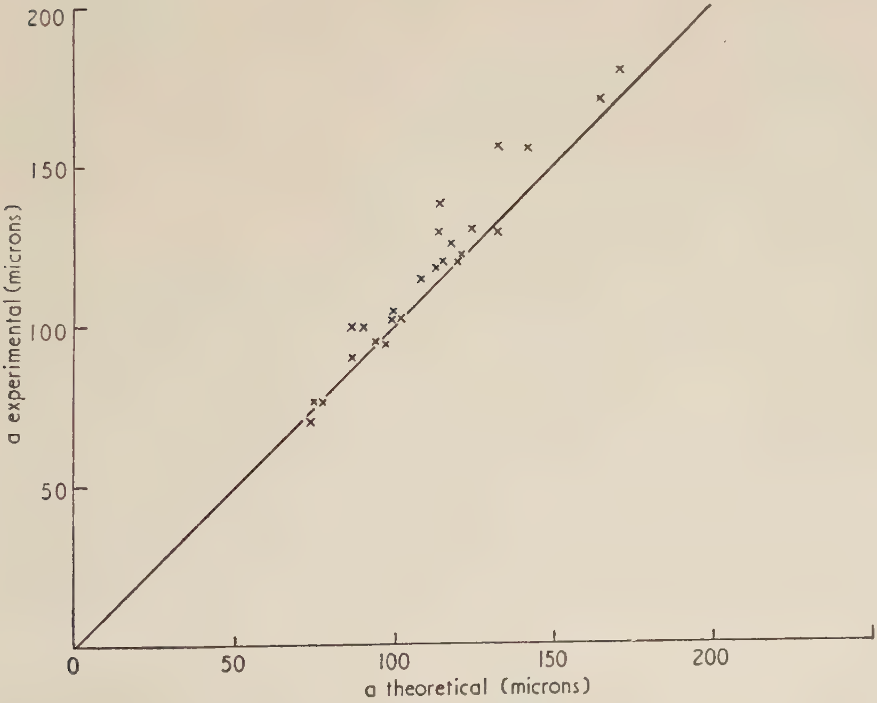

Experimental and theoretical values of the radius of the maximum area of contact. The straight line has a slope of 45°.

Equations (1)–(5) were used to obtain quantitative estimates of q_m, a and t. These equations apply to isotropic materials, so an average over the elastic moduli for different directions in InSb had to be used in calculating κ. Elastic constants for InSb are given by Potter (1956). The values finally used for the various quantities are:

density of steel spheres, $\rho = 7{\cdot}79\,\mathrm{g/cm^3}$;
κ for steel $= 1{\cdot}5 \times 10^{-13}\,\mathrm{cm^2/dyne}$;
κ for InSb $= 5{\cdot}0 \times 10^{-13}\,\mathrm{cm^2/dyne}$;
Poisson's ratio for InSb, $\nu = 0{\cdot}25$.

The velocity of impact was calculated from the height of fall using the equation

$$v = (2gh)^{1/2}, \quad . \quad . \quad . \quad . \quad . \quad . \quad . \quad . \quad . \quad (6)$$

no correction being made for atmospheric drag.

Fig. 7

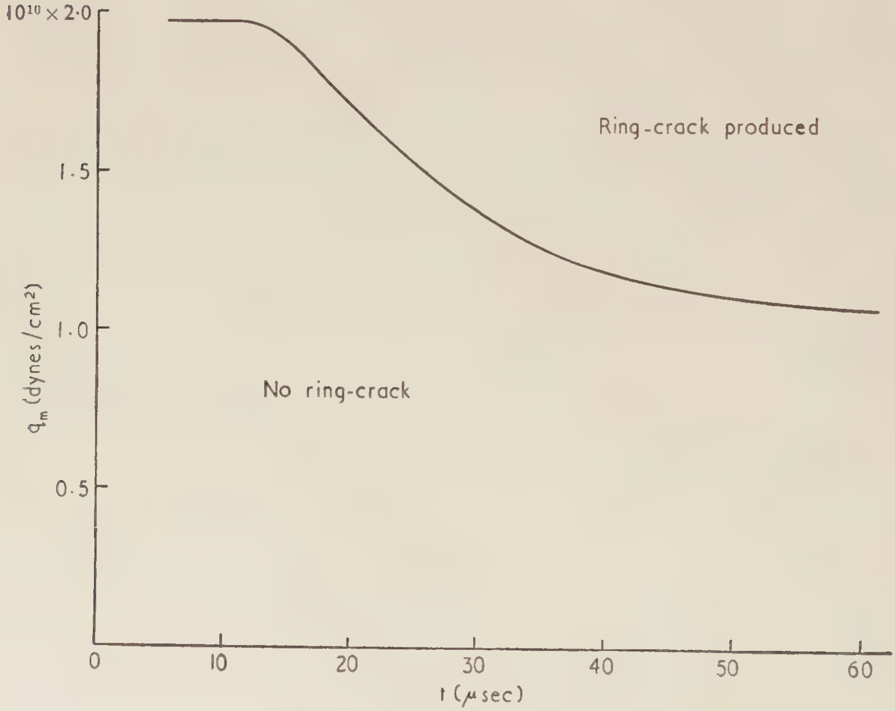

The criterion for the production of a ring-crack plotted as a function of the maximum contact pressure q_m and the total duration of contact t.

In fig. 6 the observed radius of the area of superficial damage is plotted against the theoretical value of a from eqn. (1), v and R being running parameters. The agreement is sufficiently good to give us confidence in the validity of the theory and in the choice of the numerical values for

$(\kappa_1+\kappa_2)$. In fig. 7 the criterion for the production of a ring-crack represented by the curve in fig. 5 is plotted as a function of q_m and t. It is important to bear in mind that the coordinates are not the stress and the time of application of the stress necessary to produce a ring-crack. From the fact that the ring-crack occurs at the perimeter of the maximum area of contact we can infer that the minimum stress necessary is σ_m which from eqn. (5) is approximately $\frac{1}{6}q_m$. A stress of this order of magnitude exists near the perimeter for only a fraction of the total time during which the sphere and crystal actually make contact. We may therefore say that a stress at the crystal surface of about 3×10^9 dynes/cm^2, i.e. about 1% of the shear modulus, is necessary for the production of a dislocation-crack, although a rather lower value will suffice if the stress is applied for a sufficiently long period, namely a few microseconds. The fracture stress found from static bending experiments has roughly the same value.

§ 4. Discussion of the Results

The problem immediately raised by the observations is: what is the mechanism by which dislocations are produced in these particular arrays? For various reasons a source mechanism seems unlikely if we define a source as a region of the crystal capable of propagating dislocations into neighbouring regions. Dislocations in InSb require a stress at least of the order of the fracture stress to move them at appreciable velocity at room temperature. In a dislocation-crack several millimetres in extent there may be 10^3–10^4 dislocations. This requires either that the source should be acted on by a stress orders of magnitude greater than the fracture stress, or that a volume of the crystal containing the whole dislocation-crack should be subjected to a stress of the same order as the fracture stress. In either case it is difficult to see how it is possible to have situations in which just one dislocation-crack can occur, for either the stress in a small region must be so high that considerable local fracture should appear, or there are high stresses over a large region in which case several dislocation-cracks should occur. It may be argued that the sources are some rare defect, only one or two of which are to be found in the stress fields considered. But the consistency of the ball-dropping experiments suggests the contrary, namely that dislocation-cracks are found whenever the stress is above a certain minimum. It would also be difficult to explain the phenomenon shown in fig. 3, when the dislocations lie in two parallel planes separated by a short section in a third plane, or the curved dislocation-crack shown in fig. 1. The creep of dislocations and their subsequent avalanching described in paper II is too slow by several orders of magnitude to have any appreciable effect here.

A mechanism which seems to account for all the experimental observations is shown schematically in fig. 8. The high local stress at the surface will initiate a Griffith's crack, which will tend to lie in the cleavage plane, (110). The stress concentration at the tip allows the crack to run deeply into the crystal, although side branches can run off in directions at roughly 45° to the main crack. Since the stress is inhomogeneous, as it is in all the experiments considered here, the material on the two sides of the crack will be deformed by different amounts. If the stress is then removed quickly enough, so that the atmosphere does not have time to penetrate the crack, the two sides will come together again and the crack will heal. However, because of the inhomogeneous deformation the atoms in the two approaching surfaces will not be in perfect register. Some atomic re-arrangement will then take place so that the mismatch is concentrated in dislocation lines, since this configuration has lower energy than a distributed mis-match.

Fig. 8

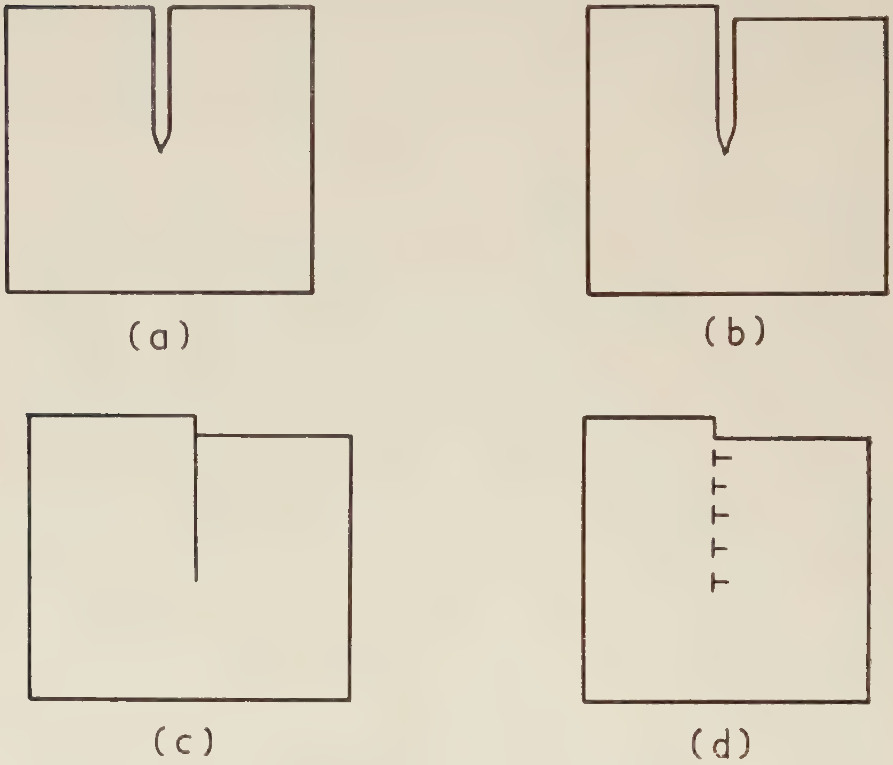

A schematic description of the production of a dislocation-crack. (*a*) A crack occurs in part of the crystal; (*b*) The crystal is inhomogeneously deformed (stages a and b will usually take place simultaneously); (*c*) The crack heals on removal of the stress; (*d*) The mis-match sorts itself out into dislocation lines. In the general case these will not all be edge dislocations and will not all have the same Burgers vector.

The morphology of a dislocation-crack is therefore that of a true crack, i.e. it tends to lie in a (110) cleavage plane instead of the (111) plane observed in slip, it can be branched, it can be curved, and it can be stepped. The steps will cause the dislocations produced to be heavily jogged and therefore immobile. The dislocations will therefore not be evenly spaced as they would be if they could move under their mutual interactions, although in limited areas where the crack follows an atomically plane cleavage surface movement might be possible and so small regions can show even spacing. Particularly high dislocation densities occur at the corners of steps, for here the mis-match is greatest. The dislocations will also be very far from straight and need not all have the same Burgers vector. The stress required to initiate a dislocation-crack will be equal to the fracture stress, but it must be applied for a very short time so that the crack does not run right across the crystal and so that the atmosphere will not have time to penetrate into it. If the stress falls off rapidly with distance from the surface it would be possible to start a crack at the surface which will not run right through the crystal however long the stress is sustained. If the time of application of such a stress field is long enough for the atmosphere to penetrate some way along the crack but not right along it the final result after the removal of the stress will be a crack beginning at the surface and merging into a dislocation-crack further in the crystal, a state of affairs often observed. The precise value of the fracture stress and the time-dependence shown in fig. 7 depend on the interaction of the crystal with the oxide film which inevitably exists on the surface after our particular chemical treatment.

§ 5. Dislocation-cracks in Other Materials

In this laboratory we have devised etches to show the presence of dislocations in the III–V semiconductors InAs, GaAs and GaP. In all three compounds dislocation-cracks were observed. These were produced during normal handling of the crystals, as described in the next section. However, their frequency of occurrence and their size appears to be much less in these materials than in InSb crystals subjected to the same treatment. We have also occasionally seen dislocation-cracks in thin germanium crystals that had been cut ultrasonically. Johnston *et al.* (1958) have also observed dislocation-cracks in germanium. In their case specimens were fractured by bending and the dislocation-cracks ran into the crystal from the fracture surfaces, as reported in paper I for InSb.

§ 6. Some Practical Consequences

The readiness with which dislocation-cracks occur in InSb and the fact that their presence is not immediately obvious has occasionally proved an embarrassment both in the study of physical properties and in the making of devices. Specimens can easily be damaged by cutting and grinding or even by being picked up with tweezers, as commonly happens. As an example, in fig. 9 (Pl. 126) a typical dislocation-crack is shown which has been produced during grinding with 850 grade Unirundum into which a speck of grit had been introduced.

Dislocations in semiconductors can have marked effects on their electrical properties, especially at low temperatures. A wall of dislocations such as is found in a dislocation-crack therefore behaves as a thin sheet of material with properties differing from that of the bulk material, and this can considerably affect electrical measurements. A detailed example has been given by Broom (1958) who showed that the presence of dislocation-cracks in n-type InSb could give rise to a negative magnetoresistance at liquid helium temperatures, while carefully prepared samples with no such defects showed the normal positive effect.

§ 7. Conclusions

The mechanism proposed above to explain the particular arrays of imperfections which we have chosen to call 'dislocation-cracks' seems adequate to account for the experimental observations, both qualitatively and quantitatively. It is interesting that it is identical in principle to the mechanism hypothesized in the text-books to describe the formation of a dislocation, in which a cut is made in a crystal, the sides of the cut are moved relative to each other, and the sides are rejoined.

The phenomenon is one which can be observed under special conditions in germanium, but is readily seen in the III-V compound semiconductors, and is likely to assume some importance as these latter materials become more widely known.

Acknowledgment

Acknowledgment is made to the Admiralty for permission to publish this paper.

References

Allen, J. W., 1957, *Phil. Mag.*, **2,** 1475; 1958, *Ibid.*, **3,** 1297.
Broom, R. F., 1958, *Proc. phys. Soc. Lond.*, **71,** 470.
Johnston, T. L., Stokes, R. J., and Li, C. H., 1958, *Acta Met.*, **6,** 713.
Potter, R. F., 1956, *Phys. Rev.*, **103,** 47.
Timoshenko, S., 1934, *Theory of Elasticity* (New York: McGraw-Hill), p. 339

The Interaction Rates of Stopped Negative Muons in Various Elements†

By W. B. Gilboy‡ and R. M. Tennent
Physics Department, University of Leeds

[Received June 2, 1959]

Abstract

The lifetimes of negative muons brought to rest in a series of elements have been measured. The mean lifetimes have been found to be: Cr, (268 ± 16)ns; Mn, (251 ± 14)ns; Fe, (205 ± 14)ns; Co, (196 ± 11)ns; Ni, (160 ± 10)ns; Cu, (168 ± 7)ns; Zn, (151 ± 13)ns. Using different assumptions, the various interaction rates have been calculated and compared with the theories of Primakoff, and Tolhoek and Luyten. Measurements of the time delays in Geiger counter discharges and photomultiplier after-pulses are described.

§ 1. Introduction

In a previous paper (Hillas *et al.* 1958), in future referred to as I, an apparatus was described which was designed to measure the mean lifetime of cosmic ray muons which had been brought to rest in different target materials. Preliminary results of measurements using targets of iron and copper were given. This paper describes the alterations and improvements made to the apparatus and results of measurements using the elements in the range of atomic number from 24 to 30 inclusive.

An experiment such as that described in I measures the mean disappearance rate of negative muons. In order to find the mean interaction rate, use must be made of the relation

$$\Lambda^- = \Lambda_i^- + \Lambda_d^- \quad . \quad . \quad . \quad . \quad . \quad . \quad . \quad . \quad . \quad (1)$$

where Λ^-, Λ_i^- and Λ_d^- are the disappearance, interaction and decay rates for negative muons brought to rest in the material considered. Recently, definite evidence of a variation of Λ_d^- with the atomic number of the target medium has been established. The measurements of this effect (Lundy *et al.* 1958, Holmstrom and Keuffel 1958, Astbury *et al.* 1959) show that the variation is slight and fairly well represented by a formula of the following type, first suggested by Porter and Primakoff (1951):

$$\Lambda_d^-(Z) = \Lambda_d^-(0)[1-(Z/137)^2].$$

As the variation is very slight for low Z, and as the absolute value of Λ_d^- is so much less than that of Λ_i^- for high Z, it is usually sufficient to take the value of Λ_d^- as fixed. The free decay rate of the negative muon has not been measured with accuracy and the value of Λ_d^- used hitherto has been the decay rate found by Bell and Hincks (1951) for positive muons brought to rest in iron. Sens *et al.* (1957) have measured the decay rate of positive muons in a carbon target and the decay rate of positive muons obtained by combining the results of these two measurements is $(4\cdot52 \pm 0\cdot03) \times 10^5\,\mathrm{sec}^{-1}$.

---

† Communicated by Professor J. G. Wilson.
‡ Now at A.W.R.E., Aldermaston.

In the table of results below, the interaction rates derived from our measurements of the disappearance rates are calculated first assuming that the decay rate of positive muons is fixed at the above value, and secondly using the weighted means of the observations of the three experiments mentioned above to provide values for Λ_d^- for the elements considered.

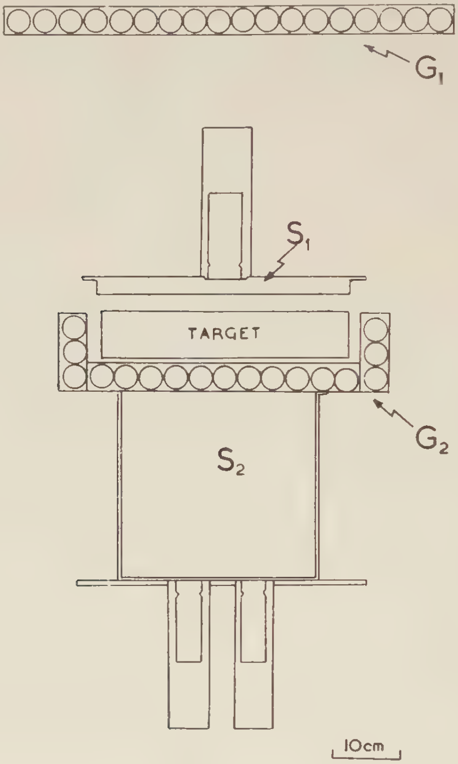

Side view of apparatus.

§ 2. APPARATUS

The figure shows a diagram of the apparatus used, showing the larger tray of counters G_1 which was used in the later experiments. This tray contained 18 counters, $3\cdot5 \times 60$ cm, compared with the earlier tray of 16 counters $2\cdot2 \times 60$ cm. The improved solid angle of acceptance of incident muons increased the counting rate by 50%. Photographs of the recording apparatus were taken following an event where a $G_1S_1\overline{G}_2\overline{S}_2$ coincidence was followed within 3 μsec by a $S_2\bar{G}_2$ coincidence. (The bar above a counter symbol represents an anticoincidence.) The time interval between the S_1 and S_2 pulses was recorded on the neon lamps of a counter chronometer scaler. The counter chronometer has been described fully by Hillas and Tennent (1958). For later experiments, the camera box was redesigned and it was made possible to record the rates of the various counters and also the output of a meter chronometer which has been described by Hillas (1958). This circuit could be used to measure time intervals of the order of microseconds, the time being recorded as a reading on a voltmeter. The meter chronometer circuit was used originally to check the counter chronometer for gross errors and later to measure the delay of neutrons captured in S_2 as described lower down.

An important improvement in the general behaviour of the apparatus was effected by stabilizing the alternating current mains input. It was found that certain of the electronic circuits, notably the fast discriminators, were sensitive to changes in the heater potentials. With the mains input stabilizer in operation the daily adjustments of discriminator settings were found unnecessary.

As the counting rate of the S_2 scintillator played such an important part in determining the background of chance coincidences, a record of its mean value for each run was obtained by a message register in the camera box. This message register recorded the output of a scaler fed with the pulses (derived from S_2) from the trigger circuit. The counter chronometer was found to be reliable. Checks were made every day but adjustments were not necessary at more than monthly intervals. As described in I the apparatus was kept running continuously and was recording useful information for more than 90% of the time.

§ 3. ANALYSIS

The counter chronometer readings were analysed in the way described in I. It was found best to determine the background counts by calculations from the various counting rates which could be determined very accurately. In this way the uncertainty in the muon lifetime resulting from the uncertainty in the estimate of the chance background was very small indeed. After deduction of the chance background, the counts in the later channels were the results of positive muons decaying with a mean lifetime of 2·2 μsec. The observed number of these counts and the known lifetime made it possible to estimate the number of positive muons at the zero of time. The final estimate of this quantity was made by successive approximations so that the number of positive muon decays plus the number of negative muon decays exactly equalled the total number of decays observed. It was not necessary to know the negative muon lifetime for this part of the analysis, since it was so much shorter than the length of the acceptance gate used.

With the estimate of the positive muon contamination decided upon, the mean lifetime of the negative muons was found using the analysis suggested by Peierls (1935). The signal-to-noise ratio of the apparatus was defined as the ratio of negative muon counts to all other counts at the start of the acceptance gate. This quantity was given the symbol λ by Peierls and for our apparatus varied between 4 and 6. A further correction to the lifetime was found to be necessary on account of a slight excess of counts in the first channel of the records which was similar to that reported by Meyer (1954). As no lead filter was used in the present experiment, the effect was slight and was estimated after a background run using a target of aluminium of similar stopping power to the targets used for the main runs.

§ 4. NEUTRON DETECTION

The original aim of the experiment was to make a direct detection and identification of the neutrons emitted following muon absorption by means of the scintillator S_2. As described in I, this was found to be very difficult. There are few cadmium salts which will remain in solution with a satisfactory scintillator and it was also found that the methanol, needed to keep the cadmium salt in solution, attacked the window seal very rapidly. However, S_2 was fitted with a new type of window, which has already been described (Tennent 1959) and a reasonable specimen of cadmium octoate was obtained.

With S_2 seeded with cadmium, the following selection scheme was used. Following a $G_1S_1\bar{G}_2\bar{S}_2$ coincidence, an $S_2\bar{G}_2$ event was required followed by a further $S_2\bar{G}_2$ event. This first $S_2\bar{G}_2$ pulse would then be the result of ionization in S_2 from protons knocked on by the incoming neutron while the second $S_2\bar{G}_2$ pulse would result from the γ-rays emitted following the capture of the thermalized neutron by a cadmium nucleus. To allow time for the neutron to be captured by a cadmium nucleus, the second gate was set at 20 μsec. With this arrangement a signal-to-noise ratio of about 30 was obtained but the counting rate was very slow. To improve the counting rate, the G_2 tray was removed and the target rested directly on top of S_2 giving an improved geometry; the apparatus being triggered on a $G_1S_1\bar{S}_2 \ldots S_2 \ldots S_2$ selection. A run on zinc was made with this arrangement but it was found that the overall time to obtain a lifetime measurement accurate to 5% was as long as that when neutron selection was not used.

This disappointing result is very probably attributable to the discoloration of the neutron scintillator. The cadmium octoate used was discoloured and the made-up scintillator was distinctly brown. Ronzio *et al.* (1958) report a very good neutron scintillator and it is likely that such a solution would have enabled a rapid and accurate lifetime measurement using the arrangement described above. It was found that the background in the zinc run was essentially flat and showed no evidence of positive muon contamination.

The meter chronometer circuit was used to measure the intervals between the two S_2 pulses in order to obtain some estimate of the neutron slowing down and capture times. Not many results were obtained, but it was found that the most probable capture time was about 7·5 μsec confirming that the gatelength of 20 μsec chosen was suitable. This value is to be compared with that of Reines *et al.* (1954) who found amost probable capture time of 4 μsec for a scintillator having a cadmium concentration about twice that used in this experiment.

The recent investigations of Litherland *et al.* (1959) indicate that the identification of neutrons by the shape of the pulses produced in S_2 might have been a better method since a smaller and more efficient scintillator would have served.

§ 5. OTHER EXPERIMENTS

5.1. *Geiger Counter Delays*

As an exercise for the counter chronometer, the delays between the S_1 pulses and the coincident G_1 pulses were measured. The delays were rather longer than quoted by other writers (den Hartog 1949, Picard and Rogozinski 1954) as the quenching circuit used was not very sensitive and triggered rather late. The distribution of delays was approximately Gaussian with a most probable delay of 0·52 μsec having width at half height of 0·20 μsec. Using a circuit of faster response to trigger the counter chronometer 'stop' pulse reduced the most probable delay to 0·12 μsec with a width at half-height of 0·15 μsec.

5.2. *Photomultiplier After-pulse Delays*

By adjusting the selection scheme, it was possible to time the intervals between a coincidence pulse in two of the S_2 photomultipliers and a delayed pulse from the third photomultiplier. Since the counting rates were not very high, most of the pulses occurring in the third photomultiplier within a short time of the coincidence pulse from the other two were 'after-pulses'. That is, the event which produced the coincidence pulse in the photomultipliers also produced a pulse in the second photomultiplier, followed by an after-pulse. The distribution of after-pulse delays was approximately exponential with a mean lifetime of 3·5 μsec; there seemed to be some evidence of fine structure in the decay curve which might fit in with the suggestions of Allen *et al.* 1954 that successive after-pulses are caused by different positive ions striking the photocathode.

§ 6. RESULTS

The mean lifetimes of negative muons in the elements investigated are shown in table 1. The interaction rates in column 5 are calculated according to eqn. (1) assuming $\Lambda_d^- = (4{\cdot}52 \pm 0{\cdot}03) \times 10^5\,\mathrm{sec}^{-1}$ while those in column 6 have been calculated using the weighted mean value of Λ_d^- referred to above: the value used being shown in column 7. In table 2, the results of this experiment are compared with those of other workers in the same field. It can be seen that the agreement is satisfactory.

Table 1. The Results of Lifetime Measurements

Element	No^-	λ	τ^-(ns)	$\Lambda_i^- - (1)$ $(\times 10^{-5}\ \mathrm{sec}^{-1})$	$\Lambda_i^- - (2)$ $(\times 10^{-5}\ \mathrm{sec}^{-1})$	Λ_d^- $(\times 10^{-5}\ \mathrm{sec}^{-1})$
Cr (24)	2120	3·7	268 ± 16	$32{\cdot}8 \pm 2{\cdot}3$	$43{\cdot}4 \pm 3{\cdot}6$	$5{\cdot}33 \pm 0{\cdot}14$
Mn (25)	2163	3·9	251 ± 14	$35{\cdot}3 \pm 2{\cdot}2$		
Fe (26)	1441	4·0	205 ± 14	$44{\cdot}2 \pm 3{\cdot}3$		
Co (27)	2042	4·2	196 ± 11	$46{\cdot}4 \pm 2{\cdot}9$		
Ni (28)	1766	4·1	160 ± 10	$58{\cdot}1 \pm 3{\cdot}8$		
Cu (29)	2899	5·5	168 ± 7	$54{\cdot}9 \pm 2{\cdot}5$	$54{\cdot}9 \pm 2{\cdot}9$	$4{\cdot}50 \pm 0{\cdot}14$
Zn (30)	528	12·5	151 ± 13	$61{\cdot}7 \pm 5{\cdot}3$	$61{\cdot}9 \pm 5{\cdot}8$	$4{\cdot}34 \pm 0{\cdot}23$

In column 5, the interaction rates are calculated from eqn. (1) assuming $\Lambda_d^- = (4{\cdot}52 \pm 0{\cdot}03) \times 10^{-5}\ \mathrm{sec}^{-1}$. In column 6, interaction rates are calculated using the value of Λ_d^- shown in column 7. The decay rates in column 7 are the weighted means of the measurements of Astbury *et al.* (1959), Holmstrom and Keuffel (1959) and Lundy *et al.* (1958).

Table 2. Measurements and Calculations of Interaction Rates

Element	Sens (1959)	Astbury *et al.* (1958)	Present work	Primakoff	Tolhoek and Luyten (Fermi)	Tolhoek and Luyten (G-T)
Cr (24)	$32{\cdot}4 \pm 0{\cdot}8$		$32{\cdot}8 \pm 2{\cdot}3$	35·1	33	23
Mn (25)	$36{\cdot}7 \pm 0{\cdot}8$	$40{\cdot}4 \pm 0{\cdot}8$	$35{\cdot}3 \pm 2{\cdot}2$	36·7	36	24
Fe (26)	$45{\cdot}3 \pm 1{\cdot}0$		$44{\cdot}2 \pm 3{\cdot}3$	45·6	43	28
Co (27)		$50{\cdot}6 \pm 0{\cdot}9$	$46{\cdot}4 \pm 2{\cdot}9$	46·6	47	29
Ni (28)	$60{\cdot}3 \pm 1{\cdot}4$	$61{\cdot}6 \pm 1{\cdot}2$	$58{\cdot}1 \pm 3{\cdot}8$	61·7	56	34
Cu (29)	$57{\cdot}9 \pm 1{\cdot}6$	$60{\cdot}0 \pm 0{\cdot}8$	$54{\cdot}9 \pm 2{\cdot}5$	54·9		
Zn (30)	$57{\cdot}6 \pm 1{\cdot}7$		$61{\cdot}7 \pm 5{\cdot}3$	61·6		

All interaction rates are in units of $10^5\ \mathrm{sec}^{-1}$. The two estimates of Tolhoek and Luyten assume the radius of the nuclear potential well to be

$$1{\cdot}40 \times 10^{-13}\, A^{1/3}\ \mathrm{cm}.$$

The experimental results are all calculated assuming

$$\Lambda_d^- = (4{\cdot}52 \pm 0{\cdot}03) \times 10^5\ \mathrm{sec}^{-1}.$$

§ 7. COMPARISON WITH THEORY

Tolhoek and Luyten (1957) have considered the elements $Z = 20$ to $Z = 28$ and have predicted the interaction rates (relative to calcium) on the basis of Gamow–Teller couplings and of Fermi couplings for the interaction. The results presented here weigh against the Fermi interaction in every case but it is doubtful if the theory is sufficiently refined to give a definite answer on this question yet. Tolhoek (1958) has considered the different theories of muon production and shown that the rather general interpolation formulae which have been suggested (e.g. Primakoff 1955) cannot be used with confidence for individual elements as the assumptions are so crude. For comparison, the predictions of Primakoff's formula and the two extreme assumptions of Tolhoek and Luyten are also shown in table 2.

Primakoff's interpolation formula is as follows:

$$\Lambda_1^- = A(Z_{\text{eff}})^4[1-\delta(A-Z)/2A]$$

and the constants used have been suggested by Sens (1959) $A = 188\,\text{sec}^{-1}$, $\delta = 3\cdot15$. The effective charge of the nucleus, Z_{eff}, has been calculated using the interpolation formula of Hillas (1958)

$$Z_{\text{eff}} = Z[1+(Z/42\cdot0)^{1\cdot47}]^{-1/1\cdot47}.$$

The interaction rates predicted by Tolhoek and Luyten have been calculated assuming the value for the interaction rate of negative muons in calcium to be $(25\cdot5 \pm 0\cdot5) \times 10^5\,\text{sec}^{-1}$ as found by Sens.

§ 8. Conclusions

The interaction rates for negative muons brought to rest in the elements $Z=24$ to $Z=30$ have been determined to an accuracy of 5–6%. The source of the negative muons was the cosmic radiation. An apparatus has been developed which detected negative muons with sufficient efficiency to enable results with accuracies of the above order to be obtained in 20 days.

Acknowledgments

We are indebted to the following firms for the loan of the large quantities of target material required. Messrs. Thomas Marshall, Leeds (zinc); Mond Nickel (nickel); Murex Ltd. (chromium); Rhokana Corporation Ltd., Northern Rhodesia (cobalt); and Union Carbide Ltd. (manganese). Messrs. Johnson-Matthey went to great trouble to supply the cadmium octoate.

We are grateful to Professor Wilson for his encouragement and to Dr. A. M. Hillas who set up much of the apparatus used. One of us (W. B. G.) is indebted to the University of Leeds for a Henry Ellison Fellowship held for part of the time during which this work was done.

References

Allen, J. S., Bergstein, J., Best, G. H., Houtz, H. E., Hoyt, H. C., and Mueller, D. W., 1954, *Nucleonics*, **12,** No. 3, 27.

Astbury, A., Kemp, M. A. R., Lipman, N. H., Muirhead, H., Voss, R. G. P., Zangger, C., and Kirk, A., 1958, *Proc. phys. Soc. Lond.*, **72,** 494.

Astbury, A., Hussein, M., Kemp, M. A. R., Lipman, N. H., Muirhead, H., Voss, R. G. P., and Kirk, A., 1959, *Proc. phys. Soc. Lond.*, **73,** 314.

Barrett, W. A., Holmstrom, F. E., and Keuffel, J. W., 1959, *Phys. Rev.*, **113,** 661.

Bell, W. E., and Hincks, E. P., 1951, *Phys. Rev.*, **84,** 1243.

den Hartog, H., 1949, *Nucleonics*, **5,** No. 3, 33.

Hillas, A. M., 1958, Thesis, Leeds University.

Hillas, A. M., Gilboy, W. B., and Tennent, R. M., 1958, *Phil. Mag.*, **3,** 109.

Hillas, A. H., and Tennent, R. M., 1958, *Nucl. Instrum.*, **3,** 344.

Holmstrom, F. E., and Keuffel, J. W., 1958, *Bull. Amer. phys. Soc.*, **3,** 408.

Litherland, A. E., Almqvist, E., Batchelor, R., and Gove, H. E., 1959, *Phys. Rev., Letters*, **2,** 104.

Lundy, R. A., Sens, J. C., Swanson, R. A., Telegdi, V. L., and Yovanovitch, D. D., 1958, *Phys. Rev., Letters*, **1,** 102.

Meyer, A. J., 1954, Thesis, Princeton University (unpublished).

Peierls, R. E., 1935, *Proc. roy. Soc.* A, **149,** 467.

Picard, E., and Rogozinski, A., 1954, *J. Phys. Radium*, **15,** 767.

Porter, C. E., and Primakoff, H., 1951, *Phys. Rev.*, **83,** 849.

Primakoff, H., 1955, Proceedings of the 5th Rochester Conference, 174.

Reines, F., Cowan, C. L., Harrison, F. B., and Carter, D. S., 1954, *Rev. sci. Instrum.*, **25,** 1061.

Ronzio, A. R., Cowan, C. L., and Reines, F., 1958, *Rev. sci. Instrum.*, **29,** 146.

Sens, J. C., 1959, *Phys. Rev.*, **113,** 679.

Sens, J. C., Swanson, R. A., Telegdi, V. L., and Yovanovitch, D. D., 1957, *Phys. Rev.*, **107,** 1464.

Tennent, R. M., 1959, *J. sci. Instrum.*, **36,** 148.

Tolhoek, H. A., and Luyten, J. R., 1957, *Nucl. Phys.*, **3,** 679.

Tolhoek, H. A., 1958, *Nucl. Phys.*, **10,** 606.

The Observation of Domain Structure in Magnetic Thin Films by Means of the Kerr Magneto-Optic Effect†

By M. Prutton
International Computers and Tabulators Ltd., Stevenage

[Received April 28, 1959]

Abstract

An apparatus is described in which the ferromagnetic domain structure in a polished surface is made clearly visible. Sufficient contrast is obtained by blooming the metal surface and by using a quarter wave plate in the viewing telescope.

Some results are described in which a film of 81 : 19 nickel iron containing a domain structure was subjected to a steady field at right angles to the anisotropy axis. These observations show that simple Bloch domain walls are not occurring and that the magnetization reversal process can proceed by simultaneous domain growth and rotation of the magnetization vectors within the domains.

§ 1. Introduction

The rotation of the plane of polarization of light reflected at the surface of a magnetized body was first used to investigate the ferromagnetic domain structure in a cobalt crystal by Williams *et al.* (1951). Subsequently Fowler and Fryer (1954, 1955, 1956) and Fowler *et al.* (1956) described the use of the longitudinal Kerr effect (the special case in which the magnetization lies in the reflecting surface and in the plane of incidence) and the Faraday effect for studying the domain structure in ferromagnetic thin films. However, the experimental techniques have been very difficult because the magnitude of the rotation is of the order of only five minutes of arc. Consequently, when the metal surface is viewed between crossed nicols the resultant image of the domain structure is one of both extremely low contrast between adjacent domains and very low brightness. Furthermore, pits, scratches and other surface imperfections cause local variations of the reflected intensity which are often greater than the contrast between adjacent domains.

Fowler and Fryer overcame this latter difficulty by combining a transparent positive photograph of the magnetically saturated surface with a transparent negative of the same surface but now containing a domain structure. By viewing this pair of photographs in transmitted light the effects of surface imperfections could be made to cancel out and the domain structure was more clearly revealed.

---

† Communicated by the Author.

This difficult photographic method can be avoided by using a blooming process first suggested by Kranz (1956) and Kranz and Drechsel (1958). If light is incident upon the magnetic surface with its plane of polarization perpendicular to the plane of incidence then Kranz and Drechsel assume that the reflection process results in a component of amplitude R with unchanged plane of polarization due to ordinary metallic reflection and a Kerr component of amplitude K polarized in the plane of incidence. If the phase difference between K and R is zero then the Kerr rotation is given by the angle between R and the vector sum of K and R. Kranz and Drechsel have shown both theoretically and experimentally that the effective Kerr rotation can be made as much as three times larger by blooming the metal surface with a quarter wavelength layer of a high refractive index dielectric such as zinc sulphide so that the amplitude of the normally reflected component R is reduced.

It has been shown in this laboratory that the contrast between adjacent domains can be further enhanced by using the fact that plane polarized light is rendered elliptically polarized in ordinary metallic reflection. This means that the vector sum of K and R is not necessarily a plane polarized wave and so exact crossing of the nicols does not give complete extinction of the transmitted light. If a quarter wave plate is inserted in the optical system before the analyser nicol the elliptically polarized beam from the metal surface can be made plane polarized and so more nearly perfect crossing of the nicols can be achieved.

§ 2. METHOD

The nickel–iron film to be investigated was mounted in a vacuum system in such a way that the intensity of green light reflected from the film at an angle of incidence of 60° could be measured while a dielectric layer was being evaporated onto it. This light covered a fairly broad spectral band as the light from a tungsten filament source was rendered green with a Wratten filter. It was then made plane polarized with a piece of suitably orientated polaroid film. Evaporation of the dielectric was continued until a minimum was observed in the intensity of the reflected beam. This method gave a dielectric layer of the correct thickness for the effective Kerr rotation to be as large as possible.

A schematic diagram of the domain viewing apparatus is shown in fig. 1. The light from a 50 w high-pressure mercury lamp was passed through an evaporated film filter of 150 Å bandwidth in order to isolate the green mercury line of 5461 Å wavelength. It was then collimated and passed through the polarizing prism and onto the reflecting surface at an angle of incidence of 60°. Both polarizer and analyser were Glan–Thompson prisms of 12 mm square aperture with a very good extinction ratio. The sample surface was viewed with a telescope using an $f2{\cdot}5$, seven inch focal length objective and a × 10 eyepiece. A mica quarter-wave plate mounted in strain free glass and the analyser prism were placed between these two components. It was found very important that the light should be monochromatic and well collimated because dispersion in the system is such that stray light from the mercury yellow lines and scattered light can seriously impair the contrast between adjacent domains.

Figure 2 (Pl. 127) shows a domain boundary in a film coated on one side with silicon monoxide (refractive index about 1·9) and on the other side with zinc sulphide (refractive index about 2·3). The centre strip is uncoated. Clearly the contrast is best when the film is coated with the dielectric of highest refractive index, while the domain pattern is barely discernable in the uncoated portion.

Fig. 1

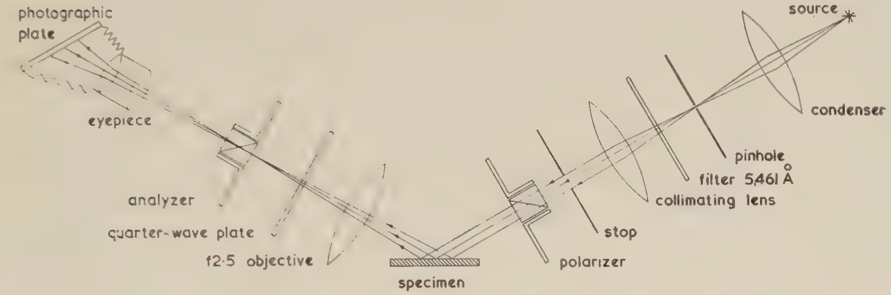

A schematic representation of the domain viewing apparatus.

§ 3. SOME OBSERVATIONS OF DOMAINS IN NICKEL–IRON THIN FILMS

Figures 3 (Pl. 128) and 4 (Pl. 129) and figs. 5 (Pl. 130) and 6 (Pl. 131) show the domain structure in a 1 cm diameter circle of 81 : 19 nickel–iron about 1500 Å thick. This film showed fairly good uniaxial behaviour (see Bradley and Prutton 1959) and was typical of the films in this composition range which have been studied in the domain viewing apparatus.

Figure 3 (Pl. 128) shows a typical domain structure which was formed by saturating the film in one direction and then applying a reverse field with a magnitude of just the coercivity. The film appears to be elliptical because the oblique incidence results in a magnification which is greater in the transverse than in the longitudinal direction. The anisotropy axis lies along the minor axis of the elliptical image so that the domains are magnetized in an antiparallel array along this direction. The first point which is immediately obvious is that the domain boundaries do not appear to be simple 180° or 90° walls but have complicated shapes. Secondly, if the same reversing field is applied several times to the saturated film then the resulting domain pattern is quite different every time. Thus it would seem that if the wall shape is determined by imperfections or grain boundaries then there are many energetically equivalent configurations and the walls need not stop at the same imperfections at each partial reversal of the magnetization.

In fig. 4 (Pl. 129), the field used to introduce the domain structure has been switched off and a field of 3·6 oersteds (or 0·78 of the anisotropy field) applied along the ‘hard direction’, i.e. at right angles to the anisotropy axis. The position of the walls is substantially unaffected but the contrast has noticeably diminished. This is interpreted as meaning that the magnetization vector in each domain has rotated towards the direction of the applied field and so the walls must have changed their structure. There was not sufficient magnification available to study the wall shape in detail. The conclusion that the magnetization within domains can rotate so that the boundary is neither a 180° nor a 90° wall is supported by the evidence given by Fuller (1958) who used the Bitter colloid technique on similar films. On removing the hard direction field the domain structure reverted to the form and contrast of fig. 3 (Pl. 128).

If a larger field is applied to the film in the hard direction the existing walls start to break up and do not revert to their original form when the field is removed. Such a situation is shown in fig. 5 (Pl. 130) for a field of 4·6 oersteds (0·96 of the anisotropy field) and in fig. 6 (Pl. 131) for a field of 4·8 oersteds. The domains in fig. 6 (Pl. 131) appear to be very thin needles but there was not sufficient magnification available to decide if these domain structures were associated with the ‘cross-tie’ walls observed by Huber *et al.* (1958), the double Bloch walls described by Williams and Sherwood (1947) or some other configuration.

§ 4. Conclusions

The Kerr magneto-optic effect alone is so small that it does not provide a very useful tool for the investigation of surface domain structure. However, if the metal surface is bloomed and a quarter-wave plate is introduced the ordinary metallic reflection can be reduced to such a level that the effective Kerr rotation is of the order of one degree and so the contrast between adjacent domains is raised to a useful level. The technique is then particularly valuable in that it provides an inertialess method of investigating ferromagnetic domain structure. Furthermore, unlike the Bitter colloid technique, it reveals domains rather than domain boundaries and by the accurate measurement of intensity a measure of the direction of magnetization could be made.

The observations on thin films of nickel–iron alloys in 81 : 19 region of composition reveal that complicated domain structures are possible as well as coherent magnetization rotation and that domain boundaries of the 180° and 90° type are not necessarily the only ones which can occur.

Acknowledgments

The author would like to take this opportunity of thanking the Directors of International Computers and Tabulators Limited for their permission to publish this paper and for providing the facilities for carrying out this research He would also like to thank Mr. J. Wells for his assistance

with the construction and operation of the Kerr apparatus and Mr. P. Astwood and Misses Farrar and Whyman who prepared and bloomed the films.

REFERENCES

BRADLEY, E. M., and PRUTTON, M. J., 1959, *J. Electron. Contr.*, **6,** 81.

FOWLER, C. A., and FRYER, E. M., 1954, *Phys. Rev.*, **94,** 52; 1955, *Ibid.*, **100,** 746; 1956, *Ibid.*, **104,** 552.

FOWLER, C. A., FRYER, E. M., and STEVENS, J. R., 1956, *Phys. Rev.*, **104,** 645.

FULLER, C. E., 1958, Proceedings of the International Conference on Magnetism, Grenoble.

HUBER, E. E., SMITH, D. O., and GOODENOUGH, J. B., 1958, *J. appl. Phys.*, **29,** 294.

KRANZ, J., 1956, *Naturwissenschaften*, **43,** 370.

KRANZ, J., and DRECHSEL, W., 1958, *Z. Phys.*, **150,** 632.

WILLIAMS, H. J., FOSTER, F. G., and WOOD, E. A., 1951, *Phys. Rev.*, **82,** 119.

WILLIAMS, H. J., and SHERWOOD, R. C., 1947, *J. appl. Phys.*, **28,** 548.

The 'Waveguide Mode' Theory of Radio Wave Propagation when the Ionosphere is not Sharply Bounded†

By D. W. Barron
University Mathematical Laboratory, Cambridge

[Received April 22, 1959]

Abstract

The propagation of radio waves to great distances can be treated by considering the space between the earth and the ionosphere as a waveguide and discussing the properties of the various waveguide modes. Previous authors have generally assumed that the upper boundary of the waveguide is a sharply bounded homogeneous ionosphere. The paper describes a method of calculating the mode characteristics for any horizontally stratified ionosphere in which the electron density and collision frequency vary with height in some arbitrary prescribed manner. The theory is given in full for a flat, perfectly conducting earth with no magnetic field, and its extension is outlined in an appendix.

The paper presents the results of some calculations carried out on EDSAC 2, the automatic digital computer at the University Mathematical Laboratory, Cambridge. The effect on the waveguide modes of changing from a sharp to a gradual boundary on an otherwise homogeneous ionosphere is investigated by considering a variation of electron density (N) with height (z) according to the law

$$N=N_0(1+\tanh\beta(z-h))$$

using a range of values of β, and mode characteristics are also calculated for an ionosphere in which the electron density increases exponentially with increasing height. The effect on the waveguide modes of changes in the parameters of the exponential model, and the difference between the modes for vertical and horizontal polarization are described.

§ 1. Introduction

When discussing the propagation of very low-frequency radio waves to great distances from the sender it is convenient to treat the space between the earth and the ionosphere as a waveguide. Several authors have considered the calculation of the attenuation, phase velocity and excitation factor for the various modes, but in almost all cases the assumption is made that the ionosphere has a sharp lower boundary and is semi-infinite in extent. At night in particular the assumption of a sharp boundary is not valid, and for frequencies below 1 kc/s it has been suggested (Wait 1958) that the E-layer does not behave as a semi-infinite medium.

Wait (1958) has extended the theory in an attempt to remove these restrictions. He has considered a model in which the ionosphere is represented by two discrete homogeneous layers with a sharp lower boundary and a sharp transition, and a model in which the variation of electron density with height is of the form

---

† Communicated by the Author.

$$N = N_0 \exp(-\alpha(z-h)), \qquad z \geqslant h,$$
$$N = 0, \qquad z < h.$$

Shmoys (1956) has derived analytic expressions for the mode characteristics for an isotropic ionosphere in which electron density and collision frequency vary exponentially with height, for horizontal polarization, and Budden (1957 a) has suggested a general method of calculation for any ionosphere. The method described in this paper, which is derived from another suggestion of Budden (1957 b) can be used to calculate the mode characteristics when the upper medium is a horizontally stratified ionosphere in which the electron density and collision frequency vary continuously with height in any specified way, and thus removes both the limitations of the theory described above. The method can take account of the earth's magnetic field and the curvature of the earth, but the calculations described in the paper are restricted to the simple case of a flat, perfectly conducting earth with no magnetic field.

The method is described in outline in §§ 3 and 4, and the detailed equations are derived in § 5. In § 6 the results are compared with those obtained using Shmoys' method, and §§ 7 and 8 present the results of some calculations which have been carried out on EDSAC 2, the automatic digital computer at the University Mathematical Laboratory, Cambridge.

§ 2. NOTATION

All electric and magnetic quantities are in rationalized units. The more important symbols are collected here for reference.

x, y, z	Cartesian coordinates: z is measured vertically upwards.
ω	$2\pi \times$ frequency of waves.
c	velocity of electromagnetic waves in free space.
k	$\omega/c = 2\pi/\lambda$ (where λ is the wavelength in free space).
s	kz.
ϵ_0	electric permittivity of free space.
μ_0	magnetic permittivity of free space.
Z_0	characteristic impedance of free space $(=(\mu_0/\epsilon_0)^{1/2})$.
e	charge on electron.
m	mass of electron.
N	electron density.
ν	collision frequency of electrons.
X	$Ne^2/\epsilon_0 m\omega^2$.
Z	ν/ω.
U	$1 - iZ$.
ψ	angle between wave normal and vertical.
C	$\cos\psi$.
S	$\sin\psi$.
μ	complex refractive index of ionosphere.

q	$(\mu^2-S^2)^{1/2}$.
E_x, E_y, E_z	components of electric field vector of wave.
H_x, H_y, H_z	components of magnetic field vector of wave.
$\mathscr{H}_x, \mathscr{H}_y, \mathscr{H}_z$	$Z_0(H_x, H_y, H_z)$.
R	reflection coefficient of ionosphere.
V	wave impedance (defined in § 5).
W	$\partial R/\partial C$.
Q	$\partial V/\partial C$.
$\mathscr{R}$	real part.
$\mathscr{I}$	imaginary part.
	A prime (′) indicates differentiation with respect to s.

§ 3. OUTLINE OF THE METHOD

The method is described here for a flat earth with no magnetic field. The extension to the general case is outlined in an appendix. If the earth is flat, the field in the waveguide mode may be considered to be made up of the fields of two plane waves, one of which is converted into the other by reflection at the ionosphere. For the nth mode, let the wave normals make an angle ψ_n with the vertical, and let $C_n=\cos\psi_n$, $S_n=\sin\psi_n$. C_n and S_n are in general complex. If the reflection coefficient of the ionosphere, measured at the ground, is $R(C)$ and the reflection coefficient of the ground is $R_g(C)$, then since after reflection at the ionosphere and subsequently at the ground the wave must be unchanged, the condition for a self-consistent mode is

$$R(C)\,.\,R_g(C)=1. \tag{1}$$

The problem is thus to find values of C which make eqn. (1) true. The mode characteristics may then be derived immediately using the relations (Budden 1951):

$$\left.\begin{aligned}\text{attenuation factor}&=(\omega/C)\mathscr{I}(S_n),\\ \text{excitation factor}&=\omega S_n,\\ \text{phase velocity}&=C/\mathscr{R}(S_n).\end{aligned}\right\} \tag{2}$$

For a homogeneous perfectly conducting earth the reflection coefficient of the ground is independent of C, being ± 1 according to the wave polarization: eqn. (1) then becomes

$$R(C)=\pm 1. \tag{1a}$$

It is possible to define a function of height $R(z)$ whose value at the ground is $R(C)$ which satisfies a first-order differential equation of the form (Budden 1955)

$$\partial R/\partial z=f(z, R, C) \tag{3}$$

which can be integrated numerically using an automatic digital computer. We require to find values of the parameter C which lead to a value of $R(C)$ satisfying eqn. (1 *a*). This can be done by successive approximations as follows. Let

$$W=\partial R/\partial C \tag{4}$$

and differentiate eqn. (3) with respect to C, thus obtaining a further equation of the form

$$\partial W/\partial z = g(z, R, C, W) \qquad . \quad . \quad . \quad . \quad . \quad . \quad . \quad (5)$$

which can be integrated simultaneously with eqn. (3) to give R and $\partial R/\partial C$ at the ground for a particular value of C. Equations (3) and (5) are not the equations used in the actual calculations: these (eqns. (13) and (16)) are similar and closely related. They are derived in § 5 below.

Now for the nth mode we have (eqn. (1 *a*))

$$R(C_n) = \pm 1.$$

Then to a first order,

$$R(C) = \pm 1 + \left(\frac{\partial R}{\partial C}\right)(C - C_n)$$

or

$$C_n = C - \left[\frac{R(C) \mp 1}{(\partial R/\partial C)}\right]. \qquad . \quad . \quad . \quad . \quad . \quad . \quad . \quad (6)$$

Starting with any value of C we can calculate R and $\partial R/\partial C$ at the ground by integrating eqns. (3) and (5), then using eqn. (6) obtain an approximate value of C_n. This value can be put into eqns. (3) and (5) to obtain new values of R and $\partial R/\partial C$ from which an improved value of C_n can be calculated. In this way we can obtain the value of C_n to the desired degree of accuracy by a series of successive approximations.

§ 4. THE ORDER OF THE MODES

The process outlined in the previous section can be used to calculate self-consistent values of C_n, but does not of itself give any indication of the order, n, of the mode. This can be found by evaluating a contour integral often called the 'phase integral'. It can be shown (Heading 1953) that the reflection coefficient of a slowly varying medium is

$$R = i \exp\left[-2ik \int_0^{z_0} q\, dz\right] \qquad . \quad . \quad . \quad . \quad . \quad (7)$$

where $q^2 = \mu^2 - S^2$ and the integral extends along a suitable contour in the complex-z plane from the ground at $z = 0$ to the complex value of z which makes $q = 0$. The zero of q chosen is that lying nearest the real-z axis on the negative imaginary side. Since q and z_0 are functions of C, R is a function of C also. For a self-consistent mode $R = \pm 1$ (eqn. (1 *a*)), the sign chosen depending on the polarization of the wave, and it follows that

$$\frac{2}{\lambda}\int_0^{z_0} q\, dz \mp \tfrac{1}{4} = n \qquad . \quad . \quad . \quad . \quad . \quad . \quad . \quad (8)$$

where n is an integer. It is convenient to choose the contour to lie on the real-z axis from 0 to $\mathscr{R}(z_0)$ and then to run parallel to the imaginary-z axis from $\mathscr{I}(z) = 0$ to $\mathscr{I}(z) = \mathscr{I}(z_0)$. Although eqn. (8) is only strictly true for a slowly varying ionosphere it is in most cases sufficiently accurate to give the relative ordering of the modes.

§ 5. THE METHOD IN DETAIL

The reflection coefficient of the ionosphere measured at the ground may be written in the form

$$R(C)=R_h(C)\,.\exp(-2ikhC) \quad \text{. . . . (9)}$$

where R_h is the reflection coefficient at the base of the ionosphere which is at a height h above the ground, and the exponent $2khC$ arises from the change of complex phase which occurs when the wave makes the double journey from the ground to the ionosphere and back. Time can be saved in the numerical computation if R_h is found by integration of the differential equation, and R is then obtained by multiplication by the exponential. The calculation of R_h can be simplified by the use of the concept of wave impedance (Barron and Budden 1959), and this method is employed. Barron and Budden in fact worked in terms of wave admittance, which is the reciprocal of the wave impedance: this is a matter of convenience, and involves no important difference of principle. For an isotropic ionosphere the differential equations satisfied by the horizontal components of the total electromagnetic field separate into two pairs, one involving E_x, $\mathscr{H}_y$ only, and the other involving E_y, $\mathscr{H}_x$ only, thus:

$$\left.\begin{aligned} E_x' &= -i(1-S^2/\mu^2)\mathscr{H}_y, \\ \mathscr{H}_y' &= -i\mu^2 E_x. \end{aligned}\right\} \quad \text{. . . . (10)}$$

$$\left.\begin{aligned} E_y' &= i\mathscr{H}_x, \\ \mathscr{H}_x' &= i(\mu^2-S^2)E_y, \end{aligned}\right\} \quad \text{. . . . . . (11)}$$

where μ is the complex refractive index given by $\mu^2=1-X/U$. The waves represented by eqns. (10) and (11) are often described as vertically and horizontally polarized respectively, and the subsequent derivation is carried out in parallel for the two cases. We define the wave impedance by

$$\left.\begin{aligned} V_1 &= E_x/\mathscr{H}_y, \\ V_2 &= E_y/\mathscr{H}_x. \end{aligned}\right\} \quad \text{. . . . . . . (12)}$$

Differentiating, and using eqns. (10) and (11) we obtain

$$\left.\begin{aligned} iV_1' &= (1-S^2/\mu^2)-\mu^2V_1^2, \quad \text{(Vertical polarization),} \\ iV_2' &= (\mu^2-S^2)V_2^2-1, \quad \text{(Horizontal polarization).} \end{aligned}\right\} \quad \text{. . (13)}$$

It can further be shown (Barron and Budden 1959) that the reflection coefficient is given in terms of the wave impedance† by

$$\left.\begin{aligned} R_1 &= \frac{C-V_1}{C+V_1}, \\ R_2 &= \frac{CV_2+1}{CV_2-1}, \end{aligned}\right\} \quad \text{. . . . . (14)}$$

and we can therefore calculate $R_h(C)$ by the integration of eqns. (13).

---

† The derivation in § 4 of Barron and Budden's paper was carried out in terms of the admittance, A, which is equal to $1/V$.

We can simultaneously calculate $\partial R/\partial C$, for let

$$\left.\begin{aligned} Q_1 &= \frac{\partial V_1}{\partial C}, \\ Q_2 &= \frac{\partial V_2}{\partial C}, \end{aligned}\right\} \quad . \quad . \quad . \quad . \quad . \quad . \quad . \quad . \quad (15)$$

and differentiate eqns. (13) and (14) with respect to C, then

$$\left.\begin{aligned} iQ_1' &= 2C/\mu^2 - 2\mu^2 V_1 Q_1, \\ iQ_2' &= 2CV_2^2 + 2(\mu^2 - S^2) V_2 Q_2, \end{aligned}\right\} \quad . \quad . \quad . \quad . \quad (16)$$

and

$$\left.\begin{aligned} \frac{\partial R_1}{\partial C} &= 2\frac{(V_1 + CQ_1)}{(C+V_1)^2}, \\ \frac{\partial R_2}{\partial C} &= -2\frac{(V_2 - CQ_2)}{(CV_2 - 1)^2}. \end{aligned}\right\} \quad . \quad . \quad . \quad . \quad . \quad . \quad (17)$$

Finally, the values of R and $\partial R/\partial C$ at the ground are given by

$$\left.\begin{aligned} R &= R_h \exp(-2ikhC), \\ \frac{\partial R}{\partial C} &= \left(\frac{\partial R}{\partial C}\right)_h \exp(-2ikhC) \quad -2ikhR. \end{aligned}\right\} \quad . \quad . \quad . \quad . \quad (18)$$

Before eqns. (13) and (16) can be integrated numerically it is necessary to find an initial solution which satisfies the physical conditions at a high level in the ionosphere (Budden 1955). If the electron density increases indefinitely with height then at a high enough level the upgoing W.K.B. solutions are satisfactory, and it is easily shown that the correct initial solutions are

$$\left.\begin{aligned} V_1 &= q/\mu^2, \qquad & Q_1 &= C/\mu^2 q, \\ V_2 &= -1/q, \qquad & Q_2 &= C/q^3. \end{aligned}\right\} \quad . \quad . \quad . \quad . \quad . \quad (19)$$

§ 6. HORIZONTAL POLARIZATION AND EXPONENTIAL INCREASE OF ELECTRON DENSITY

If the electron density varies exponentially with height so that $X = \exp(\alpha(z-h))$, eqns. (11) (which represent horizontally polarized waves) can be solved in terms of Hankel functions, and it can be shown (Shmoys 1956, Heading 1953) that

$$R = -\frac{\Gamma(1-\zeta)}{\Gamma(1+\zeta)} \cdot \left(\frac{\alpha}{k}\right)^{-2\zeta} \cdot (1-iZ)^{-\zeta} \exp(h\alpha\zeta) \quad . \quad . \quad . \quad (20)$$

where $\zeta = 2ikC/\alpha$.

It is possible to find values of C which make $R = -1$ by a process of successive approximations using eqn. (20) and this affords a valuable check on the method described in the previous sections. Tables 1 and 2 show the results of calculations made for two representative ionosphere models by the two methods, and it is seen that there is good agreement.

Table 1. Self-consistent Values of C for Ionosphere in which $X=\exp(0{\cdot}59(z-80))$ (z in km), $Z=30$, Wave Frequency $=16$ kc/s. Horizontal polarization

n	From (20) by successive approximation		By method of § 3	
	$\mathscr{R}(C)$	$\mathscr{I}(C)$	$\mathscr{R}(C)$	$\mathscr{I}(C)$
0	0·10922	0·00367	0·10919	0·00320
1	0·21826	0·00817	0·21824	0·00642
2	0·32700	0·00990	0·32706	0·00966
3	0·43553	0·01312	0·43553	0·01292
4	0·54358	0·01630	0·54358	0·01618
5	0·65115	0·01945	0·65115	0·01940
6	0·86490	0·02563	0·86490	0·02564

Table 2. Self-consistent Values of C for Ionosphere in which $X=\exp(0{\cdot}59(z-80))$ (z in km), $Z=10$, Wave Frequency $=16$ kc/s. Horizontal polarization

n	From (20) by successive approximation		By method of § 3	
	$\mathscr{R}(C)$	$\mathscr{I}(C)$	$\mathscr{R}(C)$	$\mathscr{I}(C)$
0	0·11158	0·00332	0·11157	0·00317
1	0·22303	0·00662	0·22303	0·00636
2	0·33423	0·00988	0·33423	0·00958
3	0·44506	0·01310	0·44506	0·01283
4	0·55544	0·01628	0·55544	0·01609
5	0·66532	0·01942	0·66532	0·01933
6	0·77468	0·02252	0·77468	0·02251

§ 7. THE EFFECT OF CHANGING FROM A SHARP TO A GRADUAL BOUNDARY

In this section the effect on the mode characteristics of changing from a sharply bounded to a gradually bounded homogeneous isotropic ionosphere are described. The calculations have been made for vertically polarized waves at a frequency of 16 kc/s with a constant collision frequency giving $Z=30$. The electron density variation employed is

$$X=\tfrac{1}{2}X_0(1+\tanh\beta(z-h))$$

with $X_0=200$ and $h=80$ km. This is one of the layers discussed by Epstein (1930): for $z\ll h$, $X=0$, for $z\gg h$, $X=X_0$ and the rate of transition between these values can be adjusted within wide limits by suitable choice of the parameter β. The figure shows the variation of X with height for representative values of β.

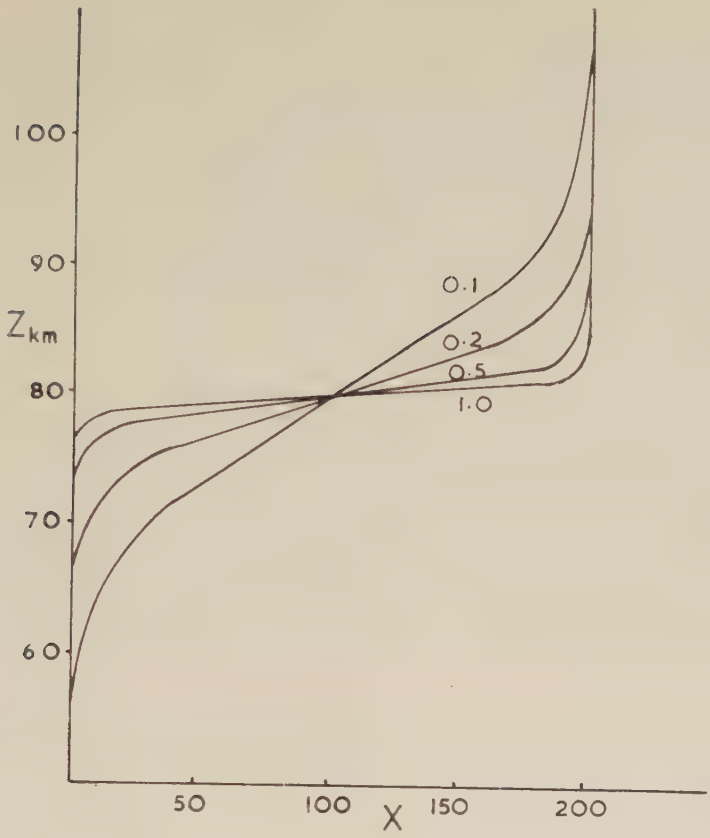

'tanh' profile $X = 100(1 + \tanh \beta(z - 80))$.
(The figure alongside each curve is the value of β.)

Table 3. Real and Imaginary Parts of S_n. $X = 100(1 + \tanh \beta(z - 80))$, ($z$ in km). $Z = 30$

n	$\beta=10$		$\beta=5$		$\beta=1$	
0	0·99811	−0·00028	0·99812	−0·00026	0·99815	−0·00018
1	0·98262	−0·00256	0·98227	−0·00233	0·98320	−0·00166
2	0·94978	−0·00667	0·95045	−0·00628	0·95228	−0·00438
3	0·89743	−0·01037	0·89860	−0·01043	0·90288	−0·00988
4	0·82456	−0·01271	0·82566	−0·01320	0·83057	−0·01609
5	0·72629	−0·01488	0·72715	−0·01557	0·72964	−0·02166
n	$\beta=0·5$		$\beta=0·2$		$\beta=0·1$	
0	0·99813	−0·00017	0·99788	−0·00025	0·99701	−0·00070
1	0·98298	−0·00157	0·98078	−0·00235	0·97376	−0·00641
2	0·95180	−0·00464	0·94595	−0·00698	0·92957	−0·01776
3	0·90246	−0·00996	0·89177	−0·01515	0·86441	−0·03536
4	0·83043	−0·01834	0·81450	−0·02916	0·77498	−0·06464
5	0·72703	−0·02924	0·70450	−0·05438	0·65790	−0·12076

The mode characteristics for a range of values of β are given in table 3. The quantities tabulated are the real and imaginary parts of S since (eqn. (2)) $\mathscr{R}(S)$ determines the phase velocity and $\mathscr{I}(S)$ the attenuation. The characteristics of the zero-order mode are not greatly affected by the change of boundary: the effect on the higher modes becomes greater as the mode order increases. $\mathscr{R}(S)$ remains roughly constant or increases slightly as β is changed from 10 km^{-1} to 0·5 km^{-1}; a further decrease in β causes $\mathscr{R}(S)$ to decrease, indicating an increase in phase velocity. $\mathscr{I}(S)$ increases with decreasing β, indicating that the attenuation increases as the boundary becomes less sharp.

§ 8. Calculations for an Exponential Ionosphere

In this section the results are presented of some calculations made using an ionosphere model in which the electron density increases exponentially with height and the collision frequency is constant. The law of variation is $X = \exp(\alpha(z-h))$, and the effect on the mode characteristics of changing α, h and the collision frequency is investigated for vertically and horizontally polarized waves. All the calculations are for a wave frequency of 16 kc/s and for a flat, perfectly conducting earth with no magnetic field.

8.1. *Comparison of Vertical and Horizontal Polarization*

The values of S for the characteristic modes for an exponential ionosphere in which $\alpha = 0{\cdot}59$ km^{-1}, $h = 80$ km and $Z = 30$ are given in table 4 for vertical and horizontal polarization. $\mathscr{I}(S)$ is always greater in magnitude for vertical polarization than for horizontal polarization indicating a greater attenuation. For the low-order modes $\mathscr{R}(S)$ is also greater for vertical polarization, but this is reversed for the high-order modes. This implies that for the low-order modes the phase velocity is less for vertical than for horizontal polarization.

Table 4. Exponential Model. $X = \exp(0{\cdot}59(z-80))$ (z in km), $Z = 30$

n	Vertical polarization		Horizontal polarization	
	$\mathscr{R}(S)$	$\mathscr{I}(S)$	$\mathscr{R}(S)$	$\mathscr{I}(S)$
0	0·99842	−0·00013	0·99403	−0·00035
1	0·98572	−0·00124	0·97592	−0·00144
2	0·95979	−0·00360	0·94506	−0·00334
3	0·91943	−0·00762	0·90029	−0·00625
4	0·86230	−0·01396	0·83958	−0·01047
5	0·78380	−0·02365	0·75938	−0·01663
6	0·67500	−0·03724	0·65289	−0·02620
7	0·51987	−0·05599	0·50452	−0·04395
8	0·26764	−0·11519	0·26245	−0·10600
9	0·07614	−0·42058	0·08355	−0·40763

8.2. *Effect of Changing Collision Frequency*

Table 5 gives the mode characteristics for the exponential ionosphere with $\alpha = 0{\cdot}59$ km^{-1}, $h = 80$ km, and $Z = 10$. These values of S should be compared with those in table 4 to see the effect of decreasing the collision frequency. The zero-order mode is almost unchanged, and there is progressively greater change in the subsequent modes. The change in S is of the same magnitude for both polarizations. The principal effect of the change in collision frequency is to change $\mathscr{R}(S)$: the change in $\mathscr{I}(S)$ is much smaller. This means that the phase velocity is changed much more than the attenuation. For the low-order modes the phase velocity increases with decreasing collision frequency: the effect is reversed for the high-order modes.

Table 5. Exponential Model. $X = \exp(0{\cdot}59(z - 80))$ (z in km), $Z = 10$

n	Vertical polarization		Horizontal polarization	
	$\mathscr{R}(S)$	$\mathscr{I}(S)$	$\mathscr{R}(S)$	$\mathscr{I}(S)$
0	0·99835	−0·00014	0·99376	−0·00036
1	0·98506	−0·00128	0·97483	−0·00146
2	0·95791	−0·00374	0·94255	−0·00339
3	0·91554	−0·00795	0·89561	−0·00637
4	0·85532	−0·01466	0·83178	−0·01075
5	0·77197	−0·02497	0·74700	−0·01722
6	0·65517	−0·03926	0·63335	−0·02753
7	0·48569	−0·05995	0·47146	−0·04796
8	0·19693	−0·15458	0·19471	−0·14567
9	0·06560	−0·47800	0·07483	−0·46362

8.3. *Effect of Varying the 'Scale Height' of the Exponential Model*

Tables 6 and 7 give the mode characteristics for the exponential models in which $Z = 30$, $h = 80$ km and $\alpha = 0{\cdot}295$ km^{-1} and $1{\cdot}18$ km^{-1}. These results should be compared with those in table 4, which refers to $\alpha = 0{\cdot}59$ km^{-1}. The parameter α determines the rate at which the electron density increases, $\alpha = 0{\cdot}295$ km^{-1} giving a 'gradual' ionosphere such as might exist at night, and $\alpha = 1{\cdot}18$ km^{-1} giving a 'sharp' ionosphere. As previously, the effect on the mode characteristics of the change in α is more pronounced as the order of the mode increases. Considering vertical polarization first, it is seen from the tables that whilst increasing α from 0·295 to 0·59 changes both $\mathscr{R}(S)$ and $\mathscr{I}(S)$ appreciably, the change from 0·59 to 1·18 has the effect of changing $\mathscr{R}(S)$ only, leaving $\mathscr{I}(S)$ almost unaltered. The change in $\mathscr{R}(S)$ is of the same order for both changes in α. For horizontal polarization the change in α has a marked effect which is of a different character, consisting principally of a change in $\mathscr{I}(S)$ with

Table 6. Exponential Model. $X=\exp(0\cdot295(z-80))$, (z in km). $Z=30$

n	Vertical polarization		Horizontal polarization	
	$\mathscr{R}(S)$	$\mathscr{I}(S)$	$\mathscr{R}(S)$	$\mathscr{I}(S)$
0	0·99851	−0·00017	0·99435	−0·00064
1	0·98661	−0·00161	0·97695	−0·00261
2	0·96264	−0·00465	0·94794	−0·00608
3	0·92619	−0·00963	0·90678	−0·01122
4	0·87619	−0·01713	0·85233	−0·01824
5	0·81022	−0·02834	0·78209	−0·02775
6	0·72331	−0·04623	0·69263	−0·04145
7	0·60355	−0·07743	0·57274	−0·06477
8	0·42512	−0·13132	0·40816	−0·11338
9	0·20315	−0·29527	0·20367	−0·27478

Table 7. Exponential Model. $X=\exp(1\cdot18(z-80))$ (z in km), $Z=30$

n	Vertical polarization		Horizontal polarization	
	$\mathscr{R}(S)$	$\mathscr{I}(S)$	$\mathscr{R}(S)$	$\mathscr{I}(S)$
0	0·99832	−0·00014	0·99376	−0·00019
1	0·98470	−0·00130	0·97482	−0·00078
2	0·95672	−0·00376	0·94242	−0·00182
3	0·91257	−0·00769	0·89512	−0·00341
4	0·84898	−0·01301	0·83044	−0·00575
5	0·76090	−0·01886	0·74389	−0·00924
6	0·64021	−0·02493	0·62660	−0·01493
7	0·46481	−0·03505	0·45575	−0·02680
8	0·11181	−0·13472	0·11873	−0·13005
9	0·03130	−0·49432	0·03899	−0·48833

a much smaller change in $\mathscr{R}(S)$. Thus the attenuation is decreased as α increases, but the phase velocity is only changed by a small amount. (Compare the result of § 7, where the attenuation also decreased as the boundary became more sharp.)

8.4. *Effect of Changing the Height of the Ionosphere*

In this section we consider the effect on the waveguide modes of moving the whole ionosphere up or down, that is of changing the value of the parameter h in the exponential model, which determines the height at which $X=1$. The modes for $h=80$ km were given in table 4: tables 8 and 9 give the mode characteristics for $h=60$ km and 100 km respectively, the other parameters being unchanged. These values represent displacements of approximately one wavelength up or down (wave frequency = 16 kc/s). The general pattern of the results is the same for both polarizations, but

Table 8. Exponential Model. $X = \exp(0{\cdot}59(z-60))$ (z in km), $Z = 30$

n	Vertical polarization		Horizontal polarization	
	$\mathscr{R}(S)$	$\mathscr{I}(S)$	$\mathscr{R}(S)$	$\mathscr{I}(S)$
0	0·99728	−0·00030	0·98984	−0·00078
1	0·97524	−0·00287	0·95884	−0·00324
2	0·92950	−0·00869	0·90518	−0·00771
3	0·85564	−0·01957	0·82502	−0·01500
4	0·74233	−0·03874	0·71024	−0·02702
5	0·56321	−0·06732	0·54080	−0·05050
6	0·25272	−0·16115	0·24791	−0·14788
7	0·08095	−0·52577	0·09347	−0·50558
8	0·05760	−0·78519	0·07805	−0·75834
9	0·04932	−0·99778	0·07505	−0·96528

Table 9. Exponential Model. $X = \exp(0{\cdot}59(z-100))$ (z in km), $Z = 30$

n	Vertical polarization		Horizontal polarization	
	$\mathscr{R}(S)$	$\mathscr{I}(S)$	$\mathscr{R}(S)$	$\mathscr{I}(S)$
0	0·99897	−0·00007	0·99607	−0·00019
1	0·99072	−0·00064	0·98420	−0·00076
2	0·97400	−0·00184	0·96413	−0·00175
3	0·94830	−0·00380	0·93555	−0·00320
4	0·91293	−0·00679	0·89745	−0·00523
5	0·86639	−0·01083	0·84876	−0·00797
6	0·80643	−0·01665	0·78762	−0·01168
7	0·72913	−0·02442	0·71094	−0·01686
8	0·62811	−0·03416	0·61310	−0·02465
9	0·49148	−0·04806	0·48186	−0·03851

the effects are of greater magnitude for horizontal polarization. The effect of lowering the ionosphere is to increase the phase velocity and decrease attenuation. The change from 100 km to 80 km has a much smaller effect than the change from 80 km to 60 km. The changes are in approximately the same ratio for all the modes, though the magnitude of the change is greater for the modes of higher order.

8.5. *Summary for the Zero-order Mode*

Since the zero-order mode is of great importance in the transmission of radio signals to great distances the value of S for this mode for the different exponential models discussed in the preceding paragraphs are collected in table 10 for purposes of comparison. It is seen that $\mathscr{R}(S)$ varies only

Table 10. Summary for Zero-order Mode, Exponential Model. $X = \exp \alpha(z-h)$

α (km^{-1})	h (km)	Z	Vertical polarization		Horizontal polarization	
			$\mathscr{R}(S)$	$\mathscr{I}(S)$	$\mathscr{R}(S)$	$\mathscr{I}(S)$
0·59	80	30	0·99842	−0·00013	0·99403	−0·00035
0·59	80	10	0·99835	−0·00014	0·99376	−0·00036
0·295	80	30	0·99851	−0·00017	0·99425	−0·00064
0·59	80	30	0·99842	−0·00013	0·99403	−0·00035
1·18	80	30	0·99832	−0·00014	0·99376	−0·00019
0·59	60	30	0·99728	−0·00030	0·98984	−0·00078
0·59	80	30	0·99842	−0·00013	0·99403	−0·00035
0·59	100	30	0·99897	−0·00007	0·99607	−0·00019

slightly for both polarizations: for vertical polarization $\mathscr{I}(S)$ also varies but slightly, though it shows a greater variation for horizontal polarization.

ACKNOWLEDGMENTS

I wish to thank Dr. K. G. Budden for much helpful advice, and Dr. M. V. Wilkes, F.R.S., Director of the University Mathematical Laboratory for permission to use EDSAC 2. I am indebted to the Department of Scientific and Industrial Research for a maintenance grant covering the period in which the research was carried out.

APPENDIX

Extensions to the Theory

(*a*) *Finite ground conductivity*

The reflection coefficient of a homogeneous imperfectly conducting earth is a function of C, and it is therefore necessary to use a more elaborate scheme of successive approximation than that defined by eqn. (6), since it is necessary to find values of C for which $R(C).R_g(C) = 1$ (eqn. (1)). This does not, however, involve any new point of principle. Expressions for $R_g(C)$ have been derived by Wait (1957).

(*b*) *Curvature of the earth*

Budden (1957 b) has formulated the differential equations in spherical polar coordinates and has shown that the wave impedance satisfies a first order differential equation analogous to eqn. (13):

$$iV' = 1 - \frac{\nu(\nu+1)}{\mu^2 S^2} - \mu^2 V^2. \qquad (21)$$

The parameter $\nu(\nu+1)$ determines the mode properties in the same way that C_n and S_n determine the characteristics for a flat earth, and it is necessary to find values of $\nu(\nu+1)$ which make $V=0$ at the ground. This can be done in exactly the same way as was used to find values of C which made $R=\pm 1$ at the ground.

(c) *Earth's magnetic field*

If the ionosphere is anisotropic the reflection coefficient becomes a matrix (Budden 1952) as does the reflection coefficient of the ground, and eqn. (1) becomes

$$\mathbf{R}(C)\,.\,\mathbf{R}_g(C)=\mathbf{I} \qquad (22)$$

where $\mathbf{I}$ is the unit matrix. The differential equation analogous to eqn. (3) satisfied by $\mathbf{R}$ can be derived in matrix form (Budden 1955) and it is thus possible to use a similar procedure to that outlined in § 3 to find values of C which are consistent with eqn. (22).

REFERENCES

BARRON, D. W., and BUDDEN, K. G., 1959, *Proc. roy. Soc.* A, **249,** 387.

BUDDEN, K. G., 1951, *Phil. Mag.*, **42,** 1 ; 1952, *Ibid.*, **43,** 1179 ; 1955, *Proc. roy. Soc.* A, **227,** 516 ; 1957 a, *N.B.S. Rep.*, 5050 1957 b, *Ibid.*, 5085.

EPSTEIN, P. S., 1930, *Proc. nat. Acad. Sci., Wash.*, **16,** 627.

HEADING, J., 1953, Ph.D. Thesis, Cambridge.

SHMOYS, J., 1956, *Proc. Inst. Radio Engrs, N.Y.*, **44,** 163.

WAIT, J. R., 1957, *Proc. Inst. Radio Engrs, N.Y.*, **45,** 760 ; 1958, *J. geophys. Res.*, **63,** 125.

CORRESPONDENCE

Lattice Dynamics of Alkali Halides

By W. Cochran
General Physics Branch, Chalk River Project, Atomic Energy of Canada Limited, Chalk River, Ontario

[Received March 9, 1959]

Many of the properties of the alkali halides, for example their cohesive energies and elastic constants, are reasonably well explained on the assumption that the atoms are fully ionized, and that the only forces between them are electrostatic forces and short-range overlap forces between closed electron shells. On this basis Kellerman (1940) has calculated dispersion curves for sodium chloride, that is, curves of frequency $(\omega/(2\pi))$ as a function of wave vector $\mathbf{q}(q=2\pi/\lambda)$ of the normal modes. His results account satisfactorily for the measured elastic constants and the infra-red absorption frequency, and lead to a frequency distribution of the normal modes which explains very well the variation of the Debye characteristic temperature (Θ) deduced from specific heat measurements (Kellerman 1941). Nevertheless this model fails to account for the dielectric properties of the alkali halides; since the ions are treated as point charges of zero polarizability, the high-frequency dielectric constant of the material should be unity, whereas that of sodium chloride is 2·25. Lyddane and Herzfeld (1938) calculated dispersion curves with the polarizability of the ions taken into account, but the agreement with observation could scarcely have been worse in that the lattice was found to be unstable against vibration modes for which $\mathbf{q}$ is close to the boundary of the Brillouin zone in the [100] direction. Neither theory gives what is believed to be the correct ratio for the frequencies of longitudinal and transverse optic modes for which $q \to 0$, namely $(\epsilon_0/\epsilon)^{1/2}$, where ϵ and ϵ_0 are the dielectric constants for electric fields of high and zero frequency respectively (Born and Huang 1954). This latter difficulty has however been resolved by the introduction of the concept of 'distortion polarization' (Szigeti 1949, Born and Huang 1954). Dick and Overhauser (1958) have shown that the distortion polarization of an ion which results from the overlap forces can be represented approximately by a mechanical model in which the ion is represented by a core and a shell which retain spherical symmetry but may be relatively displaced by either the local field or the overlap forces, thus exhibiting both field polarizability and distortion polarizability.

We have used this model with certain extensions to investigate the lattice dynamics of those alkali halides which have the NaCl type of structure. Shells and cores are treated as units which exert forces on one another in accord with the general Born–von Kármán (1912) theory of lattice dynamics. The formulae derived are however believed to have a validity which is independent of this particular model, and should be correct to the extent that the polarization in the crystal, whatever the mechanism of its origin, may be regarded as originating from small dipoles centred on ion sites. This method leads to a derivation of the well known Szigeti relations (Szigeti 1949, 1950), but with certain important modifications. The formulae obtained are:

$$\epsilon_0 - \epsilon = \frac{4\pi(\epsilon+2)^2 e^2 (1+d_1-d_2)^2}{9m\omega_0^{\,2} v} . \qquad \ldots \ldots \quad (1)$$

and
$$K = \frac{m\omega_0^{\,2}(\epsilon_0+2)}{\epsilon+2} + e^2\left(\frac{d_1^{\,2}}{\alpha_1} + \frac{d_2^{\,2}}{\alpha_2}\right) . \qquad \ldots \quad (2)$$

Here ϵ_0 and ϵ are as defined earlier, e is the electronic charge,

$$m = m_1 m_2/(m_1+m_2)$$

is the reduced mass of the ions, $v = 2r_0^{\,3}$ is the unit cell volume, α_1 and α_2 are the atomic polarizabilities of the positive and negative ions respectively and $\omega_0/(2\pi)$ is the frequency of the transverse optic mode for $q \to 0$. The definition of K is as follows: suppose the positive and negative ions to be displaced a relative distance u, the overlap force on one ion is then a restoring force Ku. The quantities d_1 and d_2 are measures of the distortion polarizabilities of the positive and negative ions respectively. On the shell model, $d_1 = KZ_1/(k_1+K)$, where Z_1 is the number of electrons in the shell of the positive ion and k_1 the force constant for small relative displacement of the shell and the core. More generally, when the shell model is used only to facilitate the calculation and its specific features do not appear in the final results. d_1 and d_2 are to be regarded as parameters whose values are to be obtained by experiment.

Comparison of eqn. (1) with the corresponding result given by Szigeti (1949) shows that the effective charge e^* which he found it necessary to introduce, is given on our treatment by

$$e^* = e(1+d_1-d_2).$$

A similar result has been obtained by Born and Huang (1954). Our derivation however shows that it is only in eqn. (1) that the effect of the unequal distortion polarizabilities of the positive and negative ions is to replace e by e^*. In the acoustic modes as $q \to 0$ neither field nor distortion polarizability has any influence on the dispersion relations, so that the elastic constants remain in principle as calculated by Kellerman (1940) and Krishnan and Roy (1952). For general values of $\mathbf{q}$ the dependence of ω on $\mathbf{q}$ involves d_1 and d_2 separately in a relatively complicated way. Equation (2) differs from that given by Szigeti (1950) by the addition of the second term to the right-hand side. This term is about 10% of the other. Values of $d_2 - d_1$ have been calculated from eqn. (1) using the experimental data collected by Born and Huang (1954). The numerical values show the trend that was to be expected, from small values for the fluorides to larger ones for the iodides. On certain reasonable assumptions our treatment predicts that $(d_2-d_1)/K$ for a particular material should be an additive property of the ions involved. Numerial values are given in table 1, and are compared with those obtained by combining the following empirical values for d/K:

Ion	Li^+	Na^+	K^+	Rb^+	F^-	Cl^-	Br^-	I^-
Value of $(d/K)\times10^6$	0	0	0	1·0	1·5	6·0	8·0	11·0

There is satisfactory agreement, and although five non-zero parameters have been used to explain eleven observations, these parameters have relative values which are reasonable. Indeed if the shell model in its simplest form were entirely adequate, it can be shown that the following relation should hold for each ion:

$$\frac{d}{K}=\frac{\alpha}{Ze^2}$$

where as before α is the (field) polarizability of the ion and Z the number of electrons in the outer shell of each ion. This equation gives values of d/K which increase from Li to I in roughly the required way, but which are too small by a factor of about two. In the above calculations we took $K=6r_0/\beta$ where β is the compressibility of the static lattice (Born and Huang 1954). Having now deduced values for d_1 and d_2 we can compare values of $6r_0/\beta$ with values of K as given by eqn. (2). The comparison is made in the last two columns of table 1; K is almost always a few percent greater than $6r_0/\beta$. It is possible that this is an indication of overlap forces between second-nearest neighbours in the crystal.

Table 1

Substance	d_2-d_1 Measured	$[(d_2-d_1)/K]\times10^6$		$[6r_0/\beta]\times10^{-4}$	$K\times10^{-4}$ from eqn. (2)
		Measured	Sum rule		
LiF	0·192	1·8	1·5	10·9	8·71
NaF	0·086	1·2	1·5	6·96	8·19
NaCl	0·257	6·1	6·0	4·24	4·40
KCl	0·217	6·1	6·0	3·59	3·87
RbCl	0·168	5·3	5·0	3·16	3·69
NaBr	0·314	8·2	8·0	3·82	3·71
KBr	0·255	8·0	8·0	3·21	3·42
RbBr	0·197	7·1	7·0	2·79	3·26
NaI	0·306	10·2	11·0	2·99	3·09
KI	0·326	11·9	11·0	2·74	2·81
RbI	0·238	9·5	10·0	2·52	2·95

Dispersion curves for sodium chloride have been calculated for **q** along each of the three symmetry axes [100], [110] and [111], using as input data $K = 4{\cdot}40 \times 10^4$, the (field) polarizabilities of the ions as given by Shockley (1946), $d_2/K = 6{\cdot}0 \times 10^{-6}$ and $d_1 = 0$. Results for **q** along [100] are shown in the figure. Not only is the lattice stable against all vibration modes, but also in general only frequencies in the longitudinal optic modes differ greatly from those obtained by Kellerman. It is therefore probable that further calculation (which however would become very cumbersome for **q** in general directions) would lead to a frequency distribution of the normal modes which differed from Kellerman's only in the high-energy range. Such modes are scarcely at all excited at low temperatures; our results therefore predict the same general dependence of Debye-Θ on temperature as was found by Kellerman. Predicted and measured values of other constants are compared in table 2. The good agreement is not entirely a matter of choice of input parameters; only three were used and their numerical values (except for that of K) have been deduced from the

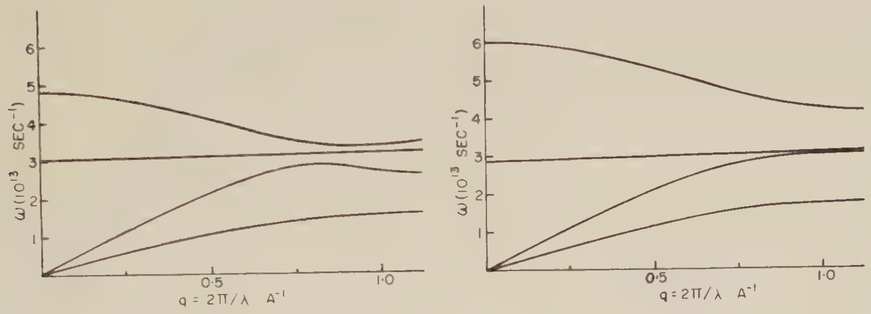

(*a*) (*b*)

(*a*) Dispersion curves for **q** along [100] according to the present theory.
(*b*) Dispersion curves for along **q** [100] according to Kellerman's theory.

Table 2

Constant	Calculated for static lattice	Experimental value
ω_0	$3{\cdot}04 \times 10^{13}$ sec^{-1}	$3{\cdot}09 \times 10^{13}$ (at room temp.)
ϵ	2·30	2·25 ,, ,, ,,
ϵ_0	5·83	5·62 ,, ,, ,,
C_{11}	$0{\cdot}522 \times 10^{12}$ dyne cm^{-2}	$0{\cdot}575 \times 10^{12}$ (at 0°K)
C_{12}	$0{\cdot}134 \times 10^{12}$	$0{\cdot}099 \times 10^{12}$,, ,,
C_{44}	$0{\cdot}134 \times 10^{12}$	$0{\cdot}133 \times 10^{12}$,, ,,

Experimental values are taken from Born and Huang (1954), except for the elastic constants, which were determined by Overton and Swim (1951). Values at 0°K are estimated by extrapolation, values at room temperature lie much closer to the calculated values.

physical properties of alkali halides in general. This approach has therefore resolved the difficulties mentioned in our introductory paragraph. The derivation of formulae utilized here will be given at a later date, when it is hoped that it will also be possible to compare theoretical dispersion curves for an alkali halide with those determined by experiment.

ACKNOWLEDGMENTS

I am indebted to Dr B. N. Brockhouse for many helpful suggestions and discussions, to Atomic Energy of Canada Limited for the award of a Fellowship, and to the University of Cambridge for granting me a year's leave of absence.

REFERENCES

BORN, M., and VON KÁRMÁN, T., 1912, *Phys. Z.*, **13,** 297.
BORN, M., and HUANG, K., 1954, *Dynamical Theory of Crystal Lattices* (Oxford: University Press).
DICK, B. G., and OVERHAUSER, A. W., 1958, *Phys. Rev.*, **112,** 90.
HANLON, J. E., and LAWSON, A. W., 1959, *Phys. Rev.*, **113,** 472.
KELLERMAN, E. W., 1940, *Phil. Trans.*, **238,** 513.
KELLERMAN, E. W., 1941, *Proc. roy. Soc.* A, **178,** 17.
KRISHNAN, K. S., and ROY, S. K., 1952, *Proc roy. Soc.* A, **210,** 481.
LYDDANE, R. H., and HERZFELD, K. F., 1938, *Phys. Rev.*, **54,** 846.
OVERTON, W. C., and SWIM, R. T., 1951, *Phys. Rev.*, **84,** 758.
SHOCKLEY, W., 1946, *Phys. Rev.*, **70,** 105.
SZIGETI, B., 1949, *Trans. Faraday Soc.*, **45,** 155.
SZIGETI, B., 1950, *Proc. roy. Soc.* A, **204,** 51.

Electron Distribution in Transition Metals

By A. J. FREEMAN and R. J. WEISS
Materials Research Laboratory, Ordnance Materials Research Office
Watertown, Massachusetts

[Received April 13, 1959]

IN a recent note Hume-Rothery *et al.* (1958) have suggested that the reason that the x-ray experiments of Weiss and DeMarco (1958) have revealed a low number of 3d atomic-like electrons in Fe and Cr is that the 3d charge density is not spherically symmetric.

We have previously investigated (Weiss and Freeman 1959 a, b) the effect of certain non-spherical charge distributions on observed atomic scattering factors in order to ascertain the way this effect would influence the x-ray measurements. In this note we are reporting the results of a new calculation on a model which exaggerates the effect of charge asphericity and which is also mathematically simple to treat. This calculation shows that only a marked change in the radial charge density can be responsible for the large reduction in the scattering factor of α Fe at the (110) (first Bragg) peak reported by Weiss and DeMarco and that *no* aspherical charge distribution of reasonable radial charge distribution *which maintains cubic symmetry* can be devised which will account for this effect.

As is well known, the electronic charge distribution must show the symmetry of its cubic environment. Two exaggerated non-spherical charge distributions which display this symmetry are illustrated in figs. 1 and 2. In fig. 1, the charge distribution consists of lines of charge pointing along the eight (111) directions (toward nearest neighbours in b.c.c. Fe), whereas in fig. 2 the charge distribution consists of lines of charge pointing along the six (100) directions (toward second nearest neighbours). It is clear that any more realistic representation of the charge distribution will show a less severe effect on the observed atomic form factor.

Fig. 1

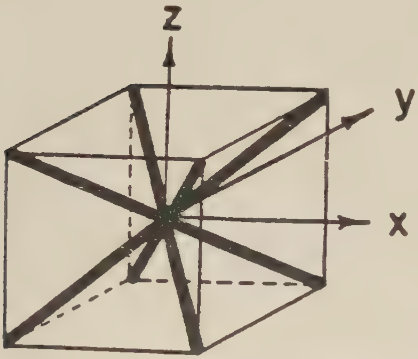

The charge distribution consists of lines of charge along the eight (111) directions.

Fig. 2

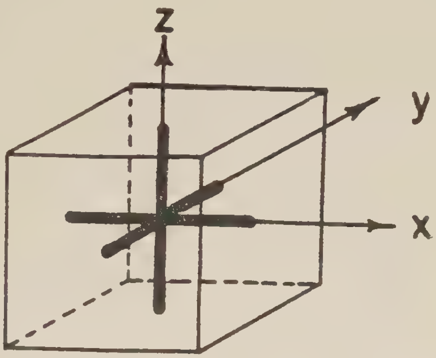

The charge distribution consists of lines of charge along the six (100) directions.

If we now choose a reasonable radial charge density, and put this density distribution along the appropriate lines of figs. 1 and 2 we may calculate the scattering factor for the various Bragg reflections. To maintain our charge normalization of six electrons (as in the free iron atom), we place 6/8 of an electron along each line of fig. 1 and one electron along each line of fig. 2.

We have chosen the radial charge density to be of the form $Ar^2 \exp(-ar)$ with a adjusted (set equal to 5·74) to give a maximum at 0·35 Å, coinciding with the peak calculated by Wood and Pratt (1957)† for the free iron atom. (This charge density also yields a form factor which agrees with the neutron form factor for iron as measured by Nathans *et al.* (1958, 1959) for the first few Bragg peaks.) The form factor may then be evaluated *analytically* for the distributions shown in figs. 1 and 2 as well as for the more usual case of spherical symmetry.

---

† This charge density has been shown to give excellent agreement with the measurements of Nathans *et al.* (1958, 1959).

For the distribution of fig. 1 the form factor is given by:

$$f_{110}{}^{(1)} = 3 + \frac{3(1-2k^2/a^2)}{(1+2k^2/3a^2)^3} \quad . \; . \; . \; . \; . \; . \; . \quad (1)$$

whereas for the distribution of fig. 2 the form factor is given by:

$$f_{110}{}^{(2)} = 2 + \frac{4(1-3k^2/2a^2)}{(1+k^2/2a^2)^3}. \quad . \; . \; . \; . \; . \; . \; . \quad (2)$$

Here $k = 4\pi \sin\theta/\lambda = 3{\cdot}1$ for the (110) reflection in α iron. The spherically symmetric result is:

$$\bar{f} = 6/(1+k^2/a^2)^2.$$

For our choice of $a = 5{\cdot}74$, $f_{110}{}^{(1)} = 3{\cdot}734$, $f_{110}{}^{(2)} = 3{\cdot}496$ and $\bar{f} = 3{\cdot}596$.

The deviation from the spherically symmetric results for these cases of exaggerated non-sphericity is seen to amount to only 3%, whereas to account for the Weiss and DeMarco x-ray results a deviation of 63% is needed. The formulae given above also allow estimates to be made quite simply of the radial distortion necessary to reduce the form factor at the (110) peak by the required amount. (This is done by changing the value of a in the exponential term of the charge density.)

From this analysis, we conclude that no angular charge distribution consistent with the requirements of cubic symmetry can produce a change in the form factor of large enough magnitude to explain the X-ray results. Only large changes in radial charge densities can account for these results.

ACKNOWLEDGMENT

We wish to acknowledge the advice of Dr. R. Harrison.

REFERENCES

HUME-ROTHERY, W., BROWN, P. J., FORSYTH, J. B., and TAYLOR, W. H., 1958, *Phil. Mag.*, **36,** 1466.

NATHANS, R., SHULL, C. G., SHIRANE, G., and ANDRESON, A., 1958, Tech. Rep. No. 3, M.I.T. Structure of Solids Group, November 19 (unpublished); 1959, *Int. J. Phys. Chem. Solids*, **10,** 133.

WEISS, R. J., and DEMARCO, J. J., 1958, *Rev. mod. Phys.*, **30,** 59.

WEISS, R. J., and FREEMAN, A. J., 1959 a, Quarterly Progress Report, Solid State and Molecular Theory Group, M.I.T. January 15; 1959 b, *Int. J. Phys. Chem. Solids*, **10,** 147.

WOOD, J. H., and PRATT, G. H., 1957, *Phys. Rev.*, **107,** 995.

Dislocation Sources in Quenched Aluminium-Based Alloys

By K. H. Westmacott, D. Hull and R. S. Barnes
Metallurgy Division, A.E.R.E., Harwell

and R. E. Smallman
Department of Physical Metallurgy, The University of Birmingham

[Received May 27, 1959]

Interest in the behaviour of vacancies in metals is considerable not only because they affect the physical and mechanical properties, but also because of their ability to form dislocations. Observation with the electron microscope has shown that dislocation loops can be formed in quenched metals from discs of aggregated vacancies (Hirsch *et al.* 1958, Hirsch and Silcox 1959, Smallman and Westmacott 1959). Similar dislocation loops have been observed in the industrially important group of alloys of the precipitation hardening type, e.g. Al–20 wt% Ag, Al–4 wt% Cu (Smallman *et al.* 1959) and Al–3·7 wt% Cu (Thomas and Whelan 1959) as expected, since these alloys are usually heat-treated and quenched. In addition, helical dislocations produced by the climb of screw dislocations were observed. Consequently since helical dislocations are not observed in pure aluminium the factors influencing their formation have been studied. It is the purpose of this letter to summarize the general findings of this investigation and to describe some dislocation sources observed.

The alloys examined included a series from each of the systems Al–Ag, Al–Si, Al–Cu and Al–Mg. In all cases foils 0·001 in. thick were used and quenched from homogeneous solid solution into one of three quenching media (brine, water or acetone at room temperature) by the method described previously (Smallman *et al.* 1959). The experiments showed that in any given alloy system the formation of helical dislocations was favoured by lowering the quenching rate or by increasing the solute concentration. Moreover, for a given quenching rate and solute concentration the formation of helices was promoted in those alloys with the greatest lattice misfit in the aluminium matrix.

During the investigation dislocation rings of the type first described by Frank and Read (1950) were observed in the Al–4% Cu alloy after quenching from 525°c into acetone. A typical area with these dislocation rings symmetrically arranged about a source is shown in fig. 1 (Pl. 132). The dislocation rings are inclined at an angle to the foil so that only a part of the second and third ring lies in the thickness of the foil. Figure 2 (Pl. 132) shows a ring with its plane lying more nearly parallel to that of the foil. Selected area diffraction of such a region confirmed that the dislocation rings were parallel to a (111) plane.

In each case there is a row of dislocation loops inside, but near to, the dislocation ring. These loops are parallel to those formed at random throughout the foil (e.g. see fig. 1) and their shapes are such that they too must lie in (111) planes. However, whereas the loops lying at random clearly lie on any of the four possible (111) planes those lying in rows inside the dislocation rings are confined to only two of the possible (111) planes and they never lie in the (111) plane of the dislocation rings.

At the centre of the concentric rings there is always a dislocation configuration which must be the source of the rings. Although often the configuration is complex, in some cases, e.g. fig. 3 (Pl. 133) the source appears as two loops with one edge common to both. This is shown more clearly in fig. 4 (Pl. 133) which is a photo-micrograph of an Al–3% Cu alloy quenched from 425°C into acetone. Region Y shows one closed dislocation ring with the source inside. This central dislocation consists of two loops lying on different (111) planes, one in the same (111) plane as that of the ring, suggesting that it is itself the next ring which has not yet broken away from the sources.

The system of concentric dislocation rings which have been shown to lie on a (111) plane must expand radially from their source by a slip process. During this process these rings climb into complex helices by acquiring some of the vacancies quenched in. A dislocation ring with its Burgers vector lying in the plane of the ring is illustrated in fig. 5 (*a*). The condensation of vacancies upon this ring would cause the line to spiral about b as illustrated in fig. 5 (*b*). Such a helical dislocation would have difficulty in slipping except in the limited region where it has perfect edge character. Under sufficient applied stress however, the dislocation could be torn away leaving behind a series of loops of about the same size and number as the turns of the helix (fig. 5 (*c*)). Loops produced in this way would lie on (111) planes and have the same Burgers vector as the original dislocation line. They would then lie only on those (111) planes which did not contain b. Thus only two of the total of four (111) planes are possible which is consistent with the observations.

The sources of these dislocation rings are of great interest and in their simplest form appear to be a dislocation loop lying on a (111) plane. Such a loop source mechanism has been predicted previously by Kuhlmann-Wilsdorf (1958). A loop formed by the collapse of a vacancy platelet and the subsequent slip of a half dislocation to remove the stacking fault has its Burgers vector in the [110] direction and could act as a dislocation source in the manner observed. Helices may be formed not only from loops expanding from sources in a slip plane but also from prismatic glide of prismatic loops. For example, such a loop has been observed to slip on the prismatic cylinder defined by the loop and its Burgers vector and the slip produces two screw dislocations separated by a distance equal to the diameter of the original loop (Hirsch *et al.* 1958). These are capable of climbing in a vacancy super-saturated into helices of opposite hand (Bontinck 1957), as observed in Al–3% Cu quenched from 550°C into acetone (fig. 6, Pl. 134) where helices of opposite hand occur in pairs separated by only a few thousand angstroms. However, this process does not generate extra dislocation lines and another process is occurring during the generation of the dislocation rings observed. Here, a part of the quenched loop must slip on a (111) plane, and as a result of the anchoring action by the rest of the loop, bow out and generate dislocation rings.

Fig 5

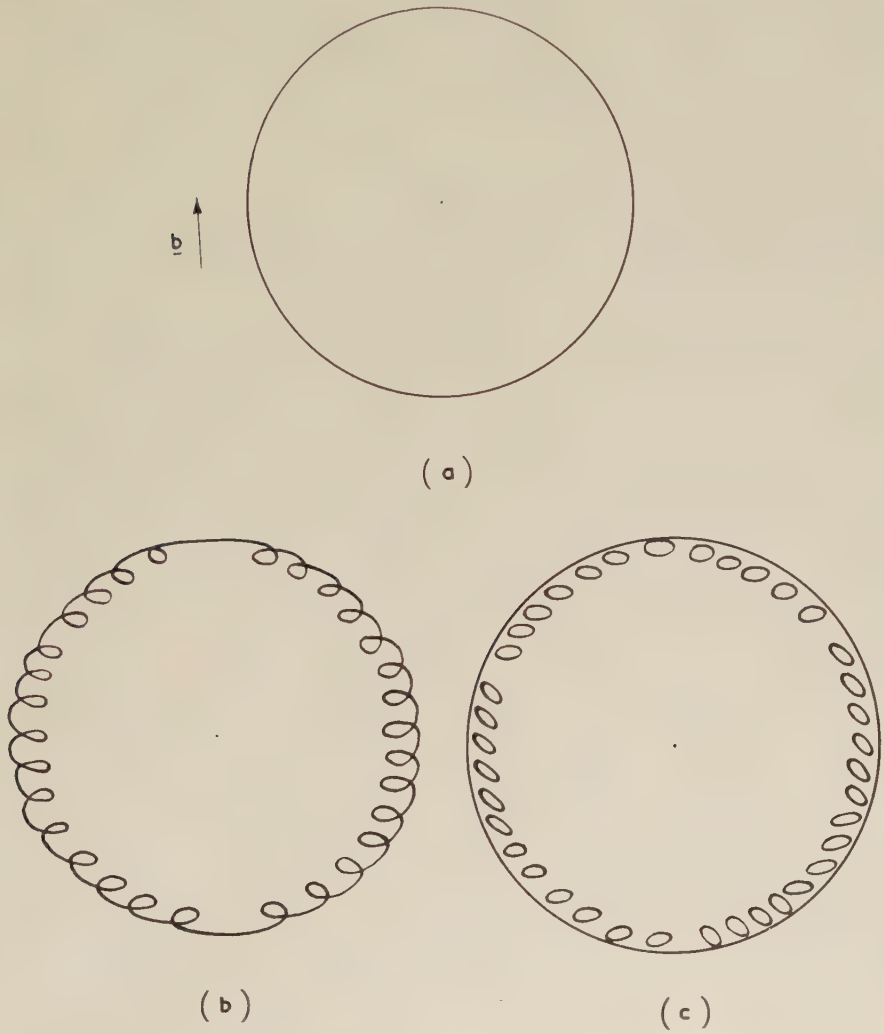

(a)

(b)

(c)

Diagrammatic illustration of the formation of closed loops inside a dislocation ring.

The recently published work of Thomas and Whelan (1959) also distinguishes the two kinds of helices produced; (*a*) from the prismatic glide of prismatic loops, and (*b*) from dislocation loops of large diameter such as might be produced by a source of slip active during quenching.

However, no observation of the source of the dislocation loops was made. Jacquet *et al.* (1958) have previously observed sources in Al–4% Cu as a result of the decoration effect of dislocation rings by θ' phase but no helices or small loops could be seen by the optical microscopic technique used. The present observations show that the dislocation loops formed by the condensation of vacancies can both slip prismatically to produce straight dislocation helices during quenching or more importantly these loops, which are not a part of the dislocation net-work (Kuhlmann-Wilsdorf *et al.* 1958) can act as Frank–Read sources and generate large numbers of dislocation rings under a sufficiently high stress.

REFERENCES

BONTINCK, W., 1957, *Phil. Mag.*, **2,** 561.
FRANK, F. C., and READ, W. T., 1950, *Phys. Rev.*, **79,** 722.
HIRSCH, P. B., SILCOX, J., SMALLMAN, R. E., and WESTMACOTT, K. H., 1958, *Phil. Mag.*, **3,** 897.
HIRSCH, P. B., SILCOX, J., 1959, *Phil. Mag.*, **4,** 56.
JACQUET, P. A., WEILL, A. R., and CALVERT, J., 1958, *Compt. rend.* **247,** 1001.
KUHLMANN-WILSDORF, D., 1958, *Phil. Mag.*, **3,** 125.
KUHLMANN-WILSDORF, D., MADDIN, R., KIMURA, H., 1958, *Z. Metallk.*, **49,** 584.
SMALLMAN, R. E., and WESTMACOTT, K. H., 1959, *J. appl. Phys.*, **30,** 603.
SMALLMAN, R. E., WESTMACOTT, K. H., and COILEY, J., 1959, *J. Inst. Metals* (in the press).
THOMAS, G., and WHELAN, M., 1959, *Phil. Mag.*, **4,** 511.

Experiments on Nuclear Cooling

By M. V. HOBDEN and N. KURTI
Clarendon Laboratory, Oxford

[Received September 30, 1959]

IN continuation of the earlier work of Kurti *et al.* (1956) we have carried out further experiments on isentropic demagnetization of copper nuclei in the metal using new apparatus and improved techniques. These lead to a somewhat different interpretation and give the interaction temperature θ_n defined below, as $1{\cdot}7\times10^{-7}$ °K. This is close to the theoretical value predicted by magnetic dipole interaction.

The specimen was similar to that used in the 1956 experiments and consisted of fine copper wires embedded in potassium chromium alum (the 'electronic stage') at 0·012°K. The copper wires acted both as thermal link and the 'nuclear stage'. It was found necessary to increase the dimensions of the thermal contact area relative to the size of the nuclear stage to ensure that the temperature of the copper before demagnetization from higher fields was indeed 0·012°K. It is now believed that the initial temperatures in the 1956 experiments were about 0·02°K for the higher initial fields.

The specimen was surrounded by a thermal shield kept at 0·35°K by means of a ^{3}He cryostat (Hobden 1960) using 0·2 cm^3 of liquid ^{3}He. The 1956 apparatus had a shield cooled by a paramagnetic salt, but this prevented reliable measurement of the temperature of the electronic stage. With a ^{3}He shield this difficulty was avoided.

The temperature of the nuclear spins was derived from the nuclear susceptibility using Curie's Law. This is a valid approximation in the range of nuclear spin temperatures obtainable by present techniques. The susceptibility was measured by a 25 c/s a.c. bridge giving a continuous pen recording starting two seconds after demagnetization. It was designed so that the presence of a copper ripple shield in the metal helium Dewar did not affect the measurements. The absolute calibration of the mutual inductance bridge was made using a paramagnetic salt at liquid helium temperatures. The amplitude of the measuring field at the specimen was of the order 0·05 oe.

The decay of the nuclear susceptibility after demagnetization was found to be exponential and the time constant τ varied inversely with the temperature T of the electronic stage, being given by $\tau T = 0{\cdot}3$ sec °K over a range of T from 0·012°K to 0·10°K. This seems to indicate that the conduction electrons in the copper remained at the temperature of the electronic stage and that τ was the relaxation time characteristic of energy transfer between nuclear spins and conduction electrons in zero external magnetic field. This interpretation is different from that of the 1956 experiments. Upon application of an external field of about 5 oe to the nuclear stage τ increased by a factor of two. These values of τT in the range 0·012°K to 0·10°K and their field dependence are similar to those of Anderson and Redfield (1957) measured at liquid helium temperatures.

The figure shows the final temperatures of the nuclear spin system after demagnetizations from fields up to 30·4 koe and initial temperatures of 0·012°K. The lowest temperature reached was $1{\cdot}2 \times 10^{-6}$°K. It can be seen that these results fit the line $T_f = 3{\cdot}1\ T_i/H_i$ where T_i and T_f are the initial and final temperatures and H_i is the initial field in oersted. Demagnetizations have also been carried out from a field of 7·6 koe with initial temperatures between 0·012°K and 0·10°K using a specimen with a larger nuclear stage.

The fact that T_f is directly proportional to T_i/H_i implies that the entropy of the nuclear spin system in zero external field is of the form

$$S/R = \log(2I+1) - b/T^2.$$

If $k\theta_n$ is defined in a naïve way as the energy separation between the successive $2I+1$ equidistant levels into which the ground state of a nuclear spin is assumed to be split by an internal field, then for $T \gg \theta_n$

$$b = \frac{I(I+1)\theta_n^2}{6}.$$

This θ_n is proportional to the root mean square splitting of the energy levels of the whole nuclear spin system in zero external field and is given by

$$I(I+1)(k\theta_n)^2 = 3\overline{(\epsilon - \bar{\epsilon})^2}.$$

Furthermore the final temperature is given by

$$T_{\mathrm{f}} = \frac{Ik\theta_n}{\mu_n}\frac{T_{\mathrm{i}}}{H_{\mathrm{i}}}$$

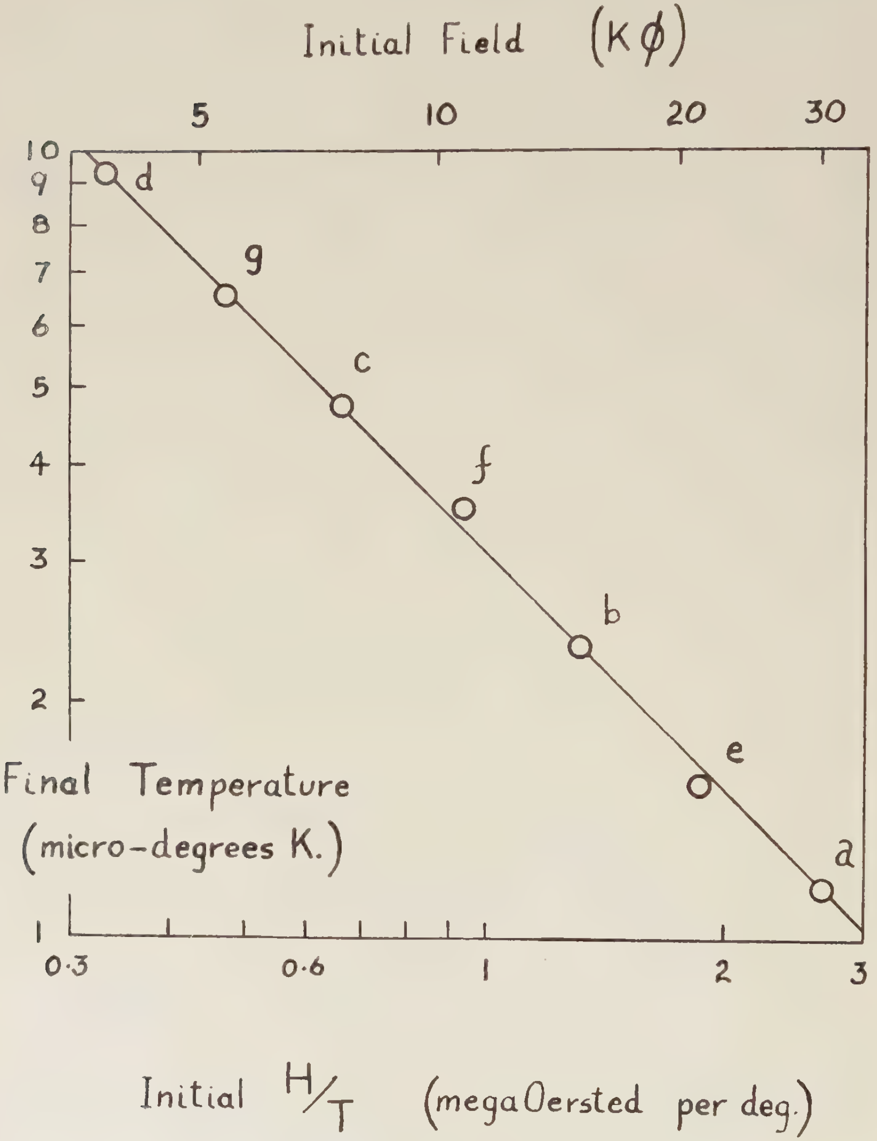

Demagnetizations from 0·012°K and various fields.

and comparison with the experimental values above shows that $\theta_n = 1{\cdot}7 \times 10^{-7}$ °K corresponding to an average effective internal field of 3·1 oe.

In the 1956 experiments the susceptibilities were measured by a ballistic method. The measuring field used (8 oe) is now known to be more than twice the average effective internal field and this led to values of θ_n which were too high.

Using Van Vleck's (1937) method for the calculation of dipolar magnetic interactions, θ_n, as defined above, has a value of $1{\cdot}9 \times 10^{-7}$ °K. The Ruderman and Kittel (1954) indirect exchange mechanism, counting nearest neighbours only, gives a value of the order 2×10^{-8} °K.

It is also interesting to compare the experimental value of $\theta_n = 1{\cdot}7 \times 10^{-7}$ °K with the Curie point given by various molecular field models of nuclear ferromagnetism. The Curie point of the Fröhlich–Nabarro (1940) theory, as computed using data given by Knight (1956, tables III and V), is $1{\cdot}9 \times 10^{-7}$ °K†. That of the simple Lorentz theory for a long specimen is also $1{\cdot}9 \times 10^{-7}$ °K. It can be seen that the lowest temperatures reached are still an order of magnitude higher than the predicted Curie point. We have observed that the relaxation time decreases as the measuring field is increased from 0·05 oe to 0·5 oe. Calculations show that this is unlikely to be due to a temperature rise of the conduction electrons through eddy current heating. However, it could possibly be explained by irreversible processes within the nuclear spin system.

Acknowledgments

We wish to thank Mr. J. R. Keyston for his assistance during these experiments. M. V. Hobden would like to thank the Department of Scientific and Industrial Research for financial assistance.

References

Anderson, A., and Redfield, A. G., 1957, *Proceedings of the Fifth International Conference on Low Temperature Physics, Madison, Wisconsin*, p. 616.
Fröhlich, H., and Nabarro, F. R. N., 1940, *Proc. roy. Soc.* A, **175,** 382.
Hobden, M. V., 1960 (to be published).
Knight, W. D., 1956, *Solid State Physics*, **2,** 93 (New York : Academic Press).
Kurti, N., Robinson, F. N. H., Simon, F. E., and Spohr, D. A., 1956, *Nature, Lond.*, **178,** 450.
Ruderman, M. A., and Kittel, C., 1954, *Phys. Rev.*, **96,** 99.
Van Vleck, J. H., 1937, *J. chem. Phys.*, **5,** 320.

---

† In the paper by Fröhlich and Nabarro, as well as in the report of the 1956 experiments, the Curie point according to this theory was given as 4×10^{-6} °K. The reason for this great discrepancy is that the recent values of the constants that enter into the formula are very different from those used in the original calculations.

REVIEWS OF BOOKS

Analysis of Straight-Line Data. By FORMAN S. ACTON. (John Wiley and Sons, Inc., 1959.) [Pp. 267+xiii.] 72*s*.

THIS book deals with statistical problems that are met with by an experimenter who has pairs of readings which are supposed to lie on or near a straight line. The author has designed it to be read by the experimenter himself and not by any statistical expert that he may desire to consult. Consequently the statistical techniques are described in great detail, with many of the byeways, that a statistician could explore for himself, discussed and with copious practical examples. Rightly, no attempt has been made to prove important results. The reader will need some statistical knowledge before reading the book: for example, some previous acquaintance with confidence limits seems necessary before p. 22 can be understood. The contents include: the classical model with one variable free from error; the bivariate normal model; both variables subject to error; comparison of several lines; orthogonal polynomials, transformations and outlying readings. The style is informal: for example in describing a bivariate probability distribution " consider the mountain to be made of uniform material, and then—with a bulldozer—push it . . . ". The book will be found useful by scientists who appreciate the need for statistical methods, have some basic statistical knowledge and wish to " fit a straight line ". The merit of the book lies in the care with which it distinguishes the various models. It is not always quite so clear in guiding the scientists' choice of which model to use. D. V. L.

Cryogenic Engineering. By RUSSELL B. SCOTT. (Van Nostrand, 1959). [Pp. 368.] 42*s*.

THE primary purpose of this book is to serve as an introduction to low-temperature engineering for engineers (not physicists) entering this field without previous cryogenic experience. The author has had long experience in low temperature work at the Bureau of Standards and is now in charge of the Bureau's Cryogenic Engineering Laboratory at Boulder.

The principal topics covered are the liquefaction of gases, the separation of gases, thermometry, thermal insulation, and the storage, transport and transfer of liquefied gases. There are also two long chapters on the properties of cryogenic fluids and structural materials.

The book is lucid and well-written and is clearly destined to be a standard work in this field. As would be expected from the author's background, the most useful and interesting sections are those dealing with the production and storage of liquid hydrogen on a large scale.

The chapter on liquefaction might be improved by including data on heat transfer to boiling cryogenic liquids, and by tabulating the values of the heat transfer coefficients for different gases under standardized conditions at various temperatures. The term ' energy ' is also rather loosely applied in the development of the thermodynamics, but these are minor blemishes easily rectified in the next edition. J. A.

Experimental Techniques in Low Temperature Physics. By G. K. WHITE. (Oxford, 1959.) [Pp. 328.] 45*s*.

THERE is an undoubted demand for a book which provides the information needed by those physicists who wish to carry out experiments at low temperatures but who have not had previous training in low temperature techniques. This book is a praiseworthy attempt to satisfy this requirement.

The ground covered includes the production and storage of liquefield gases, the measurement and control of temperature, the design of cryostats and the production of very low temperatures by adiabatic demagnetization. There are also chapters on heat exchanges and heat transfer and on thermal and electrical properties.

Wherever possible the author has discussed phenomena in terms of physical principles, and this treatment makes the book particularly suitable for a research student just starting research, or for those whose interests and training lie in other fields. In view of this, it is unfortunate that the amount of space allotted to different topics varies in a rather arbitrary way, especially in the section devoted to the design of cryostats. This is excellent on such topics as specific heat and thermal conductivity, but there is no mention, for example, of the use of microwaves either for paramagnetic resonance or for the study of metals. It is to be hoped that in a later edition the author will improve the balance between different topics and so make this book even more valuable than it is at present.

J. A.

Dendritic Crystallization. By D. D. SARATOVKIN. Translated from Russian by J. E. S. Bradley. (Consultants Bureau, Inc., New York, 1959). [Pp. 126.] $6.

THIS is not the definitive monograph on its subject which well might be written about now, and perhaps as well in the Soviet Union as elsewhere. Its principal merit lies in the careful description of simple experiments demonstrating the main phenomena involved. These may be recommended for the undergraduate laboratory.

The book is remarkably non-mathematical. Indeed the author achieves something of a *tour de force* in expounding, sufficiently for his purpose, the complex diffusion phenomena determining the dendritic growth of crystals, with only a single line of mathematics—the differential equation of diffusion in one dimension. But he gives no hint that such imprecise methods are not necessary.

The section on ‘ Effects of Surface Active Impurities on Crystallisation ’ is inferior, repeating inaccurate dogma. However it is not clear, at least from the translation, whether the author really believes the fallacious (and only) version of ‘ Wulff’s law ’ which he quotes, that the growth rate of a crystal face is proportional to its surface tension.

There follows a discussion of eutectics, and an interesting short section on contact fusion, stressing the significance of metastable eutectics.

The final section explains the solidfication of a steel ingot, and the resulting structure and distribution of impurities, in the light of what has gone before. Though no steel-man, the reviewer believes this to be sound, apart from an erroneous factor cos θ in eqn (12) and the apparent implication that the author believes iron crystals conduct heat anisotropically despite cubic symmetry. His hero is Chernov, who described dendrites in steel castings in 1879.

There are a number of stereoscopic micrographs, printed with 50 mm between centres for convenient viewing without a stereoscope.

A few photographs have been retouched: presumably it is the Russian publisher who does not realise that this is a crime in scientific works.

The occasional error, e.g. on p. 50 “ In another position we see dendrite branches on the left ” which should manifestly read “ On the left we see dendrite branches in another position ”, provides a salutary reminder that one is reading a translation, not an original text. It is a more serious matter that the original Russian title, and house and date of publication, are missing.

F. C. F.

A Supplement to 'Helium'. By E. M. LIFSHITS and E. L. ANDRONIKASHVILI. (New York: Consultants Bureau, Inc.; London: Chapman & Hall, Ltd.) [Pp. v+167.] 60*s*.

IN 1949 the Academy of Sciences of the U.S.S.R. published a translation into Russian of the well-known book *Helium* by W. H. Keesom, which itself had been published in The Netherlands in 1942. When Keesom wrote his book, one of the most interesting properties of helium, its superfluidity in the liquid phase, had hardly been investigated, but the position had changed greatly by 1949, so that Professor Lifshits and Andronikashvili each added an extra chapter to the translation, dealing respectively with the theory of superfluidity and with the relevant experimental data. The present book is a translation of these extra chapters.

A great deal of the pioneer work on superfluidity described in this book was in fact due to the Russians themselves; the work was initiated by the experiments of Kapitza and greatly stimulated by the subsequent theoretical attack by Landau. This research was of the greatest importance, and it laid the foundations for all subsequent work on the subject. However, the subsequent work itself has been important, particularly in providing a rigorous theoretical basis for Landau's semi-intuitive approach and in elucidating the mechanisms involved in the breakdown of superfluidity, so that the picture as it was in 1949 is now rather incomplete. Since this is the case, and since adequate summaries of the Russian work already exist in the English language, it is doubtful whether the publication of this translation can be considered worthwhile. W. F. V.

The Magneto-Ionic Theory and its Applications to the Ionosphere. By J. A. RATCLIFFE. (Cambridge: University Press.) [Pp. x+206.] 40*s*.

THE author defines a magneto-ionic medium as one in which free electrons and heavy positive ions are situated in a uniform magnetic field and are distributed with statistical uniformity so that there is no resultant space-charge. The ionosphere constitutes such a medium and the magneto-ionic theory plays an important part in theoretical investigations of the mode of propagation of electromagnetic waves around the earth by successive reflections between the ground and the ionosphere. After a brief historical review, the author develops this basic theory by two means of approach: the macroscopic one in which the medium is regarded as virtually continuous; and the microscopic approach in which attention is directed to the elementary wavelets which are scattered by the individual oscillating electrons. A brief discussion of the absorption suffered by a wave due to collision effects in the two cases completes the first part of the book.

In Part II the theoretical equations are interpreted graphically, and the effects of the medium on the polarization of the waves, their absorption and group velocity are discussed and illustrated. The third part of the book applies the theory to the terrestrial ionosphere and deals with the effect of the earth's magnetic field, the occurrence of a gyro-frequency and the splitting of wave echoes into two components, ordinary and extraordinary. A final section of the book discusses some miscellaneous related topics including a comparison of the phenomena involved in a magneto-ionic medium with those associated with crystal optics.

Altogether this monograph is an excellent review of the present position of the magneto-ionic theory of the ionosphere, and, together with its well-selected bibliography and brief abstracts, will form a permanent guide and introduction to this subject. Some parts of the book have not been previously published, but in view of the author's long association with, and detailed research in this field, these may be accepted as reliable as those which have withstood scientific criticism in published journals. The book is a most useful and attractive addition to the series on " Modern Radio Technique " published from Cambridge.

R. L. S-R.

Elements of Solid State Theory. By G. H. WANNIER. (Cambridge : University Press.) [Pp. 250.] 35*s*.

DR. WANNIER has succeeded in the difficult task of writing an excellent small book about a large subject. Naturally, some important topics are absent (for example, many-electron effects, and the theory of impurities and imperfections) but the scope is ample to justify the title. He has concentrated on the essential concepts, and simplified the treatment so that it should be perfectly intelligible to the average graduate physicist. Without sacrifice of rigour and precision, we are led to the key mathematical arguments of the modern theories, purged of irrelevant details and ignoring merely manipulative stages. At the same time, the so-called ' physical principles ', which guide and are created by the mathematical theory, are always clearly stated. The writing is free-flowing and relaxed, with a tang of originality that makes agreeable reading. It is surprising that the Cambridge University Press has not published this book in a larger, cheaper edition, for it should be read through, and understood, by every student of the physics of solids.

J. M. Z.

BOOK NOTICES

Lectures on the Theory of Elliptic Functions. By Harris Hancock. (New York: Dover Publications Inc.) [Pp. 498.] Price $2.55. A reprint, in the Dover Edition, of the 1st edition, published in 1958.

International Astronomical Union Symposium, No. 6. Electromagnetic Phenomena in Cosmical Physics. Stockholm, August 1956. By B. Lehnert (Cambridge University Press.) [Pp. 544.] Price 50*s.*

Annual Review of Nuclear Science, Vol. 8, 1958. Edited by E. Segre and others. (New York: Annual Reviews Inc.) [Pp. 417.] Price $7.00.

Guide to the Literature of Mathematics and Physics, 2nd edition. By Nathan Grier Parke III. (New York: Dover Publications Inc.) [Pp. 436.] Price 20*s.* A reprint, in the Dover Edition, of the 2nd edition, published in 1958.

Convex Surfaces: Interscience Tracts in Pure and Applied Mathematics, No. 6. By Herbert Busemann. (New York: Interscience Publishers Inc.) [Pp. 196.] Price 45*s.*

Elasticity, Plasticity and Structure of Matter, 2nd edition. By Dr. R. Houwink. (New York: Dover Publications Inc.) [Pp. 368.] Price 20*s.* A reprint, in the Dover Edition, of the 2nd edition, published in 1958.

Nuclear Spectroscopy Tables. By A. H. Wapstra, G. J. Nijgh and R. van Lieshout. (Amsterdam: North-Holland Publishing Co.) [Pp. 135.] Price 60*s.*

The Plasma in a Magnetic Field. A Symposium on Magnetohydrodynamics. Edited by Rolf K. M. Landshoff. (Standford University Press. London: Oxford University Press.) [Pp. 130.] Price 36*s.*

Fundamentals of Advanced Missiles. By Richard B. Dow. (New York: John Wiley & Sons Inc.; London: Chapman & Hall.) [Pp. 567.] Price 94*s.*

Colloque National de Magnetisme, Strasbourg July 1957. (Paris: Centre Nationale de la Recherche Scientifique.) [Pp. 336.] Price Fr. 4,000.

The Design of Physics Research Laboratories. Institute of Physics symposium London, November 27, 1957. (London: Chapman & Hall.) [Pp. 108.] Price 21*s.*

Proceedings of the International Symposium on Transport Processes in Statistical Mechanics, Brussels, August 1956. Edited by I. Prigogine. (Interscience Publishers, Inc.) [Pp. 436.] Price 75*s.*

[*The Editors do not hold themselves responsible for the views expressed by their correspondents.*]

Fig. 1

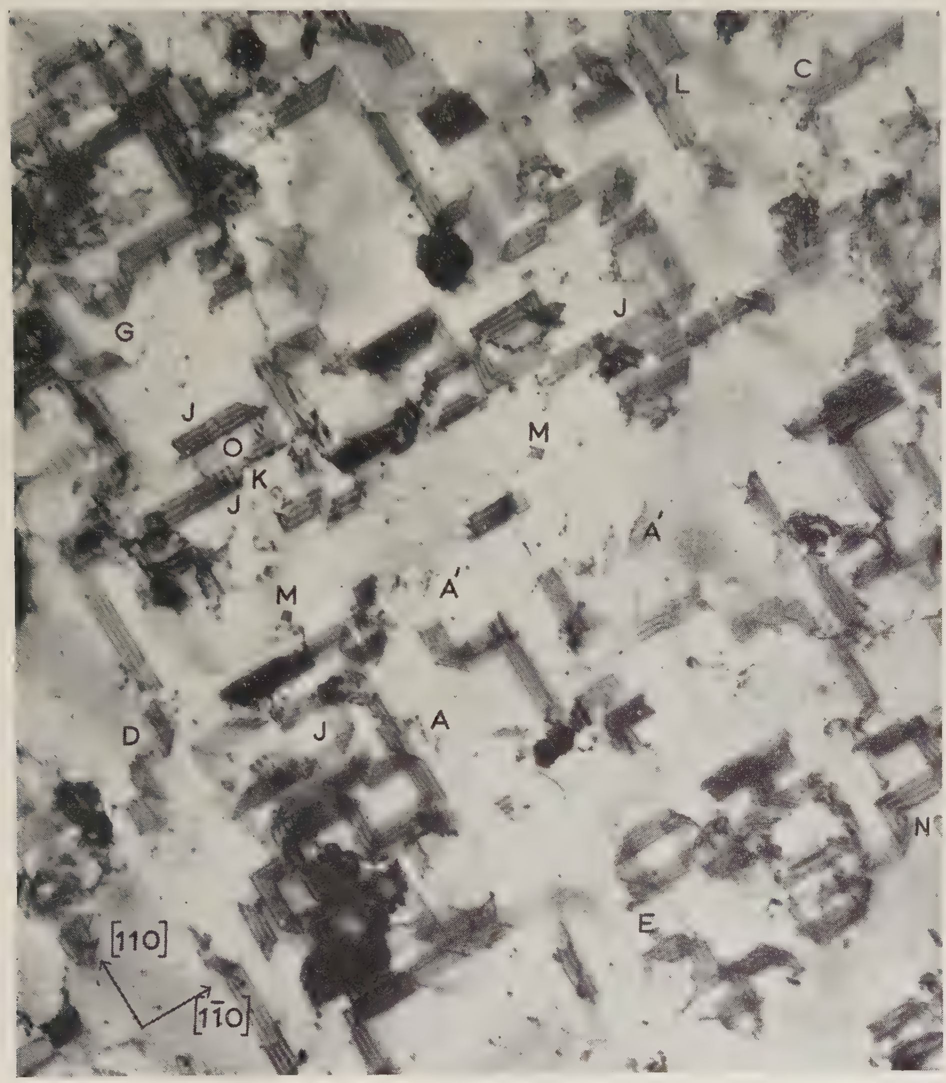

Electron micrograph of silver foil. Letters indicate position of defects discussed in the text.

Foil thickness = 500 Å.
Magnification = 88 000 ×.

Fig. 2

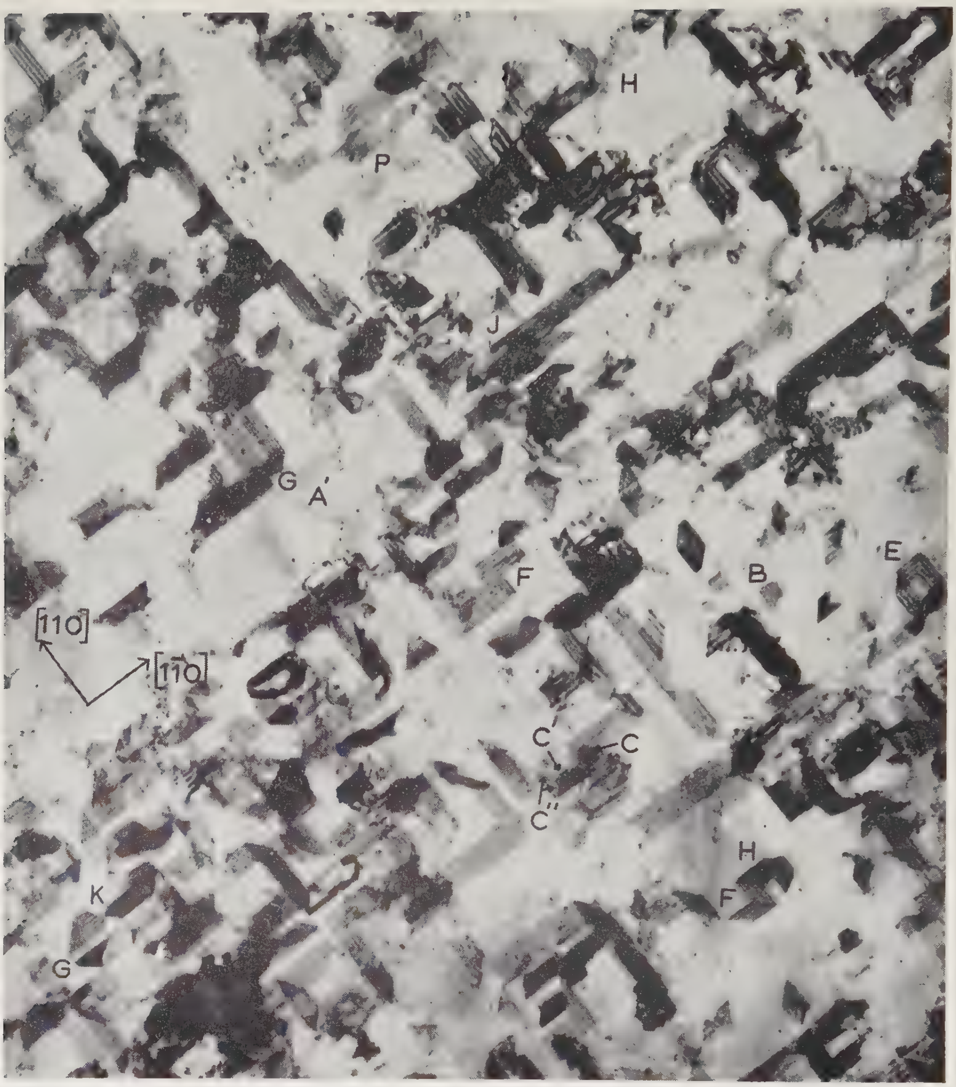

Electron micrograph of silver foil.

Foil thickness = 500 Å.
Magnification = 84 000 ×.

Fig. 3

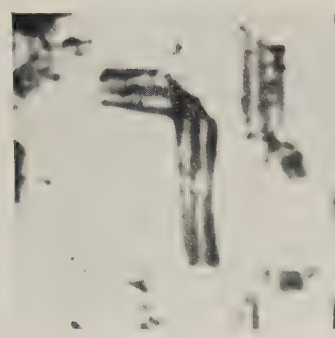

Fig. 4

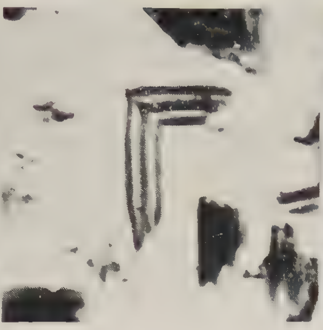

Fig. 5

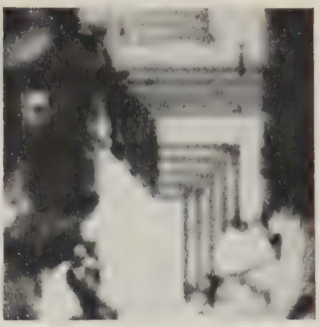

Fig. 6

Fig. 7

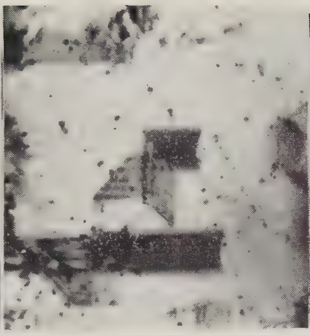

Fig. 8

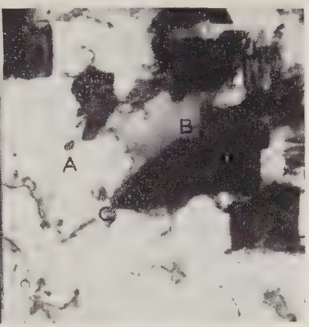

Fig. 9

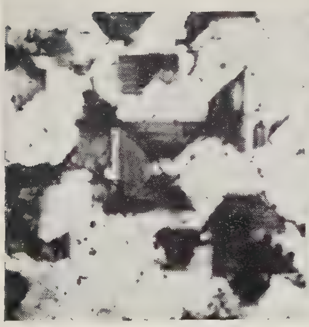

Fig. 10

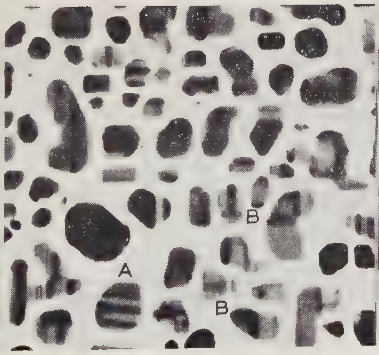

Fig. 11

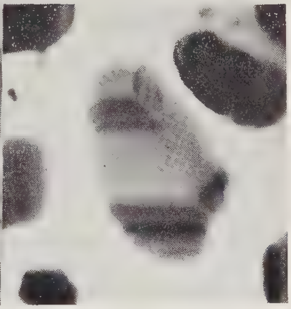

CAPTIONS TO PLATES

Fig. 3. A bent stacking fault in silver foil. The angle between the faulted planes is acute.

Foil thickness = 400 Å.
Magnification = 205 000 × .

Fig. 4. A bent stacking fault in silver foil. The angle between the faulted planes is obtuse.

Foil thickness = 400 Å.
Magnification = 205 000 × .

Fig. 5. A stacking fault in silver foil showing two bends (see fig. 14 (*e*)).

Foil thickness = 750 Å.
Magnification = 120 000 × .

Fig. 6. A defect in silver foil. The probable interpretation is drawn in fig. 18. Another example of it is seen at P in fig. 2. The interpretation of the defect at A is in doubt. It may be a dislocation loop.

Foil thickness = 500 Å.
Magnification = 155 000 × .

Fig. 7. An area of silver foil which contains an example of the defect in fig. 20.

Foil thickness = 500 Å.
Magnification = 155 000 × .

Fig. 8. A micrograph of copper foil. A dislocation loop is seen at A and BC is a stair-rod dislocation line.

Foil thickness = 1250 Å.
Magnification = 82 000 × .

Fig. 9. A micrograph of gold foil which contains a stacking fault with two bends (see fig. 14 (*f*)).

Foil thickness = 700 Å.
Magnification = 90 000 × .

Fig. 10. A micrograph of a thin deposit of gold backed with carbon. A slightly misaligned nucleus is seen at ‘ A ’. The formation of the defect in fig. 15 from nuclei joined as in fig. 27 is seen at positions ‘ B ’.

Average thickness of deposit = 70 Å.
Magnification = 120 000 × .

Fig. 11. A micrograph of a gold crystallite which shows the formation of a bent stacking fault by the coalescence of nuclei. The angle between the faulted planes is obtuse.

Average thickness of deposit = 70 Å.
Magnification = 240 000 × .

Fig. 1

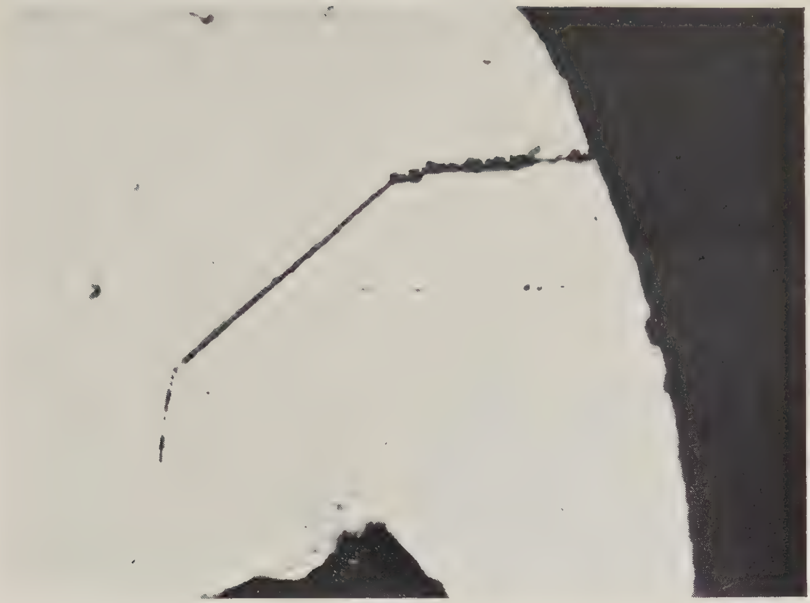

General view of a dislocation-crack. ×22.

Fig. 2

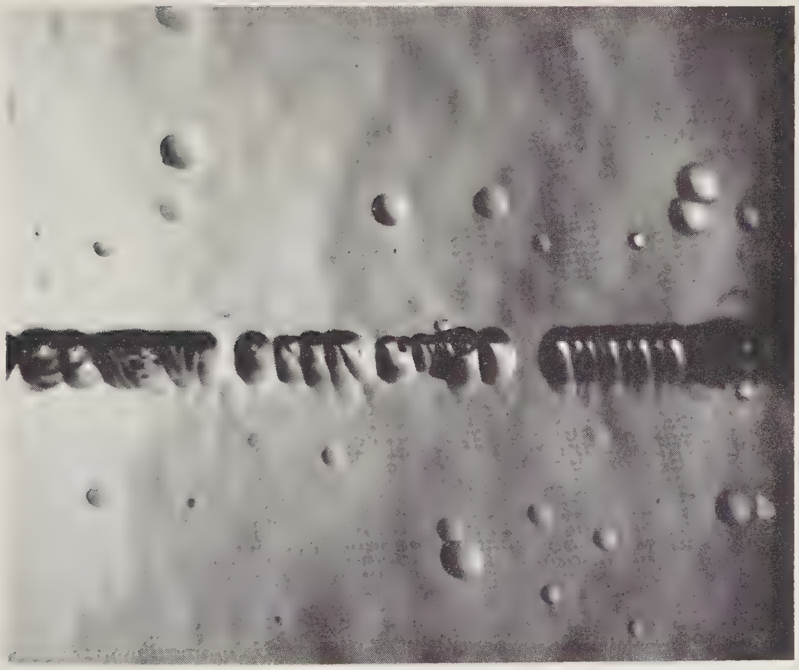

Part of a dislocation-crack under higher magnification, showing individual dislocations. ×250.

Fig. 3

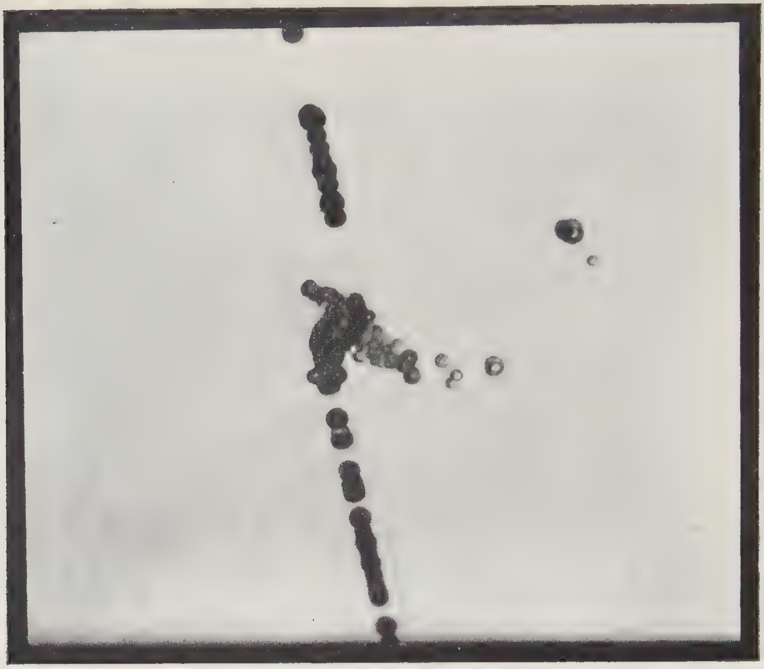

Part of a dislocation-crack showing the high density of dislocations at a change in direction. ×250.

Fig. 4

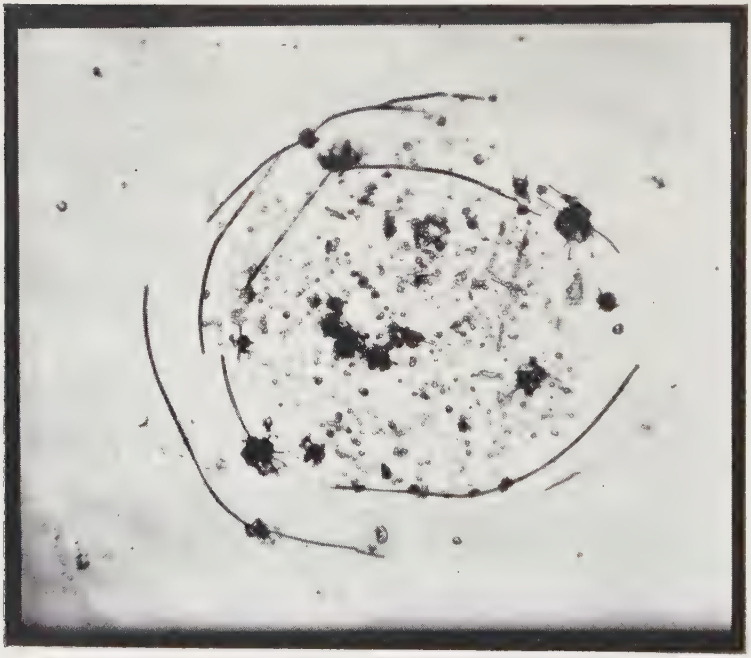

Ring-cracks and superficial damage produced by the impact of a steel sphere. ×130.

Fig. 9

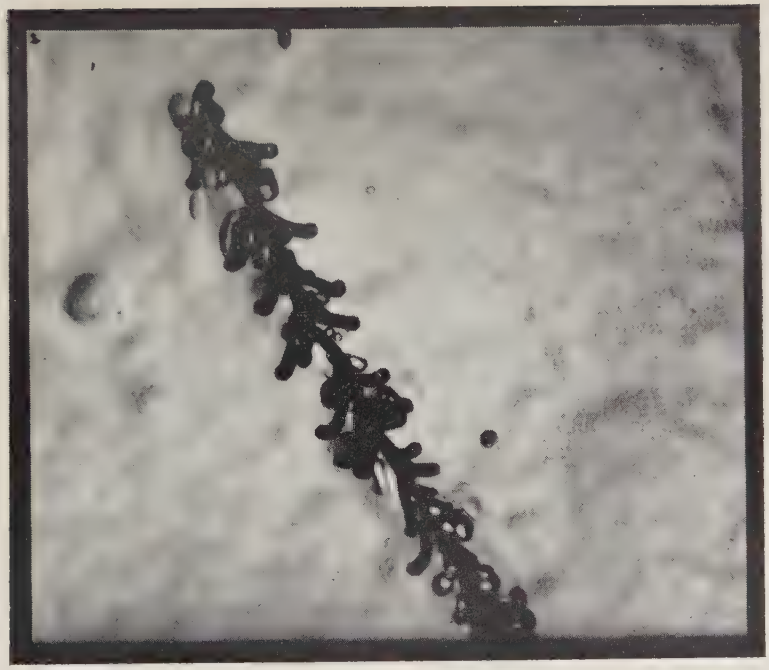

Damage produced by grit during grinding. The crystal has been lightly etched to remove the layer of general damage which is a few microns thick. ×250.

Fig. 2

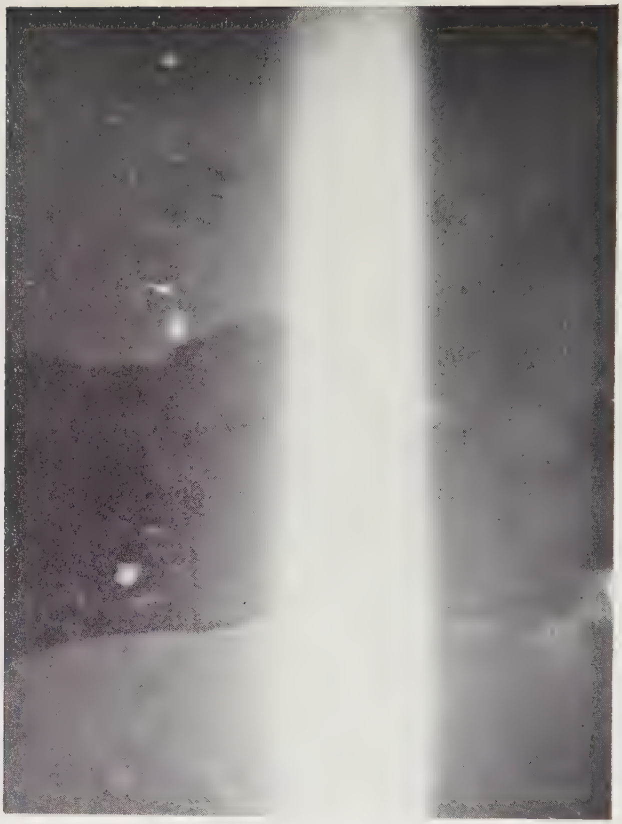

Comparison of the contrast for coated and uncoated film.
Left-hand side coated with zinc sulphide, centre uncoated, right-hand side coated with silicon monoxide.

Fig. 3

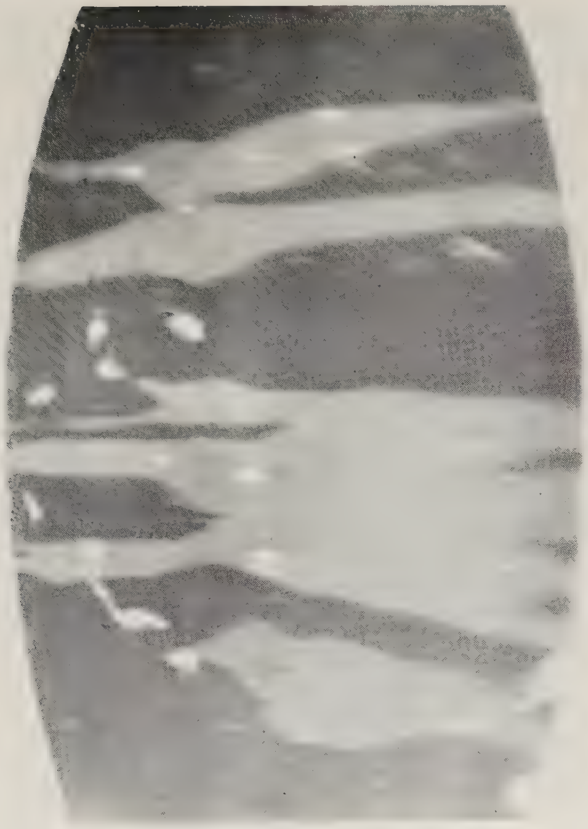

A typical domain structure in a uniaxial 81 : 19 Ni : Fe film 1500 Å thick.

Fig. 4

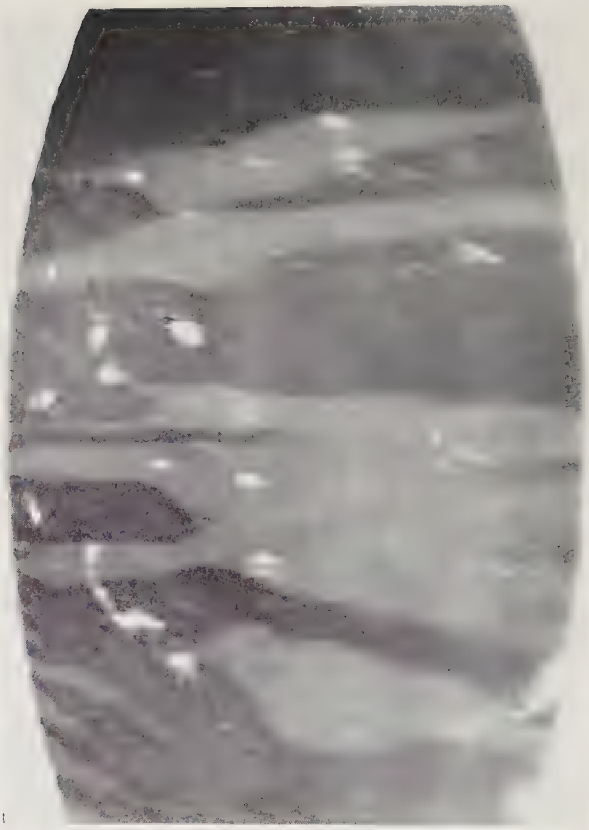

The effect of a transverse field of 0·78 of the anisotropy field upon the domain structure of fig. 3.

Fig. 5

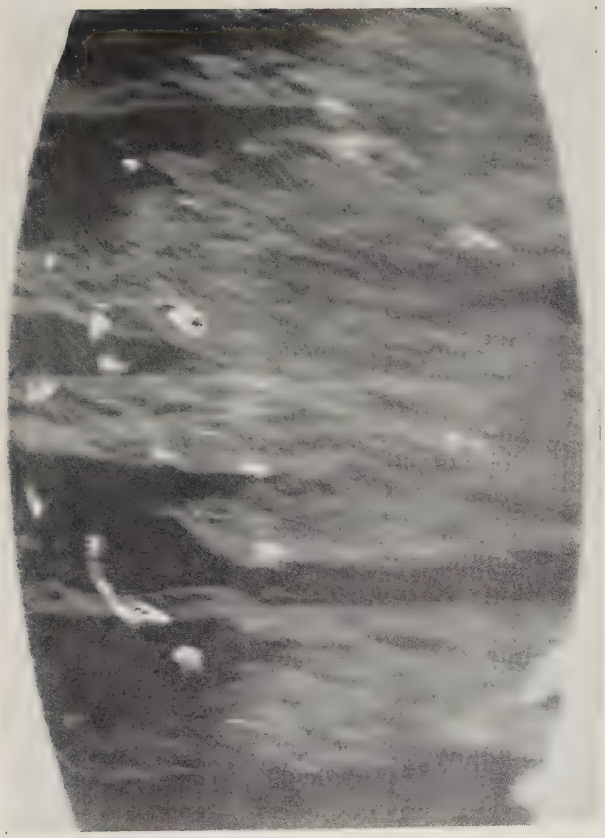

The same domain structure after the application of a transverse field of 0·86 of the anisotropy field.

Fig. 6

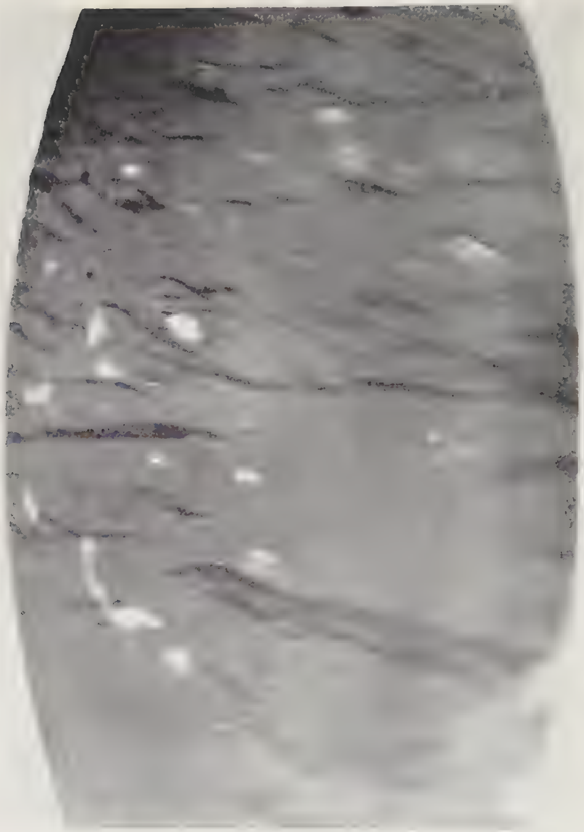

The same domain structure after the application of a transverse field equal to the anisotropy field.

Fig. 1

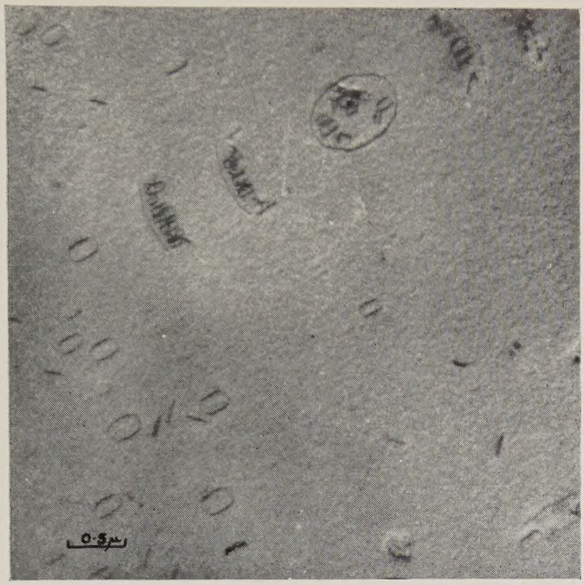

Al–4% Cu quenched from 525°c into acetone. Dislocations symmetrically arranged about a source with associated rows of loops. ×15 000.

Fig. 2

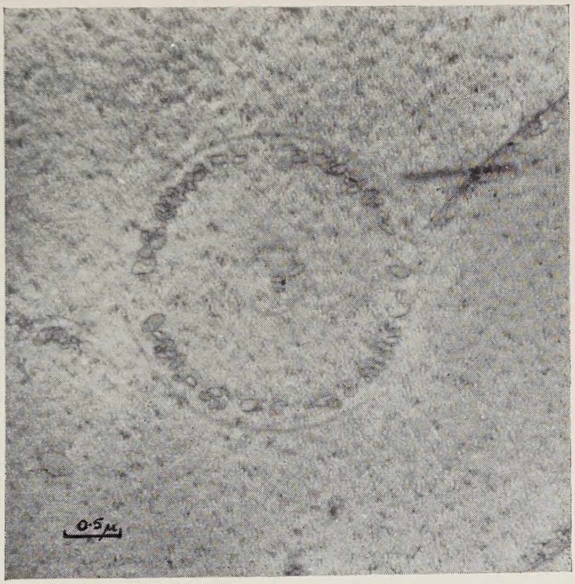

Al–4% Cu quenched from 525°c into acetone. Dislocation ring in a foil with a (111) orientation. Short sections of dislocation from other sources are also seen. ×15 000.

Fig. 3

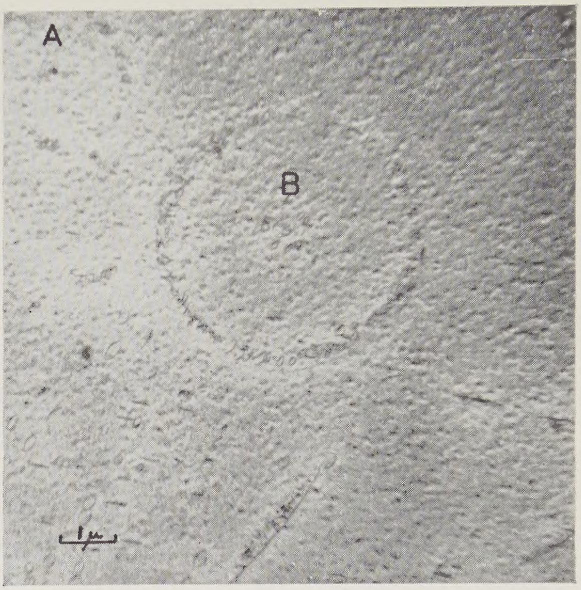

Al–4% Cu quenched from 525°c into acetone. Dislocation rings from two sources A and B. Source B consists of two small loops. ×7500.

Fig. 4

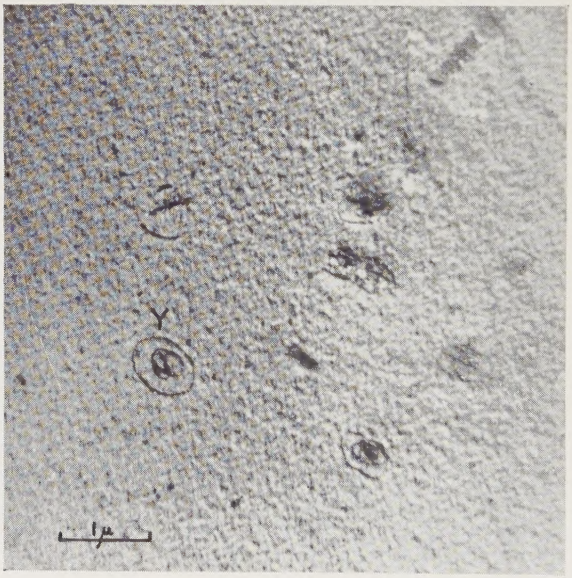

Al–3% Cu quenched from 525°c into acetone. The arrangement of the sources is shown in detail. Region (Y) consists of a complete loop around a source. ×12 000.

Fig. 6

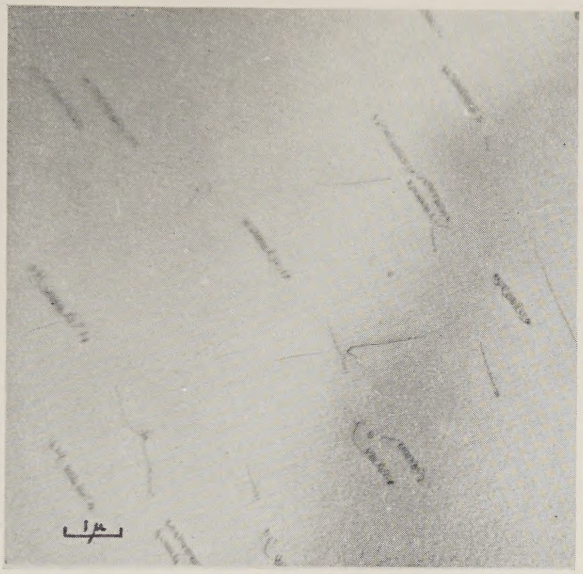

Al–3% Cu quenched from 550°c into acetone. Pairs of helical dislocations of opposite hand. ×75 000.